UC Irvine
UC Irvine Electronic Theses and Dissertations

Title
Conversion of Small Carbon Compounds by Nitrogenase Proteins

Permalink
https://escholarship.org/uc/item/1tp938hp

Author
Rebelein, Johannes Georg

Publication Date
2016

Copyright Information
This work is made available under the terms of a Creative Commons Attribution License, availalbe at https://creativecommons.org/licenses/by/4.0/

Peer reviewed|Thesis/dissertation

eScholarship.org Powered by the California Digital Library
University of California

UNIVERSITY OF CALIFORNIA,
IRVINE

Conversion of Small Carbon Compounds by Nitrogenase Proteins

DISSERTATION

submitted in partial satisfaction of the requirements
for the degree of

DOCTOR OF PHILOSOPHY

in Biological Sciences

by

Johannes Georg Rebelein

Dissertation Committee:
Professor Markus W. Ribbe, Chair
Professor Andrew Borovik
Assistant Professor Yilin Hu

2016

Portion of Chapter 2 © 2014 John Wiley and Sons
Portion of Chapter 3 © 2015 John Wiley and Sons
All other materials © 2016 Johannes Georg Rebelein

Dedication

This dissertation is dedicated
to my parents and family
for their love
and unconditional support
of all my decisions.

To Paola Tognini
and my friends
for shaping me and my life.

Table of Contents

List of Figures viii

List of Tables x

List of Abbreviations xi

Acknowledgments xiii

Curriculum Vitae xiv

Abstract of the Dissertation xvi

Chapter 1: Introduction to Nitrogenase 1

1.1 Overview of Nitrogenase 2

1.2 Comparison of Molybdenum and Vanadium Nitrogenase 4

1.2.1 The Reductase Component 4

1.2.2 The Catalytic Component 5

1.2.3 Catalytic Features 9

1.3 Aims of the Dissertation 10

1.3.1 Specific Aim 1: ATP-dependent CO_2 Reduction by Molybdenum and Vanadium Nitrogenase 11

1.3.2 Specific Aim 2: ATP-independent CO_2 Reduction by Vanadium Nitrogenase 11

1.3.3 Specific Aim 3: The Interconversion between CO and CO_2 by Nitrogenase Iron Proteins 12

1.3.4 Specific Aim 4: *In vivo* Hydrocarbon Formation by Vanadium Nitrogenase 12

1.4 Synopsis of the Dissertation 13

1.5 References 14

Chapter 2: ATP-dependent Carbon Dioxide Reduction by Molybdenum and Vanadium Nitrogenase 22

2.1 Introduction 23

2.2 Material and Methods 24

2.2.1 Reagents 24

2.2.2 Cell Growth and Protein Purification 25

2.2.3 Enzyme Assays 25

2.2.4 Activity Determination 26

2.2.5 GC-MS Analysis 26

2.3 Results and Discussion 28

2.3.1 CO_2 Reduction Products 28

2.3.2 Tracing CO_2 during Hydrocarbon Formation 29

2.4 Summary and Conclusion 34

2.5 Acknowledgments 35

2.6 References 35

Chapter 3: ATP-independent Carbon Dioxide Reduction by Vanadium Nitrogenase 40

3.1 Introduction 41

3.2 Materials and Methods 43

3.2.1 Reagents 43

3.2.2 Cell Growth and Protein Purification 43

3.2.3 Enzyme Assays 43

3.2.4 Activity Determination 44

3.2.5 GC-MS Analysis 45

3.3 Results and Discussion 45

3.3.1 C1 Products from CO_2 Reduction 45

3.3.2 Hydrocarbon Chain Products from CO_2 Reduction 47

3.3.3 Tracing the Carbon Source of the Hydrocarbon Products 48

3.4 Summary and Conclusion 49

3.5 Acknowledgments 51

3.6 References 51

Chapter 4: The Interconversion between Carbon Monoxide and Carbon Dioxide by Nitrogenase Iron Proteins 55

4.1 Introduction 56

4.2 Materials and Methods 57

4.2.1 Reagents 57

4.2.2 Protein Purification 57

4.2.3 *In vitro* CO_2 Reduction Assays 57

4.2.4 *In vitro* CO Oxidation Assays 58

4.2.5 *in vivo* CO_2 Reduction Assays 58

4.2.6 Quantification of CO and CO_2 59

4.2.7 Formate Assays 60

4.2.8 Western Blot Analysis 60

4.2.9 Midpoint Potential Determination 61

4.2.10 GC-MS Analysis 62

4.2.11 EPR Analysis 62

4.3 Results and Discussion 64

4.3.1 *In vitro* Interconversion between CO and CO_2 by Iron Proteins 64

4.3.2 EPR Analysis of CO_2- and CO-bound Iron Proteins 68

4.3.3 Comparison of Fe Proteins with Carbon Monoxide Dehydrogenase 70

4.3.4 *In vivo* Reduction of CO_2 to CO 71

4.4 Summary and Conclusion 73

4.5 Acknowledgments 74

4.6 References 74

Chapter 5: *in vivo* Hydrocarbon formation by Vanadium Nitrogenase 79

5.1 Introduction 80

5.2 Materials and Methods 81

5.2.1 Reagents 81

5.2.2 Analysis of *in vivo* CO Reduction by Nitrogenase-expressing Strains of *A. vinelandii* 81

5.2.3 Determination of Optimal CO Concentration for *in vivo* Hydrocarbon Formation 82

5.2.4 Improvement of *in vivo* Hydrocarbon Formation by Intermittent Air Exposure 83

5.2.5 GC-MS Analysis of Hydrocarbons Generated by *in vivo* CO Reduction 83

5.2.6 NanoSIMS Analysis of *A. vinelandii* Cultures Incubated with ^{12}CO and ^{13}CO 84

5.2.7 LC-MS analysis of Acetyl-CoA Formation by CO-incubated *A. vinelandii* Cultures 85

5.3 Results and Discussion 87

5.3.1 *In vivo* Hydrocarbon Formation from CO Reduction by *A. vinelandii* 87

5.3.2 The Physiological Role of the *in vivo* CO Reduction by V nitrogenase 91

5.4 Summary and Conclusions 94

5.5 Acknowledgements 96

5.6 References 96

List of Figures

Figure 1.1. The Mo nitrogenase component proteins and metalloclusters of *Azotobacter vinelandii*. 3

Figure 1.2. The V nitrogenase component proteins. 4

Figure 1.3. P-clusters of the MoFe and VFe proteins. 6

Figure 1.4. Cofactors of the MoFe and VFe proteins. 7

Figure 1.5. CO_2 conversion by nitrogenase systems. 13

Figure 2.1. Product formation by Mo and V nitrogenases in the presence of CO_2. 28

Figure 2.2. ATP-dependent product formation by V nitrogenase from CO_2. 29

Figure 2.3. GC-MS analyses of the hydrocarbon products formed by Mo and V nitrogenase. 30

Figure 2.4. Formation of hydrocarbon products by V nitrogenase. 31

Figure 2.5. ATP- and protein component dependent CH_4 formation by Mo nitrogenase in the presence of CO_2. 33

Figure 3.1. Three CO_2-reducing reaction systems based on V nitrogenase. 42

Figure 3.2. ATP-independent reduction of CO_2 to C1 products by VFe protein. 46

Figure 3.3. ATP-independent reduction and coupling of CO_2 into C2–C4 products by VFe protein. 47

Figure 3.4. GC-MS analysis of hydrocarbons generated by VFe protein in the ATP-independent reaction of CO_2 reduction. 49

Figure 3.5. C-C coupling from CO_2 reduction by the three V nitrogenase-based systems. 50

Figure 4.1. *In vitro* reduction of CO_2 to CO by Fe proteins. 65

Figure 4.2. Increase of specific activities of Fe proteins during purification. 66

Figure 4.3. Linear correlation between the activity and amount of the purified Fe protein and reproducibility of activity from different protein preparations. 67

Figure 4.4. Interactions of CO_2 and CO with the $[Fe_4S_4]$-clusters of the Fe proteins. 69

Figure 4.5. Western blot analysis of Fe protein expression. 71

Figure 4.6. *In vivo* reduction of CO_2 to CO by Fe proteins. 72

Figure 5.1. *In vivo* hydrocarbon formation from CO reduction by *A. vinelandii*. 88

Figure 5.2 Optimization of *in vivo* hydrocarbon production from CO reduction. 89

Figure 5.3. *In vivo* CO reduction as a secondary metabolic pathway. 92

Figure 5.4. Assimilation of N via N_2 reduction by *A. vinelandii*. 93

List of Tables

Table 3.1. Nitrogenase Reactions. 41

Table 4.1. Reduction Potential of NifH and VnfH $[Fe_4S_4]^{+1}$-Clusters in the presence of CO_2. 64

List of Abbreviations

ATP	adenosine triphosphate
A. vinelandii	*Azotobacter vinelandii*
C-C	carbon-carbon single bond
C=C	carbon-carbon double bond
C≡C	carbon-carbon triple bond
C_2H_2	acetylene
C_2H_4	ethene
C_2H_6	ethane
C_3H_6	propene
C_3H_8	propane
C_4H_8	butene
C_4H_{10}	butane
CO	carbon monoxide
CO_2	carbon dioxide
Da	dalton
$E^{0'}$	standard electrode potential
e^-	electron
Eu^{II} DTPA	europium(II) diethylenetriaminepentaacetate
EXAFS	Extended X-ray absorption fine structure
FeS	iron-sulfur
FID	flame ionization detector
GC	gas chromatography

h	hour
k	kilo
L	liter
M	molar
M cluster	Iron molybdenum cofactor (FeMoco)
min	minute
N_3^-	azide
OD_λ	optical density at wavelength λ [nm]
rpm	rotations per minute
SDS-PAGE	sodium dodecyl sulfate polyacrylamide gel electrophoresis
SmI_2	Samarium(II) iodide
Tris	tris-(hydroxymethyl)-amino methane
UV/Vis	ultra violet and visible spectrum of light
V cluster	Iron vanadium cofactor (FeVco)
v/v	volume per volume
w/v	weight per volume
XAS	X-ray absorption spectroscopy

Acknowledgments

First and foremost, I would like to thank my advisor, Professor Markus W. Ribbe, for giving me the opportunity to work on several fascinating and exciting scientific projects. The combination of basic research with the outlook of an imminent application, particularly of ammonia, intrigued and motivated me. I greatly value his guidance and positive approach as well as his enthusiasm for research.

I would like to thank my co-advisor Professor Yilin Hu for the fantastic projects we collaborated on. I am especially grateful for the support she provided regarding the molecular biology of *Azotobacter vinelandii* and the construction of strains used for my thesis work.

I would also like to thank my committee member Professor Andy Borovik for his constant guidance and support during my graduate work and for a wonderful lecture on metallobiochemistry.

I owe much gratitude to my co-workers in the Ribbe lab: Dr. Jared Wiig, Dr. Chi Chung Lee, Dr. Nathanial Sickerman, Dr. Kazuki Tanifuji, Dr. Aaron Fay, Dr. Martin Stiebritz, Lee Rettberg, Megan Newcomb, Caleb Hiller and Jasper Liedtke. I especially thank Dr. Jared Wiig and Dr. Chi Chung Lee for their nurturing and mentoring, as well as their suggestions and improvements of my writing, for which I also thank Dr. Nathanial Sickerman. Also, the after-hours discussions about research and beyond were greatly appreciated and made me feel home.

I would like to thank John Wiley and Sons for the permission to include portions of Chapter 2 and 3 in my dissertation, which were originally published in Angewandte Chemie International Edition and ChemBioChem, respectively. Furthermore, I would also like to thank the Nature Publishing Group for publishing portions of Chapter 4 and 5 in Nature Chemical Biology and Nature Communications, respectively. Financial support was provided by the National Institutes of Health (Grant GM 67626), by the Department of Energy (BES) Award DE-SC0014470, a Hellman Fellowship to Dr. Yilin Hu and funds from UC Irvine to Dr. Markus W. Ribbe and Dr. Yilin Hu.

Curriculum Vitae

JOHANNES GEORG REBELEIN

EDUCATION

University of California, Irvine — Irvine, CA, USA

Ph.D., Biological Sciences — 11/22/2016

TU Braunschweig — Braunschweig, Germany

M.S., Biotechnology — 2012

B.S., Biotechnology — 2010

FELLOWSHIPS AND AWARDS

UC Carbon Slam – 3rd place at the UC-wide short talk competition about carbon neutrality — 2016

UCI's Public Impact Fellowship — 2015-2016

William F. Holcomb Scholarship of the Ayala School of Biological Sciences, UCI — 2015

Poster Award of the American Chemical Society at the Enzymes Coenzymes and Metabolic Pathways - Gordon Research Conference — 2015

Research Abroad Grant by the German National Academic Foundation — 2012

Scholarship of the German National Academic Foundation — 2010-2012

Academic excellence scholarship of the TU Braunschweig, Germany — 2009-2011

CONFERENCE PRESENTATIONS

1. "NifEN: A Structural and Functional Homolog of the Nitrogenase Catalytic Component" **Rebelein JG,** Fay AW, Blank MA, Lee CC, Ribbe MW, Hedman B, Hodgson KO, Hu Y. Poster presentation at the Metallocofactors – Gordon Research Conference. June 2016, Easton, MA
2. „Reduction of CO_2 by Molybdenum and Vanadium Nitrogenase"; **Rebelein JG,** Hu Y, Ribbe MW. Poster presentation at the Enzymes, Coenzymes & Metabolic Pathways – Gordon Research Conference. July 2015, Waterville Valley, NH
3. „Heterometal Insertion into the FeMoco-Precursor"; **Rebelein JG,** Hu Y, Ribbe MW. Poster presentation at the Iron-Sulfur Enzymes – Gordon Research Conference. June 2014, Easton, MA

SERVICE AND AFFILIATION

Elected member of the graduate student government, UCI — 2013-2015

Elected student council member, TU Braunschweig, Germany — 2007-2012

Volunteer work as paramedic at the German Red Cross — 2007-2009

PEER REVIEWED PUBLICATIONS

1. **Rebelein JG**, Lee CC, Hu Y, Ribbe MW. (2016) In vivo Hydrocarbon Formation by Vanadium Nitrogenase: A Novel Secondary Metabolic Pathway. *Nat. Commun.* (In Press)

2. **Rebelein JG**, Stiebritz M, Lee CC, Hu Y. (2016) Activation and Reduction of Carbon Dioxide by Nitrogenase Iron Proteins. *Nat. Chem. Biol.* (In Press)

3. Fay AW*, Blank MA*, **Rebelein JG***, Lee CC, Ribbe MW, Hedman B, Hodgson KO, Hu Y. (2016) Assembly scaffold NifEN: A Structural and Functional Homolog of the Nitrogenase Catalytic Component. *Proc Natl Acad Sci U S* A. 113(34):9504-8 (* Authors contributed equally to this work)

4. **Rebelein JG**, Hu Y, Ribbe MW. (2015) Widening the Product Profile of Carbon Dioxide Reduction by Vanadium Nitrogenase. *ChemBioChem.* 16(14):1993-6.

5. **Rebelein JG**, Hu Y, Ribbe MW. (2014) Differential Reduction of CO_2 by Molybdenum and Vanadium Nitrogenases. *Angew Chem Int Ed Engl.* 53(43): 11543-6.

6. Wiig JA, **Rebelein JG**, Hu Y. (2014) Nitrogenase Complex. *eLS*2014, (John Wiley & Sons, Ltd.)

7. Moser J, Lange C, Krausze J, **Rebelein JG**, Schubert WD, Ribbe MW, Heinz DW, Jahn D. (2013) Structure of ADP-Aluminium $Fluoride^-$Stabilized Protochlorophyllide Oxidoreductase Complex. *Proc Natl Acad Sci U S A*. 110(6): 2094-8.

Abstract of the Dissertation

Conversion of Small Carbon Compounds by Nitrogenase Proteins

By

Johannes Georg Rebelein

Doctor of Philosophy in Biological Sciences

University of California, Irvine, 2016

Professor Markus Walter Ribbe, Chair

Nitrogenases are complex metalloenzymes capable of catalyzing two of the most challenging reactions in Nature: the reduction of atmospheric dinitrogen to ammonia and the reduction of carbon monoxide (CO) to hydrocarbons. The *Azotobacter vinelandii* molybdenum (Mo) and vanadium (V)-nitrogenases are homologous systems consisting of two components: the reductase component (Fe protein) and the catalytic component (MoFe or VFe protein, respectively). The reductase component contains a [Fe_4S_4]-cluster, whereas the catalytic component contains two unique metal clusters, the P-cluster and the M or V cluster for Mo- and V-nitrogenase, respectively.

This dissertation focuses on the conversion of small carbon compounds such as the toxic exhaust CO and the greenhouse gas carbon dioxide (CO_2) by nitrogenase proteins. The CO_2 reducing capability of Mo- and V-nitrogenase was investigated under physiologically relevant assay conditions. Indeed, both nitrogenases reduce CO_2 to CO, but only

V-nitrogenase reduces CO_2 to hydrocarbons. These studies demonstrated that V-nitrogenase directly couples CO_2 or CO_2-derived species to hydrocarbon chains.

Building on this, the efficiency of this reaction was improved by using the strong reductant europium(II) diethylenetriaminepentaacetate, rendering the ATP-dependent electron transfer obsolete and increasing the hydrocarbon chain length as well as the yield.

Excitingly, the reductase component of V- and Mo-nitrogenase alone can reduce CO_2 to CO. Strikingly, the reverse reaction, the oxidation of CO to CO_2, is catalyzed under oxidizing conditions by Fe protein. The interconversion of CO and CO_2 establishes the reductase component housing a $[Fe_4S_4]$-cluster as simple Fe/S-based mimic of CO dehydrogenase. The physiological relevance of this reduction is suggested by the observation that *A. vinelandii* strains expressing only the Fe protein component form CO_2-derived CO *in vivo.*

These discoveries led to the question of whether V-nitrogenase expressing *A. vinelandii* strains could also *in vivo* form hydrocarbons from CO or CO_2. Indeed, this strain can convert CO to hydrocarbons *in vivo.* Furthermore, this process is a secondary metabolism since the carbon from CO is not incorporated into the cell mass, but released. Coupling the two *in vivo* processes could result in a biofuel process that catalytically converts CO_2 into combustible hydrocarbon fuels.

Chapter 1: Introduction to Nitrogenase

1.1 Overview of Nitrogenase

Nitrogenase is a group of complex metalloenzymes that is best known for its function in the global nitrogen cycle, catalyzing the reduction of atmospheric dinitrogen (N_2) to ammonia (NH_3) under ambient conditions (1, 2). The overall reaction is usually depicted as $N_2 + 8H^+ + 16MgATP + 8e^- \rightarrow 2NH_3 + H_2 + 16MgADP + 16P_i$ (2). The physiological function of providing a bioavailable form of nitrogen (NH_3) aside, this reaction embodies the formidable chemistry of breaking the exceptionally stable N≡N triple bond only achieved by nitrogenases.

So far three homologous nitrogenases, the molybdenum (Mo), the vanadium (V), and the iron (Fe)-only nitrogenases, have been identified (3, 4). The best-studied homolog of this family is the Mo nitrogenase from *Azotobacter vinelandii*, which consists of two protein components. The first component, designated Fe protein (*nifH* encoded), is a γ_2-dimer that contains a subunit-bridging $[Fe_4S_4]$-cluster per dimer and an ATP binding site within each subunit (Figure 1.1) (5-13). The surface-exposed $[Fe_4S_4]$-cluster of NifH is ligated symmetrically through two cysteines (i.e., Cys^{97} and Cys^{132}) (9) from each subunit and can assume three oxidation states (i.e., 0, +1 and +2), although the $[Fe_4S_4]^{2+/1+}$ couple is generally believed to be utilized under physiological conditions (11, 14, 15). The second component is designated MoFe protein (*nifDK* encoded) and is a $\alpha_2\beta_2$-tetramer that contains two unique metalloclusters per αβ-dimer: the P-cluster, a $[Fe_8S_7]$ subunit-bridging cluster and the M cluster (FeMoco), a $[MoFe_7S_9C$-homocitrate$]$ cluster within the α-subunit (Figure 1.1) (16-20). While the P-cluster is located 10 Å below the surface of the protein and coordinated at the αβ-subunit interface of NifDK by six ligands ($Cys^{\alpha62}$, $Cys^{\alpha88}$, $Cys^{\alpha154}$, $Cys^{\beta70}$, $Cys^{\beta95}$, and $Cys^{\beta153}$), the M cluster is buried within the α-subunit NifD 14 Å away from the P-cluster and ligated by only two amino acids ($His^{\alpha442}$ and $Cys^{\alpha275}$) (Figure 1.1b) (19, 20). Structurally, the

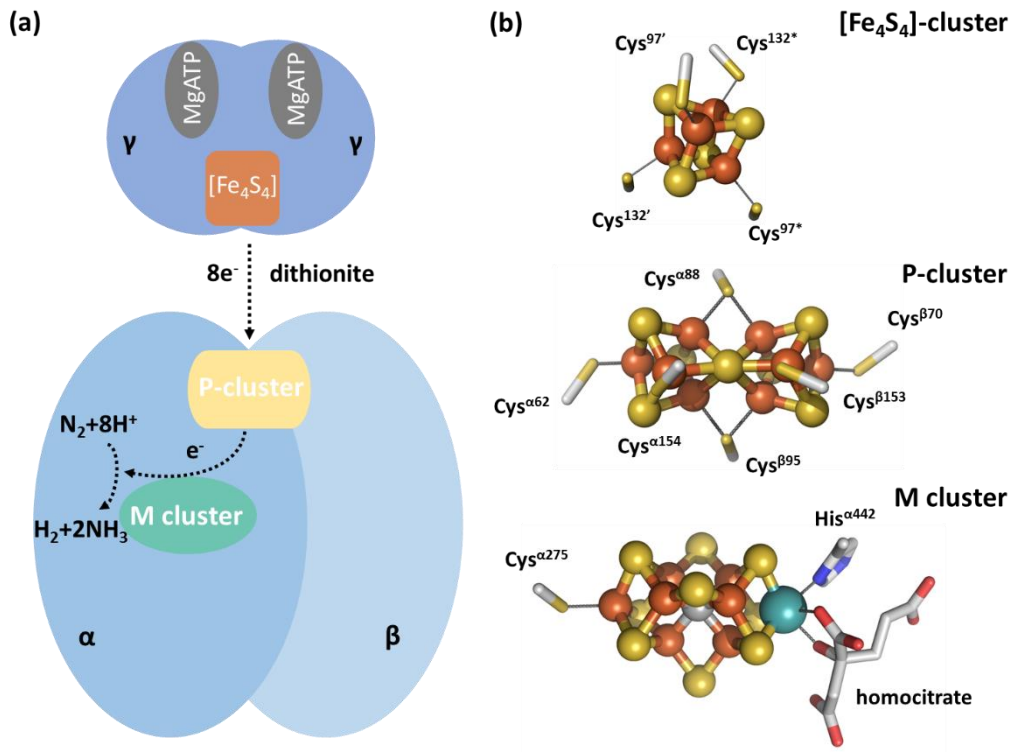

Figure 1.1. The Mo nitrogenase component proteins and metalloclusters of *Azotobacter vinelandii*. (a) Schematic representation of the γ2-homodimeric reductase component, $NifH_2$ (top) and the αβ-half of the catalytic component NifDK (bottom). The reductase component contains a $[Fe_4S_4]$-cluster at the subunit interface and an ATP-binding site within each subunit. The catalytic component harbors the subunit-bridging P-cluster ($[Fe_8S_7]$) and within the α-subunit resides the M cluster ($[MoFe_7S_9C$-homocitrate$]$). (b) Structures of the Mo-nitrogenase metalloclusters based on crystallographic data. From top to bottom: $[Fe_4S_4]$-cluster, P-cluster and M cluster. Clusters are shown as ball-and-stick models, with the atoms colored as follows: Fe (orange), S (yellow), Mo (cyan), O (red), C (grey), and N (blue). PYMOL was used to generate the structures in this figure based on coordinates of PDB entries 1M1N and 1N2C.

P-cluster can be viewed as two $[Fe_4S_3]$ cubanes that are bridged by one μ_6-sulfide (19-21), while the M cluster can be regarded as a $[MoFe_3S_3]$ and a $[Fe_4S_3]$ cubane bridged by three μ_2-sulfides and a central μ_6-carbide atom (17-20, 22). Catalysis by the Mo nitrogenase involves the complex formation between homodimeric $NifH_2$ and heterotetrameric $Nif(DK)_2$ (8, 12) and the ATP-dependent transfer of electrons from the $[Fe_4S_4]$-cluster of NifH, via the P-cluster, to the M cluster of NifD, where substrate reduction occurs (Figure 1.1a).

1.2 Comparison of Molybdenum and Vanadium Nitrogenase

Like Mo nitrogenase, V nitrogenase is a binary system consisting of two components (Figure 1.2); the γ_2-dimeric Fe protein (or reductase component encoded by *vnfH*) and the $\alpha_2\beta_2\delta_4$-heterooctameric VFe protein (or catalytic component encoded by v*nfDGK)* (3, 23, 24). Both nitrogenases share a high degree of homology regarding primary sequence, cluster composition, spectroscopic and catalytic features. Mo and V nitrogenase follow the same mode of action during catalysis, forming a functional complex that allows the ATP-dependent electron transfer from the $[Fe_4S_4]$-cluster of the reductase component via the P-cluster to the V cluster, the M cluster counterpart of V nitrogenase, in the catalytic component (Figure 1.2). In addition, both nitrogenases are known to reduce other substrates besides N_2, such as protons (H^+), acetylene (C_2H_2), azide (N_3^-), cyanide (CN^-) and carbon monoxide (CO), albeit at different rates and preferences (3, 24-28).

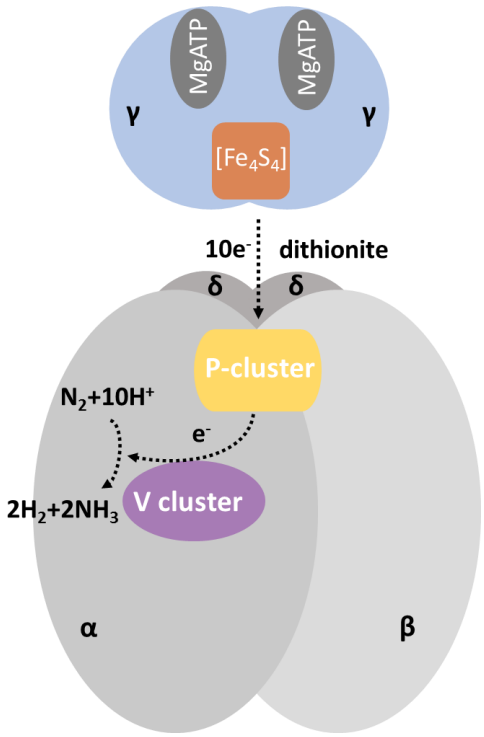

Figure 1.2. The V nitrogenase component proteins. Schematic representation of the γ2-homodimeric reductase component, $VnfH_2$ (top) and the $\alpha\beta\delta_2$-half of the catalytic component $VnfDKG_2$ (bottom). The reductase component contains a $[Fe_4S_4]$-cluster at the subunit interface and an ATP-binding site within each subunit. The catalytic component harbors the subunit-bridging P-cluster, and within the α-subunit resides the V cluster.

1.2.1 The Reductase Component

The reductase components (Fe proteins) of Mo and V nitrogenase, encoded by ni*fH* and vn*fH* respectively, are dimers with a molecular weight of ~60 kDa. The sequences of *nifH* and *vnfH*

show an identity of 91 %, with the ATP-binding motif Gly-X-Gly-X-X-Gly and the two cysteines binding the subunit-bridging [Fe_4S_4]-cluster being conserved in both sequences (23). Moreover, the spectroscopic features of NifH and VnfH, as derived from X-ray absorption spectroscopy (XAS) and electron paramagnetic resonance (EPR) analyses, are overwhelmingly similar, although the Fe K-edge XAS analysis reveals slightly less ferric Fe atoms for VnfH (15). However, the EPR spectra of the dithionite-reduced [Fe_4S_4]$^{1+}$-cluster of both Fe proteins display a mixture of S = 1/2 and S = 3/2 EPR signals (29, 30). Moreover, the mid-point potential of both reductase components drops after the binding of MgATP by ~100 mV (28). In the MgADP-bound state, the mid-point potential of both Fe proteins is similar. Furthermore, the [Fe_4S_4]-cluster of both components can assume the three oxidation states 0, +1 and +2 (31). Taken together, these characteristics point towards a striking similarity between the two Fe proteins and their [Fe_4S_4]-clusters.

1.2.2 The Catalytic Component

The catalytic component is called MoFe protein for Mo nitrogenase (encoded by *nifDK*) and VFe protein for V nitrogenase (encoded by *vnfDGK*). MoFe protein forms a heterotetrameric complex ($\alpha_2\beta_2$) with a molecular weight of ~240 kDa, while the VFe protein has an additional small subunit (encoded by *vnfG*) and forms a heterooctameric complex ($\alpha_2\beta_2\delta_4$) with a molecular weight of ~270 kDa (26, 28, 32). The sequence identity of *nifD* and *nifK* to its respective *vnf* counterpart is 33 % and 32%, respectively. The anchoring ligands for both

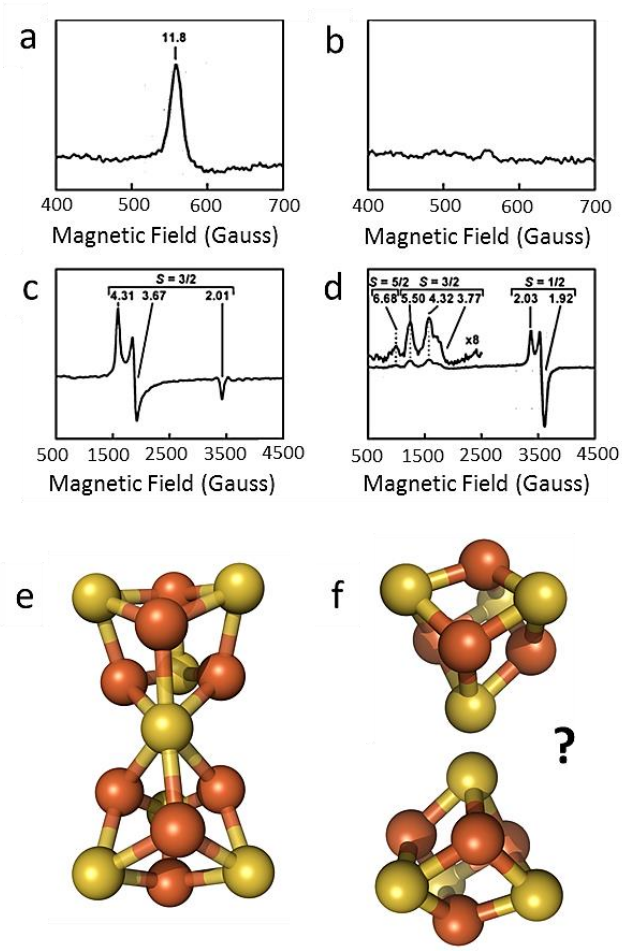

Figure 1.3. P-clusters of the MoFe and VFe proteins. (a, b) Parallel mode EPR spectra of indigo disulfonate (IDS)-oxidized MoFe (a) and VFe (b) proteins. (c, d) Perpendicular mode EPR spectra of dithionite-reduced MoFe (c) and VFe (d) proteins. The g values are indicated. Spectra (a, b, c, d) were collected at 50 mW and 15 K. (e, f) Crystal structure of the P-cluster in MoFe protein (e) and the proposed structure of the P-cluster in VFe protein (f). The clusters are shown as ball-and-stick models, with the atoms colored as follows: Fe (orange), S (yellow) PYMOL was used to create the figure.

clusters, the P-cluster and the M cluster/V cluster are conserved in both catalytic components.

Until recently, it was assumed that the P-cluster of MoFe and VFe protein is a [Fe_8S_7] cluster. However, EPR analysis of VFe protein in comparison to the MoFe protein suggests otherwise (Figure 1.3) (26). The most notable difference emerges from the indigo disulfonate (IDS)-oxidized state of the catalytic proteins. The P-cluster of MoFe protein displays a strong S = 2 signal at g = 11.8 (Figure 1.3a) in the parallel mode associated with +2 oxidation state of the P-cluster (P^{2+}) (33, 34). In contrast, this signal cannot be identified in the spectrum of the oxidized VFe protein (Figure 1.3b) (26). Instead, the EPR spectrum of the dithionite-reduced VFe protein shows an S = 1/2 signal at g = 2.03 and 1.92 distributed to the P-cluster (Figure 1.3d) (26, 35), which is not present in the spectrum of the reduced MoFe protein (Figure 1.3c). Moreover, an S = 5/2 signal at g = 6.85 seems to be associated with the P-cluster since it follows the same temperature and redox dependency

as the S = 1/2 signal (26). Previously, it was shown that the partially oxidized P-cluster of MoFe protein in the P^{1+}-state shows an analogous S =1/2 signal at g = 2.06 and 1.95 as well as a similar S = 5/2 signal at g = 6.70 (36), indicating that the P-cluster of VFe protein might exist in a more oxidized state than the P-cluster of MoFe protein. This difference of oxidation state could originate from a structural difference as observed in the Fe K-edge XAS/extended X-ray absorption fine structure (EXAFS) analysis of the cofactor-deficient VFe protein (35). Instead of the 'standard' [Fe_8S_7] P-cluster (Figure 1.3e) of MoFe protein, the P-cluster of VFe protein could reassemble a pair of [Fe_4S_4]-clusters (Figure 1.3f) (35).

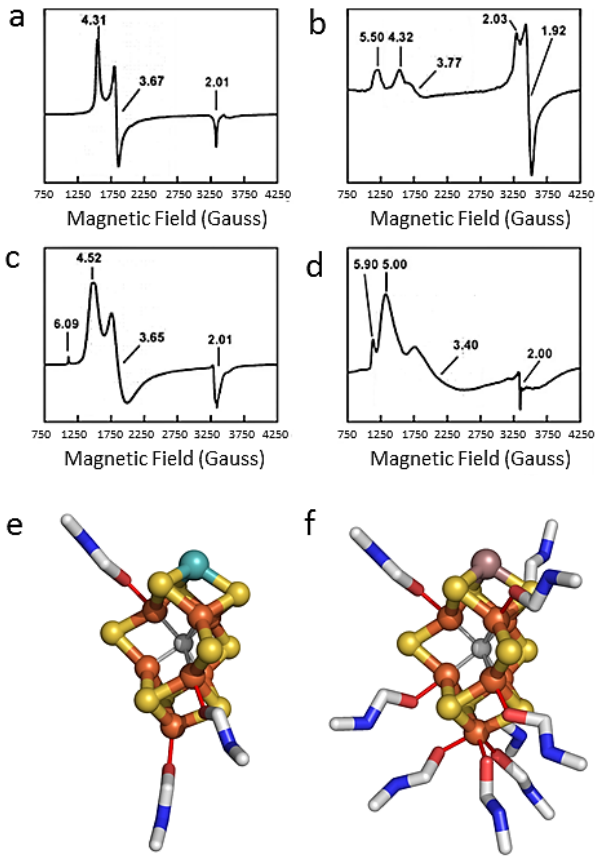

Figure 1.4. Cofactors of the MoFe and VFe proteins. (a, c) Perpendicular mode EPR spectra of dithionite-reduced MoFe protein (a) and NMF-extracted M cluster (c). Perpendicular mode EPR spectra of dithionite-reduced EPR spectra of VFe protein (b) and NMF-extracted V cluster (d). The g values are indicated. Spectra were collected at 15 K (a, b, c) and at 6 K (d) (e, f) The XAS/EXAFS-derived structures of NMF-extracted M cluster (e) and V cluster (f). The clusters are shown as ball-and-stick models, whereas the NMF molecules are represented by sticks, with the atoms colored as follows: Fe (orange), S (yellow), Mo (cyan), V (lilac), O (red), C (grey), and N (blue). PYMOL was used to create the figure.

Besides the fact that Mo is replaced by V in the V cluster of VFe protein, it was shown that both catalytic cofactors M- and V cluster contain a central carbide atom and are structurally similar (17, 18, 37). Yet, both clusters have differences in their electronic properties and the interactions with the protein environment, which is evident by

much weaker, broader and less-resolved EPR-features of the dithionite-reduced V cluster (Figure 1.4b), in comparison to the M cluster (Figure 1.4a). The V cluster causes the $S = 3/2$ signal at $g = 5.50$, 4.32 and 3.77 (Figure 1.4b) in the protein-bound state (26). The $S = 3/2$ signal seems to originate from different species since the $g = 5.50$ feature behaves differently than the other two features upon temperature and redox treatment (26, 30). The NMF-extracted V cluster (Figure 1.4d) gives rise to an $S = 3/2$ signal at $g = 5.00$ and 3.40 that corresponds to the features at $g = 4.32$ and 3.77 of the protein-bound V cluster, respectively (38). The disappearance of the $g = 5.50$ feature indicates that it is indeed a different $S = 3/2$ species and originates from the interaction of the cofactor with the protein environment. The additional features at $g = 5.90$ of the V cluster spectra (Figure 1.4d) and $g = 6.09$ of the M cluster spectra (Figure 1.4c) may originate from the interactions of M cluster and V cluster with the thiolate groups in thiophenol and 1,4-benzenedithiol.

The Fe K-edge XAS/EXAFS analyses of both extracted cofactors confirm the similarity between the cluster, yet also show the differences (Figure 1.4e, f). On the one hand, the 'Fe cages' of both clusters closely resemble each other. On the other hand, the V cluster is surrounded by a well-defined sphere of NMF molecules, in contrast to the M cluster. This observation implies a difference in the electronic structure, at least without the protein background (38). Moreover, the V cluster displays a more elongated structure than the M cluster, which might render the V cluster more susceptible to solvent binding (38). Overall, the distinctive electronic structure of the V cluster to the M cluster can at least in part be attributed to the different hetero metals Mo and V, respectively.

1.2.3 Catalytic Features

Like Mo nitrogenase, V nitrogenase reduces N_2 and H^+, NH_3 and H_2, but V nitrogenase shows an increased preference for H^+ resulting in the following equation: $N_2 + 10H^+ + 20MgATP + 10e^- \rightarrow 2NH_3 + 2H_2 + 20MgADP + 20P_i$ (26). The shift towards increased co-evolution of H_2 is also observed under C_2H_2 (30, 39). Moreover, V nitrogenase catalyzes the $4e^-$ and the $8e^-$ reduction of C_2H_2, to form C_2H_4 (95%) and C_2H_6 (~5%), respectively, while Mo nitrogenase, catalyzes exclusively the $4e^-$ reduction of C_2H_2 to C_2H_4 (40, 41).

In 2010 Lee *et al.* discovered that V nitrogenase reduces CO to hydrocarbons such as C_2H_4, C_2H_6, C_3H_6 and C_3H_8 (42). A year later, in 2011, the Ribbe lab demonstrated that Mo nitrogenase can reduce CO to the same hydrocarbon products (25), but the amount of hydrocarbons formed is only ~0.1% of the yield achieved with V nitrogenase. Furthermore, it was shown that the replacement of H_2O by D_2O led to a decrease of D_2 evolution by ~30% for both nitrogenase systems. Employing D_2O as the solvent resulted in the rerouting of the electrons towards CO reduction, displayed by an increased hydrocarbon formation of ~12% for V nitrogenase and a dramatic 21-fold increase for Mo nitrogenase (25, 42). Besides these discrepancies in the CO reduction activities, the product profile differs between Mo and V nitrogenase. Although the product distribution is quite different in H_2O, the discrepancy shrinks in D_2O. The shared similarities are as follows: i) hardly any CH_4 is produced; ii) the main product is C_2H_4; and iii) at a hydrocarbon chain length of ≥C3, the saturated hydrocarbons are predominantly formed (25, 42). These observations demonstrate that nitrogenase prefers C-C bond formation over the complete hydrogenation of CO to CH_4.

The ability of nitrogenase to reduce CO to hydrocarbons mirrors the capacity of late transition metal catalysts in the Fischer-Tropsch (FT) synthesis (43). In contrast to the FT

synthesis, nitrogenase uses H^+/e^- instead of H_2 as the hydrogen source for product formation but requires the participation of the two component proteins and hydrolysis of ATP for electron transfer. Moreover, nitrogenase catalyzes the reaction at ambient conditions, while the FT process runs at elevated temperatures (200-240°C) and pressures (20-35 bar) (44-46). The advantages of the protein system for the CO conversion to hydrocarbons illustrate the potential of nitrogenase as a blueprint for the development of cost-efficient strategies for renewable fuel production.

1.3 Aims of the Dissertation

The central theme of this dissertation is the exploration of the catalytic capabilities of nitrogenase for the conversion of small carbon compounds such as CO and CO_2. Based on the groundbreaking work done by the Ribbe lab on the nitrogenase-based (26, 28, 42, 47) and the cofactor-based (48, 49) conversion of CO to hydrocarbons, we set out to extend our knowledge of this process by investigating the physiological relevance of this process for *A. vinelandii*. Furthermore, there is still a lack of understanding for the determining factors of the small carbon compound processing and hydrocarbon formation by nitrogenase proteins. To further illuminate this process, we subjected the potential substrate CO_2 to nitrogenase assays. The *in vivo* conversion of CO and the *in vitro* conversion of CO_2 allow us to extend our knowledge for exploiting nitrogenase as a clean and efficient template for hydrocarbon formation. Moreover, substituting CO with CO_2 as the feedstock would enable us to develop an environmentally friendly process that converts the greenhouse gas CO_2 directly into fuels.

1.3.1 Specific Aim 1: ATP-dependent CO_2 Reduction by Molybdenum and Vanadium Nitrogenase

Considering the work on the reduction of CO by the nitrogenase enzyme system done in the Ribbe lab (25, 42), the conversion of CO_2 by the ATP-dependent two component system of Mo and V nitrogenase was explored. These studies revealed that both nitrogenase systems can convert CO_2 to CO, under physiologically relevant assays conditions (50). In contrast to Mo nitrogenase, V nitrogenase can convert CO_2 to hydrocarbons such as CH_4, C_2H_4 and C_2H_6. Detailed characterizations of the CO_2 conversion allowed us to illuminate the mechanism of this process. V nitrogenase directly couples CO_2 or CO_2-derived intermediates to hydrocarbon chains. These results are presented in Chapter 2.

1.3.2 Specific Aim 2: ATP-independent CO_2 Reduction by Vanadium Nitrogenase

Based on the discovery that V nitrogenase can reduce CO_2 to hydrocarbons in an ATP-dependent fashion (Chapter 2) and the establishment of nitrogenase cofactor-based assay conditions for the ATP-independent reduction of CO (48, 49) and CO_2 (51) to hydrocarbons, we set out to combine the propitious features of both systems. The rationale was to use stronger reductants to deliver electrons directly to the V cluster, rendering the ATP-dependent electron transfer of the reductase component obsolete while retaining a higher V cluster stability by keeping it in its natural protein environment. Indeed, these improvements resulted in a system superior to the V nitrogenase-based ATP-dependent and the cofactor-based ATP-independent system. The ATP-independent, VFe protein-based system, detailed in Chapter 3 exhibits the formation of longer hydrocarbon chains (e.g. butene and butane) as well as higher turnover numbers (52).

1.3.3 Specific Aim 3: The Interconversion between CO and CO_2 by Nitrogenase Iron Proteins

While running control experiments for the ATP-dependent reduction of CO_2 by Mo and V nitrogenase (Chapter 2), we were surprised that Fe protein (NifH and VnfH) under dithionite reduces CO_2 in low amounts to CO. Following up on these exciting results; we discovered that Fe protein is a Fe/S-based mimic of nickel CO-dehydrogenase (53). Apart from reducing CO_2 under dithionite and europium(ii) diethylenetriaminepentaacetate (Eu^{II} DTPA) to CO, Fe protein can also catalyze the reverse reaction under IDS-oxidizing conditions. Furthermore, the function of Fe protein as a CO_2 reductase might be of physiological relevance, since *A. vinelandii* strains expressing NifH or VnfH, but not the catalytic component MoFe or VFe protein, convert CO_2 to CO *in vivo*. The biological implications of the CO_2-reductase function of Fe protein and its potential for biotechnological applications are discussed in Chapter 4.

1.3.4 Specific Aim 4: *In vivo* Hydrocarbon Formation by Vanadium Nitrogenase

The observation that V nitrogenase can catalyze the reduction of CO with a rate of 16 nmol reduced carbon/nmol protein/min (42) led to the question of whether cells expressing V nitrogenase can reduce CO *in vivo* to hydrocarbons. If this would be the case, it remained to be seen if cells incorporate the CO-derived carbon into the cell mass or simply release the hydrocarbons as byproducts. The physiological relevance of the *in vivo* reduction of CO and its potential for biotechnological applications in conjunction with *in vivo* reduction of CO_2 (Chapter 4) are discussed in Chapter 5 (54).

1.4 Synopsis of the Dissertation

This dissertation focuses on the conversion and activation of CO_2 by nitrogenase based systems summarized in Figure 1.5. V nitrogenase, System I of Figure 1.5 consisting of the Fe protein VnfH and VFe protein converts CO_2 ATP-dependently to CO and hydrocarbons (HCs), described in Chapter 2. The electrons are delivered by dithionite to the $[Fe_4S_4]$-cluster of the Fe protein. Concomitant with the hydrolysis of two molecules ATP, one electron is transferred from the $[Fe_4S_4]$-cluster of the Fe protein to the P-cluster of VFe protein which funnels the electrons to the V cluster, in the active site of VFe protein, to reduce CO_2 (50).

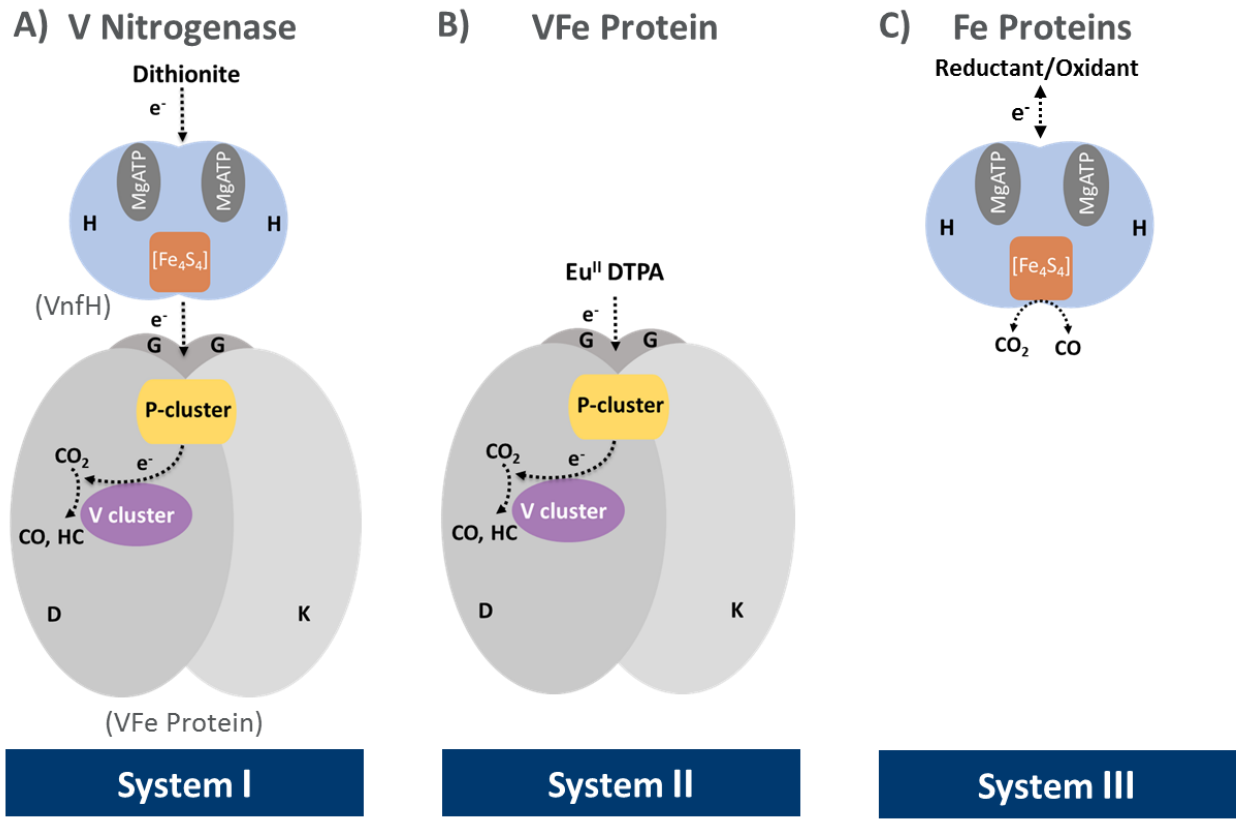

Figure 1.5. CO_2 conversion by nitrogenase systems. A) System I: V nitrogenase consisting of the Fe protein (encoded by *vnfH*) and VFe protein (encoded by *vnfDKG*) affords ATP-dependent reduction of CO_2 to CO and hydrocarbons (HCs). B) System II: VFe protein plus Eu^{II} DTPA affords ATP-independent reduction of CO_2 to CO and HCs. C) System III: Fe proteins (encoded by *vnfH* or *nifH*) plus the reductants dithionite or Eu^{II} DTPA afford ATP-independent reduction of CO_2 to CO. Whereas, Fe proteins plus the oxidant indigo disulfonate (IDS) afford ATP-independent oxidation of CO to CO_2.

To overcome the ATP-requirement, we simplified System I by omitting the Fe protein and replacing dithionite (E°' = - 0.436 V, (55)) by a stronger reductant Eu^{II} DTPA (E°' = - 1.14 V, (56)) resulting in System II, Figure 1.5. System II allows the direct transfer of electrons from Eu^{II} DTPA to the V cluster of VFe protein and the formation of CO and HCs derived from CO_2 in an ATP-independent manner (52), described in Chapter 3.

In contrast to the V cluster based Systems I and II, System III of Figure 1.5 focuses on the catalytic capabilities of the $[Fe_4S_4]$-cluster in the subunit interface of the Fe proteins VnfH and NifH. Chapter 4 describes the reduction of CO_2 to CO by Fe proteins driven by the reductants dithionite or Eu^{II} DTPA as well as the reverse reaction, the oxidation of CO to CO_2, by Fe proteins driven by the oxidant indigo disulfonate (IDS). Furthermore, we demonstrated that Fe proteins reduce *in vivo*, inside *A. vinelandii* cells, CO_2 to CO (53).

Based on the *in vivo* reduction of CO_2 to CO, an *A. vinelandii*-strain expressing the complete V nitrogenase was employed to reduce *in vivo* CO to hydrocarbons such as ethene, ethane and propane, described in Chapter 5. Moreover, the yield of these reactions could be increased more than 10-fold by cycling between CO-incubations and air-incubations, keeping this reaction going for four days. In addition to this, we established that the carbon of CO is not incorporated into the cell mass of *A. vinelandii* but rather released as a novel secondary metabolite (54).

1.5 References

1. Howard JB & Rees DC (1996) Structural Basis of Biological Nitrogen Fixation. *Chem Rev* 96(7):2965-82.

2. Burgess BK & Lowe DJ (1996) Mechanism of Molybdenum Nitrogenase. *Chem Rev* 96(7):2983-3012.

3. Eady RR (1996) Structure-Function Relationships of Alternative Nitrogenases. *Chem Rev* 96(7):3013-30.

4. Joerger RD & Bishop PE (1988) Bacterial alternative nitrogen fixation systems. *Crit Rev Microbiol* 16(1):1-14.

5. Chiu H, Peters JW, Lanzilotta WN, Ryle MJ, Seefeldt LC, Howard JB, & Rees DC (2001) MgATP-Bound and nucleotide-free structures of a nitrogenase protein complex between the Leu 127 Delta-Fe-protein and the MoFe-protein. *Biochemistry* 40(3):641-50.

6. Georgiadis MM, Komiya H, Chakrabarti P, Woo D, Kornuc JJ, & Rees DC (1992) Crystallographic structure of the nitrogenase iron protein from Azotobacter vinelandii. *Science* 257(5077):1653-9.

7. Jang SB, Seefeldt LC, & Peters JW (2000) Insights into nucleotide signal transduction in nitrogenase: Protein with MgADP bound. *Biochemistry* 39(48):14745-52.

8. Schindelin N, Kisker C, Sehlessman JL, Howard JB, & Rees DC (1997) Structure of ADP center dot AIF(4)(-)-stabilized nitrogenase complex and its implications for signal transduction. *Nature* 387(6631):370-6.

9. Schlessman JL, Woo D, Joshua-Tor L, Howard JB, & Rees DC (1998) Conformational variability in structures of the nitrogenase iron proteins from Azotobacter vinelandii and Clostridium pasteurianum. *J Mol Biol* 280(4):669-85.

10. Schmid B, Einsle O, Chiu HJ, Willing A, Yoshida M, Howard JB, & Rees DC (2002) Biochemical and structural characterization of the cross-linked complex of

nitrogenase: Comparison to the ADP-AlF(4)(-)-stabilized structure. *Biochemistry* 41(52):15557-65.

11. Strop P, Takahara PM, Chiu HJ, Angove HC, Burgess BK, & Rees DC (2001) Crystal structure of the all-ferrous [4Fe-4S](0) form of the nitrogenase iron protein from Azotobacter vinelandii. *Biochemistry* 40(3):651-6.

12. Tezcan FA, Kaiser JT, Mustafi D, Walton MY, Howard JB, & Rees DC (2005) Nitrogenase complexes: Multiple docking sites for a nucleotide switch protein. *Science* 309(5739):1377-80.

13. Owens CP, Katz FE, Carter CH, Luca MA, & Tezcan FA (2015) Evidence for Functionally Relevant Encounter Complexes in Nitrogenase Catalysis. *J Am Chem Soc* 137(39):12704-12.

14. Lawson DM & Smith BE (2002) Molybdenum nitrogenases: a crystallographic and mechanistic view. *Met Ions Biol Syst* 39:75-119.

15. Blank MA, Lee CC, Hu Y, Hodgson KO, Hedman B, & Ribbe MW (2011) Structural models of the [Fe4S4] clusters of homologous nitrogenase Fe proteins. *Inorg Chem* 50(15):7123-8.

16. Wiig JA, Hu Y, Lee CC, & Ribbe MW (2012) Radical SAM-dependent carbon insertion into the nitrogenase M-cluster. *Science* 337(6102):1672-5.

17. Spatzal T, Aksoyoglu M, Zhang L, Andrade SL, Schleicher E, Weber S, Rees DC, & Einsle O (2011) Evidence for interstitial carbon in nitrogenase FeMo cofactor. *Science* 334(6058):940.

18. Lancaster KM, Roemelt M, Ettenhuber P, Hu Y, Ribbe MW, Neese F, Bergmann U, & DeBeer S (2011) X-ray emission spectroscopy evidences a central carbon in the nitrogenase iron-molybdenum cofactor. *Science* 334(6058):974-7.

19. Einsle O, Tezcan FA, Andrade SL, Schmid B, Yoshida M, Howard JB, & Rees DC (2002) Nitrogenase MoFe-protein at 1.16 A resolution: a central ligand in the FeMo-cofactor. *Science* 297(5587):1696-700.

20. Kim J & Rees DC (1992) Crystallographic structure and functional implications of the nitrogenase molybdenum-iron protein from azotobacter vinelandii. *Nature* 360(6404):553-60.

21. Peters JW, Stowell MH, Soltis SM, Finnegan MG, Johnson MK, & Rees DC (1997) Redox-dependent structural changes in the nitrogenase P-cluster. *Biochemistry* 36(6):1181-7.

22. Kim J & Rees DC (1992) Structural models for the metal centers in the nitrogenase molybdenum-iron protein. *Science* 257(5077):1677-82.

23. Bishop PE & Premakumar R (1992), eds Stacy G, Burris RH, & Evans HJ (Chapman and Hall, New York), pp 736-62.

24. Hales BJ (1990) Alternative nitrogenase. *Adv Inorg Biochem* 8:165-98.

25. Hu Y, Lee CC, & Ribbe MW (2011) Extending the carbon chain: hydrocarbon formation catalyzed by vanadium/molybdenum nitrogenases. *Science* 333(6043):753-5.

26. Lee CC, Hu Y, & Ribbe MW (2009) Unique features of the nitrogenase VFe protein from Azotobacter vinelandii. *Proc Natl Acad Sci U S A* 106(23):9209-14.

27. Fisher K, Dilworth MJ, & Newton WE (2006) Azotobacter vinelandii vanadium nitrogenase: formaldehyde is a product of catalyzed HCN reduction, and excess

ammonia arises directly from catalyzed azide reduction. *Biochemistry* 45(13):4190-8.

28. Hu Y, Lee CC, & Ribbe MW (2012) Vanadium nitrogenase: a two-hit wonder? *Dalton Trans* 41(4):1118-27.

29. Eady RR, Richardson TH, Miller RW, Hawkins M, & Lowe DJ (1988) The vanadium nitrogenase of Azotobacter chroococcum. Purification and properties of the Fe protein. *Biochem J* 256(1):189-96.

30. Hales BJ, Langosch DJ, & Case EE (1986) Isolation and characterization of a second nitrogenase Fe-protein from Azotobacter vinelandii. *J Biol Chem* 261(32):15301-6.

31. Bergstrom J, Eady RR, & Thorneley RNF (1988) The Vanadium-Containing and Molybdenum-Containing Nitrogenases of Azotobacter-Chroococcum - Comparison of Mid-Point Potentials and Kinetics of Reduction by Sodium Dithionite of the Iron Proteins with Bound Magnesium Adenosine 5'-Diphosphate. *Biochem J* 251(1):165-9.

32. Ribbe MW, Hu Y, Hodgson KO, & Hedman B (2014) Biosynthesis of nitrogenase metalloclusters. *Chem Rev* 114(8):4063-80.

33. Tittsworth RC & Hales BJ (1993) Detection of Epr Signals Assigned to the 1-Equiv-Oxidized P-Clusters of the Nitrogenase Mofe-Protein from Azotobacter-Vinelandii. *J Am Chem Soc* 115(21):9763-7.

34. Pierik AJ, Wassink H, Haaker H, & Hagen WR (1993) Redox properties and EPR spectroscopy of the P clusters of Azotobacter vinelandii MoFe protein. *Eur J Biochem* 212(1):51-61.

35. Hu Y, Corbett MC, Fay AW, Webber JA, Hedman B, Hodgson KO, & Ribbe MW (2005) Nitrogenase reactivity with P-cluster variants. *Proc Natl Acad Sci U S A* 102(39):13825-30.

36. Tittsworth RC & Hales BJ (1996) Oxidative titration of the nitrogenase VFe protein from Azotobacter vinelandii: an example of redox-gated electron flow. *Biochemistry* 35(2):479-87.

37. Lee CC, Fay AW, Weng TC, Krest CM, Hedman B, Hodgson KO, Hu Y, & Ribbe MW (2015) Uncoupling binding of substrate CO from turnover by vanadium nitrogenase. *Proc Natl Acad Sci U S A* 112(45):13845-9.

38. Fay AW, Blank MA, Lee CC, Hu Y, Hodgson KO, Hedman B, & Ribbe MW (2010) Characterization of isolated nitrogenase FeVco. *J Am Chem Soc* 132(36):12612-8.

39. Robson RL, Eady RR, Richardson TH, Miller RW, Hawkins M, & Postgate JR (1986) The Alternative Nitrogenase of Azotobacter-Chroococcum Is a Vanadium Enzyme. *Nature* 322(6077):388-90.

40. Dilworth MJ, Eady RR, & Eldridge ME (1988) The Vanadium Nitrogenase of Azotobacter-Chroococcum - Reduction of Acetylene and Ethylene to Ethane. *Biochem J* 249(3):745-51.

41. Dilworth MJ, Eady RR, Robson RL, & Miller RW (1987) Ethane Formation from Acetylene as a Potential Test for Vanadium Nitrogenase Invivo. *Nature* 327(6118):167-8.

42. Lee CC, Hu Y, & Ribbe MW (2010) Vanadium nitrogenase reduces CO. *Science* 329(5992):642.

43. Roferdepoorter CK (1981) A Comprehensive Mechanism for the Fischer-Tropsch Synthesis. *Chem Rev* 81(5):447-74.

44. Schulz H (1999) Short history and present trends of Fischer-Tropsch synthesis. *Applied Catalysis a-General* 186(1-2):3-12.

45. Bezemer GL, Bitter JH, Kuipers HPCE, Oosterbeek H, Holewijn JE, Xu XD, Kapteijn F, van Dillen AJ, & de Jong KP (2006) Cobalt particle size effects in the Fischer-Tropsch reaction studied with carbon nanofiber supported catalysts. *J Am Chem Soc* 128(12):3956-64.

46. Dry ME, Boshoff LJ, & Shingles T (1972) Rate of Fischer-Tropsch Reaction over Iron Catalysts. *Journal of Catalysis* 25(1):99-&.

47. Hu Y & Ribbe MW (2016) Nitrogenases-A Tale of Carbon Atom(s). *Angew Chem Int Ed Engl* 55(29):8216-26.

48. Lee CC, Hu YL, & Ribbe MW (2012) ATP-Independent Formation of Hydrocarbons Catalyzed by Isolated Nitrogenase Cofactors. *Angewandte Chemie-International Edition* 51(8):1947-9.

49. Lee CC, Hu YL, & Ribbe MW (2015) Insights into Hydrocarbon Formation by Nitrogenase Cofactor Homologs. *Mbio* 6(2).

50. Rebelein JG, Hu Y, & Ribbe MW (2014) Differential reduction of CO(2) by molybdenum and vanadium nitrogenases. *Angew Chem Int Ed Engl* 53(43):11543-6.

51. Lee CC, Hu YL, & Ribbe MW (2015) Catalytic Reduction of CN-, CO, and CO2 by Nitrogenase Cofactors in Lanthanide-Driven Reactions. *Angewandte Chemie-International Edition* 54(4):1219-22.

52. Rebelein JG, Hu Y, & Ribbe MW (2015) Widening the Product Profile of Carbon Dioxide Reduction by Vanadium Nitrogenase. *ChemBioChem* 16(14):1993-6.

53. Rebelein JG, Stiebritz M, Lee CC, & Hu Y (2016) Activation and Reduction of Carbon Dioxide by Nitrogenase Iron Proteins. *Nat Chem Biol* (In Press).

54. Rebelein JG, Lee CC, Hu Y, & Ribbe MW (2016) In vivo Hydrocarbon Formation by Vanadium Nitrogenase: A Novel Secondary Metabolic Pathway. *Nat Commun* (In Press).

55. Mayhew SG (1978) The redox potential of dithionite and SO-2 from equilibrium reactions with flavodoxins, methyl viologen and hydrogen plus hydrogenase. *Eur J Biochem* 85(2):535-47.

56. Vincent KA, Tilley GJ, Quammie NC, Streeter I, Burgess BK, Cheesman MR, & Armstrong FA (2003) Instantaneous, stoichiometric generation of powerfully reducing states of protein active sites using Eu(II) and polyaminocarboxylate ligands. *Chem Commun (Camb)* (20):2590-1.

Chapter 2: ATP-dependent Carbon Dioxide Reduction by Molybdenum and Vanadium Nitrogenase

2.1 Introduction

Nitrogenase catalysis by the 'conventional' Mo nitrogenase is well characterized through more than 70 years of active research (1-4). Various aspects of the catalysis were studied including the ATP hydrolysis concomitant with complex formation between the reductase (*nifH*- or *vnfH*-encoded Fe protein) and the catalytic component (*nifDK*-encoded MoFe or *vnfDGK*-encoded VFe protein) (5-8), the reduction of N_2 (1, 4, 9), and the reduction of alternative substrates like acetylene, azide and hydrogen cyanide (4, 10, 11) as well as the inhibition of the Mo nitrogenase particularly by carbon monoxide (CO) (see Chapter 1) (12, 13).

Recently, it was recognized that CO is a substrate for nitrogenase, this originates from the observation that CO has differential inhibitory effects on the hydrogen (H_2) evolution of Mo and V nitrogenase. In the presence of 100 % CO, the hydrogen evolution of V nitrogenase is inhibited by ~76 % whereas the H_2 evolution of Mo nitrogenase is barely affected (14). At the same time, the ATP hydrolysis is comparable for Mo and V nitrogenase under 100 % CO, indicating a similar electron flux for both nitrogenases (15). Further investigation of this phenomenon led to the discovery of the conversion of CO to ethene (C_2H_4), ethane (C_2H_6), propene (C_3H_6) and propane (C_3H_8) by V nitrogenase (15).

For a 130-fold upscaled CO reaction assay, additional hydrocarbon products like methane (CH_4), butene (C_4H_8) and butane (C_4H_{10}) were identified (16). Moreover, the same C1-C3 products were identified for the 'conventional' Mo nitrogenase in these upscaled assays (16). The striking difference between Mo and V nitrogenase is that V nitrogenase is showing a nearly 1000 times higher overall activity for the reduction of CO than Mo nitrogenase (16). Contrasting the reduction of N_2 to NH_3, which is catalyzed twice as fast by Mo than V

nitrogenase (14). Furthermore, the replacement of H_2O by D_2O increases the specific activity of Mo nitrogenase by 21-fold but of V nitrogenase only by 12 % (16, 17).

The CO reduction by nitrogenase was a very exciting discovery in the field of nitrogenase research and the general field of bioinorganic chemistry. It renders nitrogenase as the first enzyme capable of reductively coupling CO to alkanes and alkenes and suggesting nitrogenase as a blueprint for an industrial conversion of CO into fuels.

This discovery of the CO reduction by nitrogenase triggered the question, whether nitrogenase can also reduce the greenhouse gas carbon dioxide (CO_2). The conversion of CO_2 is not only interesting from an academic standpoint, but could also offer new insights in a CO_2-fixation reaction to decrease climate change while providing a sustainable hydrocarbon source for fuels and other chemicals.

A comparative study for the CO_2 reduction by the ATP-dependent two component systems of Mo and V nitrogenase was carried out, to address 1) whether the two nitrogenases can reduce CO_2 to hydrocarbons and 2) whether the discrepancies of the CO reduction between the two nitrogenase systems are similar for the conversion of CO_2.

2.2 Material and Methods

2.2.1 Reagents

Unless noted otherwise, all chemicals were purchased from Fisher Scientific and Sigma-Aldrich. $^{12}CO_2$ (99.998% purity) was purchased from Praxair, and $^{13}CO_2$ (≥ 98% isotopic purity), D_2O and deuterated Tris were purchased from Cambridge Isotope Labs.

2.2.2 Cell Growth and Protein Purification

Azotobacter vinelandii strains expressing His-tagged MoFe and VFe proteins and non-tagged *vnfH*- and *nifH*-encoded Fe proteins (designated VnfH and NifH, respectively) were grown in 180 L batches in a 200 L New Brunswick fermentor (New Brunswick Scientific) in Burke's minimal medium supplemented with 2 mM ammonium acetate (Note that the Mo in Burke's medium was replaced by 30 μM sodium orthovanadate for the growth of VFe protein). The growth rate was measured by cell density at 436 nm using a Spectronic 20 Genesys. Cells were harvested in the late exponential phase by using a flow-through centrifuge (Cepa). The cell paste was washed with a buffer containing 50 mM Tris-HCl (pH 8.0). Published methods were used for the purification of His-tagged MoFe and VFe proteins, and non-tagged *nifH*- and *vnfH*-encoded Fe proteins (18-21).

2.2.3 Enzyme Assays

Each H_2O-based reaction of CO_2 reduction was carried out in a 37.5 ml reaction vial with a total volume of 25 ml, which contained 100 mM Tris-HCl (pH 8.0), 20.4 mM MgATP, 43.2 mM $MgCl_2$, 245 mM creatine phosphate, 420 U/ml creatine phosphokinase, 20 mM sodium dithionite and 1 M $NaHCO_3$ as a CO_2 source. This reaction mixture was allowed to equilibrate for 1 h, followed by the adjustment of the pH to 8.5. The reaction was started by the addition of 150 mg NifH plus 100 mg MoFe protein, or 150 mg VnfH plus 100 mg VFe protein. Subsequently, the reaction was incubated with continuous shaking in a water bath at 30 °C and samples were taken at 0, 30, 60, 120 and 180 min, respectively. $NaHCO_3$ was omitted from the assays to address whether the hydrocarbons generated by CO_2 reduction were derived indirectly from CO reduction. In these assays, 110 ppm CO was added in the headspaces of the vials and equilibrated, which represented the maximum amount of CO

produced during CO_2 reduction. The D_2O-based assays had the same composition as the H_2O-based assays except that all components were dissolved in 100 mM (D11)-Tris [i.e., $(DOCD_2)_3CND_2$] buffer. In addition, all protein samples used in these assays were exchanged into the same deuterated buffer. The pD of this buffer was adjusted to 8.0 with DCl and NaOD by using the pH indicator strips and subsequently determined by a previously established equation (22): pD = measured pH + 0.40. For GC-MS analysis (see below), the H_2O- or D_2O-based assays of CO_2 reduction were prepared as described above except for the substitution of $NaH^{12}CO_3$ by $NaH^{13}CO_3$.

2.2.4 Activity Determination

The products CH_4, C_2H_4 and C_2H_6, were quantified by GC-FID using a previously published method (14-16). For each assay, a total of 250 µl headspace was injected onto a Grace activated alumina column, which was held at 55 °C for 1 min, heated to 180 °C at 12.5 °C/min, and held at 180 °C for another 2.6 min. The quantities of these products were determined based on a Scott standard gas mixture containing 15 ppm of each hydrocarbon compound. The product, CO was quantified by a GC coupled to an SRI reduction gas detector. For each assay, a total of 250 µl headspace was applied onto a Grace molecular sieve column, which was held at a constant temperature of 50 °C. The quantity of CO was determined based on a linear standard curve ($R^2 \geq 98$) derived from the injection of varying amounts of ^{12}CO (99.5 % purity). The detection limits for the products were, in nmol product/µmol protein, 0.38 (CH_4), 0.23 (C_2H_4), 0.36 (C_2H_6) and 0.1 (CO).

2.2.5 GC-MS Analysis

The hydrocarbon products were identified by GC-MS using an Agilent 6890 GC system coupled to a Waters GCT-Premier time-of-flight mass spectrometer. The identities of CH_4,

CD_4, C_2D_4 and C_2D_6 were confirmed by comparing their masses and retention times with those of the Scott standard alkane and alkene gas mixture. For each assay, a total of 50 µl headspace was injected into a split/splitless injector operated at 125 °C in split mode, with a split ratio of 5. A 1 mm ID liner was used to optimize sensitivity. Separation of gas was achieved with an Agilent 0.320 mm (ID) x 30 m (length) HP-PLOT-Q capillary column, which was held at 40 °C for 1 min, heated to 45 °C at a rate of 5 °C/min, heated further to 200 °C at a rate of 20 °C/min, and held at 200 °C for another 4 min. The carrier gas, helium, was passed through the column at a rate of 1.1 ml/min. The mass spectrometer was operated in electron impact (EI) ionization mode.

2.3 Results and Discussion

2.3.1 CO_2 Reduction Products

Consistent with an earlier report (23), Mo nitrogenase can reduce CO_2 to CO (Figure 2.1 A, triangles) in an ATP-dependent reaction using dithionite (20 mM) as a reductant at pH 8.5. The V nitrogenase shows under these conditions the same efficiencies for the reduction of CO_2 to CO in H_2O-based reactions over a period of 180 minutes (Figure 2.1 A). Moreover, both nitrogenases exhibited roughly the same increase in activity for the formation of CO from CO_2 upon substitution of H_2O by D_2O, reaching a maximum increase of activity at 120 minutes (Figure 2.1 A). Apart from CO, CH_4, which is a further reduced C1 product, could be detected in the reaction mixtures in the presence of Mo and V nitrogenase when CO_2 was supplied as a substrate (Figure 2.1 B). However, Mo nitrogenase forms 7.3 nmol CH_4 per µmol of protein under H_2O which decreases to 0 under D_2O (Figure 2 B, ▾ vs. ▿) whereas the activity of CH_4 formation by the V nitrogenase increased from 0 under H_2O to a maximum of 22.2 nmol per µmol of protein under D_2O (Figure 2.1 B, • vs. ○). Such a disparate D_2O effect implies a difference in the routes to CH_4 formation taken by the two nitrogenases.

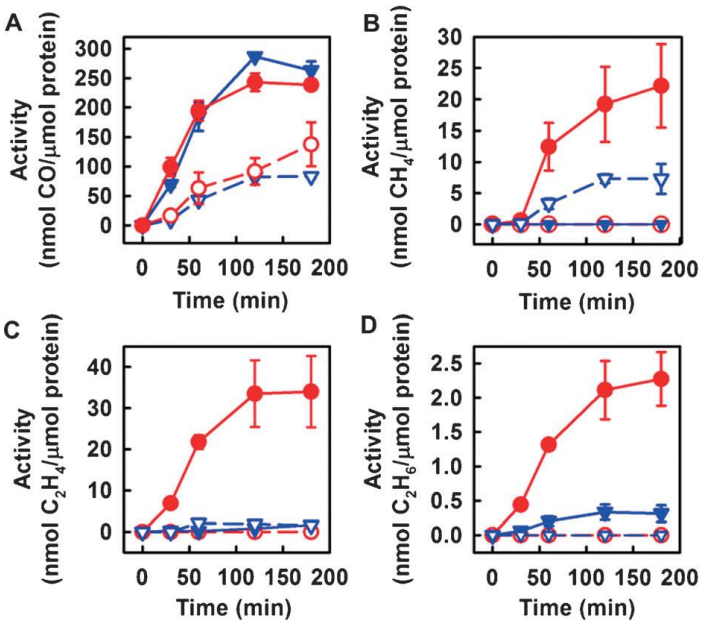

Figure 2.1. Product formation by Mo and V nitrogenases in the presence of CO_2. Time-dependent formation of CO (A), CH4 (B), C2H4 (C), and C2H6 (D) by the Mo nitrogenase in H_2O (▿, – – –) or D2O (▾, —) and by the V nitrogenase in H_2O (○, – – –) or D2O (•, —). Data are presented as mean ± SD (N=3) after background correction.

The difference between the V and Mo nitrogenases in CO_2 reduction is further illustrated by the difference in their abilities to use CO_2 as a substrate to form C-C bonds. In the presence of H_2O, little or no C2 products was detected during CO_2 reduction by either the Mo or the V nitrogenase (Figure 2.1 C and D, ▿ and ○). In the presence of D_2O, however, C_2D_4 (Figure 2.1 C, •) and C_2D_6 (Figure 2.1 D, •) were detected as products of CO_2 reduction by the V nitrogenase, whereas these C2 products were hardly detectable in the same reaction catalyzed by the Mo nitrogenase (Figure 2.1 C and D, ▾). Thus, as was observed in the case of CH_4 formation, there was a clear increase in the activities of C_2D_4 and C_2D_6 formation by the V nitrogenase upon replacment of D_2O for H_2O, whereas these activities remained marginal in the reaction catalyzed by the Mo nitrogenase following such a substitution. Moreover, like the formation of CH_4, the formation of C2 products by the V nitrogenase was ATP-dependent, as C_2D_4 and C_2D_6 could not be detected in the absence of ATP (Figure 2.2).

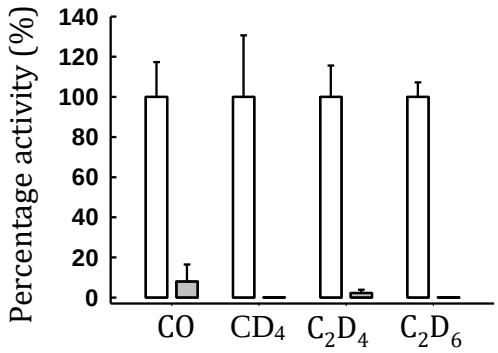

Figure 2.2. ATP-dependent product formation by V nitrogenase from CO_2. Percentage activities of product formation by V nitrogenase from CO_2 in the presence (white bars) or absence (grey bars) of ATP in D_2O based reactions. The percentage activities in the absence of ATP were calculated relative to those in the presence of ATP, with the latter set to 100 %. The actual specific activities of product formation in the presence of ATP are, in nmol/μmol protein/h 194 ± 17 (CO), 12.4 ± 3.8 (CD_4), 21.8 ± 1.7 (C_2D_4) and 1.31 ± 0.05. (C_2D_6).

2.3.2 Tracing CO_2 during Hydrocarbon Formation

GC-MS analysis supplied further evidence for the differences between the Mo and V nitrogenase in hydrocarbon formation from CO_2. When $^{12}CO_2$ was replaced by $^{13}CO_2$, $^{13}CD_4$ could be detected in the V nitrogenase-catalyzed reaction in D_2O (Figure 2.3 B);

however, $^{13}CH_4$ was absent from the Mo nitrogenase catalyzed reaction in H_2O (Figure 2.3 A). This observation confirmed CO_2 as the carbon source for CD_4 generated by the V nitrogenase while suggesting a different carbon source for the same C1 product formed by the Mo nitrogenase. Aside from CD_4, CO_2 also gave rise to the C2 products in the V nitrogenase catalyzed reaction, as $^{13}C_2D_4$ (Figure 2.3 C) and $^{13}C_2D_6$ (Figure 2.3 D) could be detected in the presence of D_2O upon substitution of $^{13}CO_2$ for $^{12}CO_2$. Together, the GC-MS and activity data highlight the difference between the reactions of CO_2 reduction by the V and Mo nitrogenase, showing the ability of the V nitrogenase to form C1 and C2 hydrocarbons along with CO and the inability of its Mo counterpart to generate products other than CO under these experimental conditions. Given the previous observation that the V nitrogenase can reduce CO to hydrocarbons (15, 16), the co-production of CO and hydrocarbons by this enzyme as products of CO_2 reduction raises the relevant question, whether it is the CO_2-derived CO that gives rise to the hydrocarbon products.

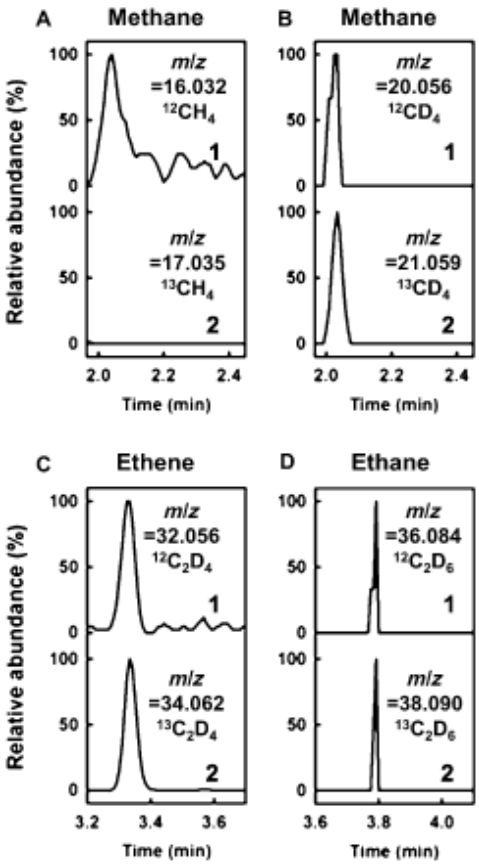

Figure 2.3. GC-MS analyses of the hydrocarbon products formed by Mo and V nitrogenase. The products were generated by the Mo nitrogenase in H_2O (A) or by the V nitrogenase in D_2O (B-D) when $^{12}CO_2$ (1) or $^{13}CO_2$ (2) was supplied. The mass-to-charge (m/z) ratios at which the products were traced are indicated.

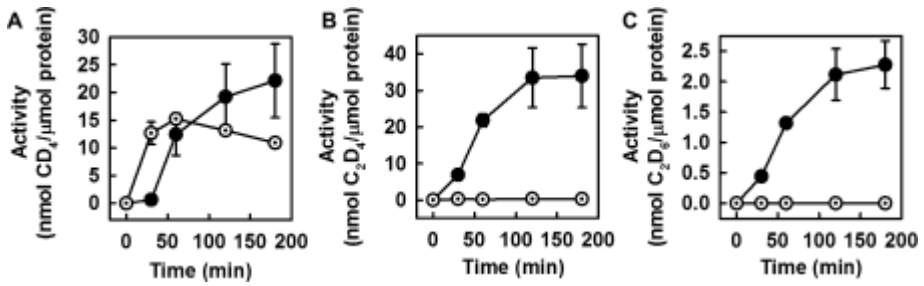

Figure 2.4. Formation of hydrocarbon products by V nitrogenase. Time-dependent formation of CD_4 (A), C_2D_4 (B), and C_2D_6 (C) from CO_2 (●) or CO (⊙) by the V nitrogenase in D_2O. CO was added at a concentration of 110 ppm in assays involving the direct formation of products from CO, which was equivalent to the maximum concentration of CO generated from the CO_2 reduction by the V nitrogenase (see also Figure 2.1). Data are presented as mean ±SD (N=3), after background correction.

This question can be addressed by directly supplying CO to the V nitrogenase in a concentration simulating the maximum concentration of CO achieved in the "equilibrated state" of CO_2 reduction by this enzyme (see Figure 2.1 A) and monitoring the formation of the C1 and C2 hydrocarbons in D_2O over a time period of 180 minutes. Interestingly, the CO-based formation of CD_4 by the V nitrogenase (Figure 2.4, ○) displayed a product increase of 12.6 nmol per µmol of protein between 0 and 30 minutes, whereas the CO_2-based formation of CH_4 exhibited a nearly identical increase of 11.8 nmol per µmol of protein between 30 and 60 minutes after an initial lag phase between 0 and 30 minutes (Figure 2.4, •). This observation suggests the possibility for the V nitrogenase to direct the formation of C1 hydrocarbons via CO, as the 30-minute delay could be correlated with a need for the enzyme to accumulate a sufficient amount of CO_2-derived CO to initiate further reduction of CO to CD_4. Furthermore, the divergence of the CD_4 formation after 60 min from CO (Figure 2.4 A, ⊙) and CO_2 (Figure 2.4 A, ●) could be explained by a slight decrease of the CO concentration in the CO-assay whereas CO concentration in the CO_2 assay remains constant (see Figure 2.1 A).

Unlike CD_4, both C_2D_4 and C_2D_6 seem to be produced by the V nitrogenase along a CO-independent route, as no C2 products could be detected (Figure 2.4 B and C, ⊙) upon direct addition of the same amount of CO as produced by the V nitrogenase through CO_2 reduction in the equilibrated state (see Figure 2.1 A). This observation suggests that instead of CO, CO_2 and/or other CO_2-derived intermediates are responsible for the formation of C2 hydrocarbon products by the V nitrogenase. The lack of contribution of CO to the generation of C2 hydrocarbons, in this case, could be explained by an insufficient CO concentration achieved by the reduction of CO_2, which does not allow the formation of C-C bonds. More excitingly, it defines the ability of the V nitrogenase to use CO_2 directly as a substrate for the initial C-C coupling and the subsequent carbon chain extension.

The ability of certain variants of the Mo nitrogenase to reduce CO_2 to CH_4 was reported recently (24). To our surprise, contrary to what has been described for these variants of the Mo nitrogenase (24), the wild-type Mo nitrogenase cannot reduce CO_2 to CH_4; rather, it uses an unknown carbon source to generate CH_4 in the presence of CO_2 and H_2O. Considering the presence of an interstitial carbide (25-28) and a homocitrate-moiety in the M cluster (25, 27) it can be postulated that in H_2O, CO_2 or its derivative somehow promotes the release of the central carbide ligand or carbon-containing groups of the homocitrate in the form of CH_4. Alternatively, the side-chain groups of certain amino acids at the active site of the Mo nitrogenase may also serve as a carbon source for the production of CH_4 in the presence of

CO_2. Remarkably, despite the unclear nature of the carbon source, the formation of CH_4 by the Mo nitrogenase is ATP-dependent and requires the presence of both component proteins; moreover, it only occurs in the presence of CO_2 and H_2O (Figure 2.5). This observation points to a redox-dependent mechanism for this reaction, as the requirement for ATP and both components is specifically associated with the transfer of electrons through the enzyme system, which may permit the initial binding and processing of CO_2 or its derivative in H_2O and the subsequent interaction between CO_2 or CO_2-derived intermediate(s) and the carbon species that eventually gives rise to CH_4. Given the overall homology between the Mo and V nitrogenases, one would expect V nitrogenase to catalyze the same unspecific formation of CH_4 from a different carbon source than CO_2 as its Mo counterpart. Although this possibility cannot be ruled out, our current data (see Figure 2.3 B) clearly demonstrate that the CH_4 formed by V nitrogenase is derived, at least in part, from CO_2. Further investigations of the origin of the different routes taken by the two nitrogenases to CH_4 formation could be informative, particularly with regard to the initial binding and processing of CO_2 by this enzyme system.

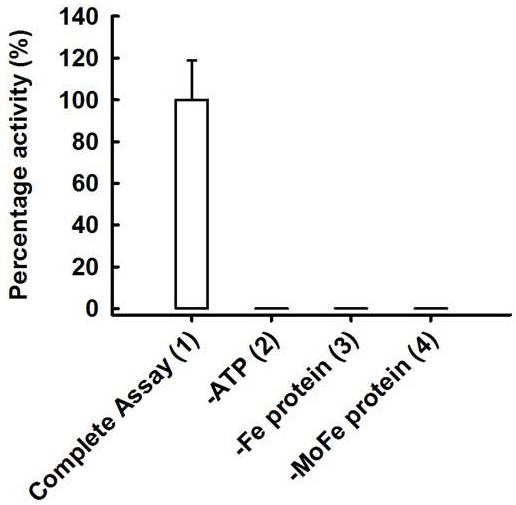

Figure 2.5. ATP- and protein component dependent CH_4 formation by Mo nitrogenase in the presence of CO_2. Percentage activities of CH_4 formation by Mo nitrogenase in a complete assay containing ATP and both component proteins (1), in the absence of ATP (2), in the absence of Fe protein (3), and in the absence of MoFe protein (4) all in H_2O-based reactions. The percentage activity in the absence of ATP or either component of the Mo-nitrogenase was calculated relative to that in the presence of ATP and dithionite, with the latter set to 100 %. The actual specific activity of CH_4 formation in the presence of ATP and dithionite is 3.7 + 0.7 nmol/μmol protein/h.

2.4 Summary and Conclusion

Based on the hydrocarbon products identified thus far in the gas phase, V nitrogenase generates carbon-containing compounds at a slow rate from CO_2 reduction, forming 0.3 mol CO, 0.02 mol CH_4, 0.04 mol C_2H_4, and 0.002 mol C_2H_6 per mol of protein. Nevertheless, the ability of V nitrogenase to form hydrocarbons, particularly the C2 products, from CO_2, is a most remarkable finding, because it adds another exciting reaction to the catalytic repertoire of this unique enzyme system. As was observed in the case of CO reduction (16), the V nitrogenase is superior to its wild-type Mo counterpart in generating hydrocarbons from CO_2. The disparate CO-reducing activities of the V and Mo nitrogenases were compared with the differential capacities of synthetic V and Mo compounds to reductively couple two CO moieties into functionalized acetylene ligands (29). Furthermore, an alteration of the CO-reducing activities was reported for the MoFe protein variants that contained modified residues at the active site (30). By analogy, the disparate CO_2 reducing activities of the two nitrogenases could also stem from the structural/redox differences between V- and M cluster, as well as the protein environments surrounding the two cofactors (see Chapter 1). Moreover, the different structural/redox properties of the P-clusters in the two nitrogenases could further contribute to the differences between their abilities to reduce CO_2 (see Chapter 1.2). In fact, the ability of the nitrogenases to generate hydrocarbons from CO_2 was first described for a cofactor-deficient variant of the MoFe protein (31) and attributed to its unique P-cluster, which contains a $[Fe_4S_4]$-like cluster pair instead of the normal $[Fe_8S_7]$ P-cluster (32). Interestingly, the P-cluster of the V nitrogenase also consists of a pair of $[Fe_4S_4]$-like clusters (14, 17, 33) and could, in principle, serve as a site for CO_2 reduction on its own; only in the case of the holo form of the V nitrogenase, the presence of the cofactor

"downstream" of the P-cluster along the electron transfer pathway (see Chapter 1) may effectively "funnel" the electrons towards the cofactor site and only allow a small amount of CO_2 reduction at the P-cluster site. The possibility of two reactive sites (i.e., P-cluster and cofactor) and different reaction routes (i.e., via CO or other CO_2-derived intermediates) for CO_2 reduction makes it a challenging task to elucidate the mechanistic details of this reaction. Nevertheless, the work reported herein provides an essential framework for systematic investigations of this unique reaction in the future, which will hopefully lead to the development of nitrogenase-based strategies to recycle the greenhouse gas CO_2 into useful carbon fuels.

2.5 Acknowledgments

I would like to thank Dr. Yilin Hu (University of California, Irvine) for the construction of the *A. vinelandii* strain YM68A. I also thank John Wiley and Sons for the permission to include portions of Chapter 2 in my dissertation, which were originally published in *Angewandte Chemie International Edition* (34). This work is supported by the National Institute of Health Grant GM 67626.

2.6 References

1. Hoffman BM, Lukoyanov D, Yang ZY, Dean DR, & Seefeldt LC (2014) Mechanism of nitrogen fixation by nitrogenase: the next stage. *Chem Rev* 114(8):4041-62.
2. Hu Y & Ribbe MW (2011) Historic overview of nitrogenase research. *Methods Mol Biol* 766:3-7.

3. Seefeldt LC, Hoffman BM, & Dean DR (2009) Mechanism of Mo-dependent nitrogenase. *Annu Rev Biochem* 78:701-22.

4. Burgess BK & Lowe DJ (1996) Mechanism of Molybdenum Nitrogenase. *Chem Rev* 96(7):2983-3012.

5. Duval S, Danyal K, Shaw S, Lytle AK, Dean DR, Hoffman BM, Antony E, & Seefeldt LC (2013) Electron transfer precedes ATP hydrolysis during nitrogenase catalysis. *Proc Natl Acad Sci U S A* 110(41):16414-9.

6. Tezcan FA, Kaiser JT, Howard JB, & Rees DC (2015) Structural evidence for asymmetrical nucleotide interactions in nitrogenase. *J Am Chem Soc* 137(1):146-9.

7. Owens CP, Katz FE, Carter CH, Luca MA, & Tezcan FA (2015) Evidence for Functionally Relevant Encounter Complexes in Nitrogenase Catalysis. *J Am Chem Soc* 137(39):12704-12.

8. Tezcan FA, Kaiser JT, Mustafi D, Walton MY, Howard JB, & Rees DC (2005) Nitrogenase complexes: Multiple docking sites for a nucleotide switch protein. *Science* 309(5739):1377-80.

9. Rees DC, Akif Tezcan F, Haynes CA, Walton MY, Andrade S, Einsle O, & Howard JB (2005) Structural basis of biological nitrogen fixation. *Philos Trans A Math Phys Eng Sci* 363(1829):971-84; discussion 1035-40.

10. Yates MG (1992) *Biological Nitrogen Fixation* (Chapman and Hall, New York).

11. Rivera-Ortiz JM & Burris RH (1975) Interactions among substrates and inhibitors of nitrogenase. *J Bacteriol* 123(2):537-45.

12. Cameron LM & Hales BJ (1995), eds Tikhonovich IA, Provorov NA, Romanov VI, & Newton WE (Springer Netherlands, Dordrecht), pp 109-13.

13. Christiansen J, Seefeldt LC, & Dean DR (2000) Competitive substrate and inhibitor interactions at the physiologically relevant active site of nitrogenase. *J Biol Chem* 275(46):36104-7.

14. Lee CC, Hu Y, & Ribbe MW (2009) Unique features of the nitrogenase VFe protein from Azotobacter vinelandii. *Proc Natl Acad Sci U S A* 106(23):9209-14.

15. Lee CC, Hu Y, & Ribbe MW (2010) Vanadium nitrogenase reduces CO. *Science* 329(5992):642.

16. Hu Y, Lee CC, & Ribbe MW (2011) Extending the carbon chain: hydrocarbon formation catalyzed by vanadium/molybdenum nitrogenases. *Science* 333(6043):753-5.

17. Hu Y, Lee CC, & Ribbe MW (2012) Vanadium nitrogenase: a two-hit wonder? *Dalton Trans* 41(4):1118-27.

18. Ribbe MW, Hu Y, Guo M, Schmid B, & Burgess BK (2002) The FeMoco-deficient MoFe protein produced by a nifH deletion strain of Azotobacter vinelandii shows unusual P-cluster features. *J Biol Chem* 277(26):23469-76.

19. Hu Y, Fay AW, Dos Santos PC, Naderi F, & Ribbe MW (2004) Characterization of Azotobacter vinelandii nifZ deletion strains. Indication of stepwise MoFe protein assembly. *J Biol Chem* 279(52):54963-71.

20. Burgess BK, Jacobs DB, & Stiefel EI (1980) Large-scale purification of high activity Azotobacter vinelandII nitrogenase. *Biochim Biophys Acta* 614(1):196-209.

21. Hu Y, Fay AW, & Ribbe MW (2005) Identification of a nitrogenase FeMo cofactor precursor on NifEN complex. *Proc Natl Acad Sci U S A* 102(9):3236-41.

22. Glasoe PK & Long FA (1960) Use of glass electrodes to measure acidities in deuterium oxide. *J Phys Chem* (64):188-9.

23. Seefeldt LC, Rasche ME, & Ensign SA (1995) Carbonyl sulfide and carbon dioxide as new substrates, and carbon disulfide as a new inhibitor, of nitrogenase. *Biochemistry* 34(16):5382-9.

24. Yang ZY, Moure VR, Dean DR, & Seefeldt LC (2012) Carbon dioxide reduction to methane and coupling with acetylene to form propylene catalyzed by remodeled nitrogenase. *Proc Natl Acad Sci U S A* 109(48):19644-8.

25. Einsle O, Tezcan FA, Andrade SL, Schmid B, Yoshida M, Howard JB, & Rees DC (2002) Nitrogenase MoFe-protein at 1.16 A resolution: a central ligand in the FeMo-cofactor. *Science* 297(5587):1696-700.

26. Lancaster KM, Roemelt M, Ettenhuber P, Hu Y, Ribbe MW, Neese F, Bergmann U, & DeBeer S (2011) X-ray emission spectroscopy evidences a central carbon in the nitrogenase iron-molybdenum cofactor. *Science* 334(6058):974-7.

27. Spatzal T, Aksoyoglu M, Zhang L, Andrade SL, Schleicher E, Weber S, Rees DC, & Einsle O (2011) Evidence for interstitial carbon in nitrogenase FeMo cofactor. *Science* 334(6058):940.

28. Wiig JA, Hu Y, Lee CC, & Ribbe MW (2012) Radical SAM-dependent carbon insertion into the nitrogenase M-cluster. *Science* 337(6102):1672-5.

29. Carnahan EM, Protasiewicz JD, & Lippard SJ (1993) The 15 years of reductive coupling: what have we learned? *Acc Chem Res* 26(3):90-7.

30. Yang ZY, Dean DR, & Seefeldt LC (2011) Molybdenum nitrogenase catalyzes the reduction and coupling of CO to form hydrocarbons. *J Biol Chem* 286(22):19417-21.

31. Corbett MC, Hu Y, Naderi F, Ribbe MW, Hedman B, & Hodgson KO (2004) Comparison of iron-molybdenum cofactor-deficient nitrogenase MoFe proteins by X-ray

absorption spectroscopy: implications for P-cluster biosynthesis. *J Biol Chem* 279(27):28276-82.

32. Lee CC, Hu Y, & Ribbe MW (2012) ATP-independent substrate reduction by nitrogenase P-cluster variant. *Proc Natl Acad Sci U S A* 109(18):6922-6.

33. Hu Y, Corbett MC, Fay AW, Webber JA, Hedman B, Hodgson KO, & Ribbe MW (2005) Nitrogenase reactivity with P-cluster variants. *Proc Natl Acad Sci U S A* 102(39):13825-30.

34. Rebelein JG, Hu Y, & Ribbe MW (2014) Differential reduction of CO(2) by molybdenum and vanadium nitrogenases. *Angew Chem Int Ed Engl* 53(43):11543-6.

Chapter 3: ATP-independent Carbon Dioxide Reduction by Vanadium Nitrogenase

3.1 Introduction

The enzyme catalyzed CO_2 reduction in an ATP-dependent fashion by V nitrogenase not only added another substrate to the already impressive list of remarkable nitrogenase reactions (see Table 3.1) (1-4); it renders nitrogenase the first enzyme to convert CO_2 into hydrocarbons. This discovery generated a lot of interest for nitrogenase as a possible template for the design of cost-efficient strategies to convert the greenhouse gas CO_2 into products of economic value (see Chapter 2) (5). However, the ATP-dependent conversion of CO_2 by the complete V nitrogenase (Figure 3.1 A, system I) is rather slow, and the amount of formed products is with 0.3 mol CO, 0.02 mol CH_4, 0.04 mol C_2H_4, and 0.002 mol C_2H_6 per mol of protein very low and the hydrocarbon chains are rather short. A second approach taken by Lee *et al.* (2015) to reduce CO_2 to hydrocarbons employed the isolated cofactors of nitrogenase proteins, receiving the electrons directly from a strong reductant samarium(II) iodide (SmI_2; $E^{0'}$ = −1.55 V in THF, SHE (6)), in an organic solvent (Figure 3.1 C, system III). This approach renders the ATP-dependent electron transfer obsolete and increases the turnover number (TON) from 0.4 for system I to 1.8 for system

Table 3.1. Nitrogenase Reactions.

Substrate	Reaction
Acetylene	$C_2H_2 + 2H^+ + 2e^- \rightarrow C_2H_4$
Azide	$N_3^- + 3H^+ + 2e^- \rightarrow N_2 + NH_3$
Carbon dioxide[(a)]	$CO_2 + 2H^+ + 2e^- \rightarrow CO + H_2O + CH_4 + C_2H_4 + C_2H_6$
Carbon monoxide[(a)]	$CO + H^+ + e^- \rightarrow CH_4 + C_2H_4 + C_2H_6 + C_3H_6 + C_3H_8 + C_4H_8 + C_4H_{10}$
Carbonyl Sulfide	$COS + 2H^+ + 2e^- \rightarrow CO + H_2S$
Cyclopropene	$3\triangle + 6H^+ + 6e^- \rightarrow 2C_3H_6 + \triangle$
Hydrazine	$N_2H_4 + 2H^+ + 2e^- \rightarrow 2NH_3$
Hydrogen cyanide	$HCN + 6H^+ + 6e^- \rightarrow CH_4 + NH_3$ $HCN + 4H^+ + 4e^- \rightarrow CH_3NH_2$
Methyl isonitrile	$CH_3NC + 6H^+ + 6e^- \rightarrow CH_3NH_2 + CH_4$
Nitrogen	$N_2 + 8H^+ + 8e^- \rightarrow 2NH_3 + H_2$
Propargyl alcohol	$HC{\equiv}CCH_2OH + 2H^+ + 2e^- \rightarrow CH_2{=}CHCH_2OH$

[(a)] **The overall stoichiometry has not been established.**

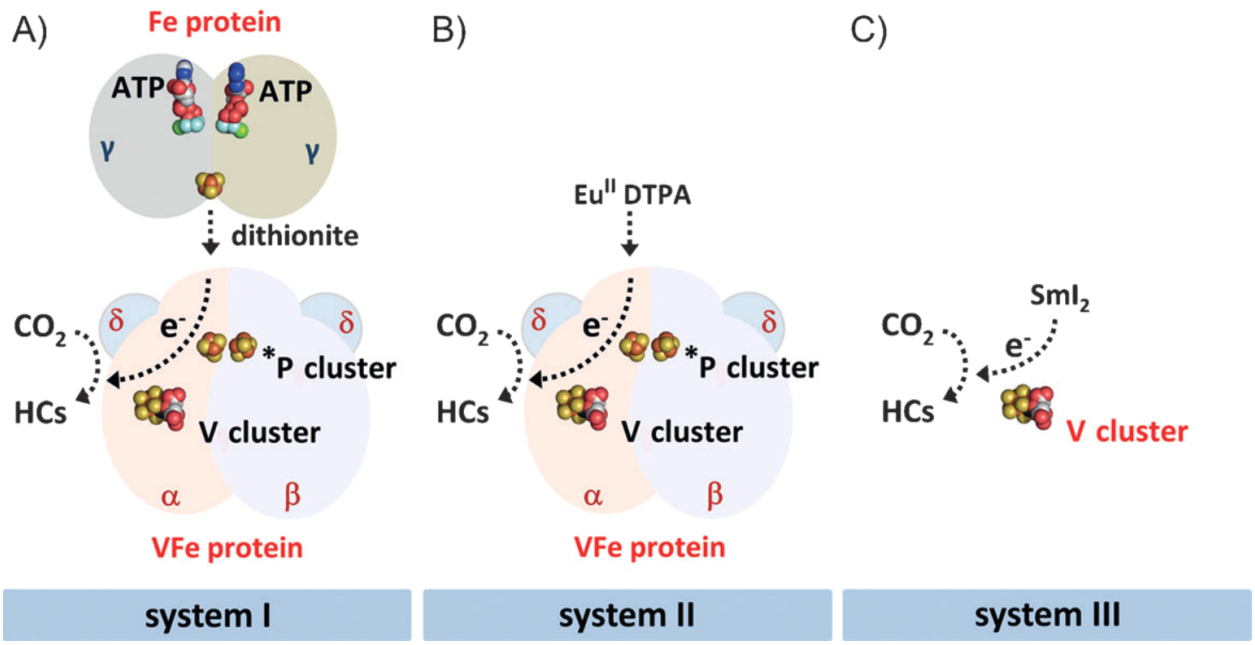

Figure 3.1. Three CO_2-reducing reaction systems based on V nitrogenase. A) System I: V nitrogenase plus dithionite affords ATP-dependent transfer of electrons from the $[Fe_4S_4]$ cluster of the Fe protein to the V cluster (cofactor) of the VFe protein in aqueous buffer. B) System II: VFe protein plus Eu^{II} DTPA affords ATP-independent electron transfer from Eu^{II} DTPA to the V cluster of the VFe protein in aqueous buffer. C) System III: V cluster plus SmI_2 affords ATP-independent electron transfer from SmI_2 to the isolated V cluster in organic solvent. For clarity, only half of the VFe protein is shown. HC: hydrocarbon.

III. Although C3 hydrocarbon chains such as propene (C_3H_6) and propane (C_3H_8) were identified and the overall activity is elevated in the SmI_2 driven system III, the product profile is shifted from hydrocarbon chains towards C1 products (CO and CH_4). C1 products constitute 97.3 % of all products in system III, compared to 79.2 % C1 products for the ATP-dependent system I. Furthermore, the instability of the isolated V cluster and its laborious isolation hampers a further increase of the efficiency as well as the application in upscaled approaches (7).

The elevated TON in combination with identification of C3 hydrocarbon chains prompted us to combine the features of the isolated cofactor system with the desirable features of the ATP-dependent enzyme system such as better ratios of hydrocarbon chains to C1 products

and a higher stability of the cofactor. This resulted in a water based, ATP-independent, reductant driven reaction system using the VFe protein bound V cluster as a standalone catalyst for the improved production of hydrocarbons (Figure 3.1 B, system II). Such a system was generated by combining europium(II) DTPA ($E^{\circ\prime}$ = −1.1 V, SHE) (8, 9) with VFe protein in an aqueous buffer.

3.2 Materials and Methods

3.2.1 Reagents

Unless noted otherwise, all chemicals were purchased from Fisher Scientific and Sigma-Aldrich. $^{12}CO_2$ (99.998% purity) was purchased from Praxair, and $^{13}CO_2$ (≥ 98% isotopic purity), D_2O and deuterated Tris were purchased from Cambridge Isotope Labs.

3.2.2 Cell Growth and Protein Purification

Azotobacter vinelandii strain (YM68A) expressing the His-tagged VFe protein was grown in 180 L batches in a 200 L New Brunswick fermentor (New Brunswick Scientific) in Burke's minimal medium supplemented with 2 mM ammonium acetate and 30 μM sodium orthovanadate. The growth rate was measured by cell density at 436 nm using a Spectronic 20 Genesys. Cells were harvested in the late exponential phase by using a flow-through centrifuge (Cepa). The cell paste was washed with a buffer containing 50 mM Tris-HCl (pH 8.0). Published methods were used for the purification of His-tagged VFe proteins (10-13).

3.2.3 Enzyme Assays

Each H_2O-based reaction of CO_2 reduction was carried out in a 27 ml reaction vial with a total volume of 15 ml, which contained 100 mM Tris-HCl (pH 8.0), 20 mM Eu^{II} DTPA and 1 M $NaHCO_3$ as a CO_2 source. This reaction mixture was allowed to equilibrate for 1 h, followed

by the adjustment of the pH to 8.3. The reaction was started by the addition 100 mg VFe protein. Subsequently, the reaction was incubated with continuous shaking in a water bath at 30 °C and samples were taken at 0, 10, 30, 60, 120, 180, 240, 300 and 360 min, respectively. The D_2O-based assays had the same composition as the H_2O-based assays except that all components were dissolved in 100 mM (D11)-Tris [i.e., $(DOCD_2)_3CND_2$] buffer. In addition, all protein samples used in these assays were exchanged into the same deuterated buffer. The pD of this buffer was adjusted to 8.0 with DCl and NaOD by using the pH indicator strips and subsequently determined by a previously established equation (14): pD = measured pH + 0.40. For GC-MS analysis (see below), the H_2O- or D_2O-based assays of CO_2 reduction were prepared as described above except for the substitution of $NaH^{12}CO_3$ by $NaH^{13}CO_3$. For experiments using CO as a substrate, $NaHCO_3$ was omitted, and CO was added to the the reaction vial in a concentration mimicking that achieved by VFe protein from CO_2 reduction at 180 min: 136 ppm for H_2O-based assays, or 178 ppm for D_2O-based assays.

3.2.4 Activity Determination

The products, CH_4, C_2H_4, C_2H_6, C_3H_6, C_3H_8, C_4H_8 and C_4H_{10} were quantified by GC-FID using a previously published method (15-17). For each assay, a total of 250 µl headspace was injected onto a Grace activated alumina column, which was held at 55 °C for 1 min, heated to 180 °C at 12.5 °C/min, and held at 180 °C for another 2.6 min. The quantities of these products were determined based on a Scott standard gas mixture containing 15 ppm of each hydrocarbon compound. The product CO was quantified by a GC coupled to an SRI reduction gas detector. For each assay, a total of 250 µl headspace was applied onto a Grace molecular sieve column, which was held at a constant temperature of 50 °C. The quantity of CO was determined based on a linear standard curve ($R^2 \geq 98$) derived from the injection of varying

amounts of ^{12}CO (99.5 % purity). The detection limit for the products in nmol product/µmol protein was as follows: 0.27 (CH_4), 0.11 (C_2H_4), 0.091 (C_2H_6), 0.087 (C_3H_6), 0.066 (C_3H_8), 0.086 (C_4H_8), 0.053 (C_4H_{10}), and 0.1 (CO).

3.2.5 GC-MS Analysis

The hydrocarbon products were identified by GC-MS using an Agilent 6890 GC system coupled to a Waters GCT-Premier time-of-flight mass spectrometer. The identities of CH_4, C_2H_4, C_2H_6, C_3H_6, C_3H_8, C_4H_8 and C_4H_{10} and their deuterated counterparts were confirmed by comparing their masses and retention times with those of the Scott standard alkane and alkene gas mixture. For each assay, a total of 50 µl headspace was injected into a split/splitless injector operated at 125 °C in split mode, with a split ratio of 5. A 1 mm ID liner was used to optimize sensitivity. Separation of gas was achieved with an Agilent 0.320 mm (ID) x 30 m (length) HP-PLOT-Q capillary column, which was held at 40 °C for 1 min, heated to 45 °C at a rate of 5 °C/min, heated further to 200 °C at a rate of 20 °C/min, and held at 200 °C for another 4 min. The carrier gas, helium, was passed through the column at a rate of 1.1 ml/min. The mass spectrometer was operated in electron impact (EI) ionization mode.

3.3 Results and Discussion

3.3.1 C1 Products from CO_2 Reduction

Employing a water based, ATP-independent system, the VFe protein was directly driven by Eu^{II} DTPA and able to reduce CO_2 to CO (Figure 3.2 A) and CH_4 (Figure 3.2 B). The conversion of CO_2 into CO was consistently higher in D_2O than in H_2O (Figure 3.2 A). In contrast, CH_4 formation could not be detected in the presence of D_2O (Figure 3.2 B, ○), but reached 30 nmol/µmol protein after 180 min in H_2O (Figure 3.2, ▽). Interestingly, when CO was supplied

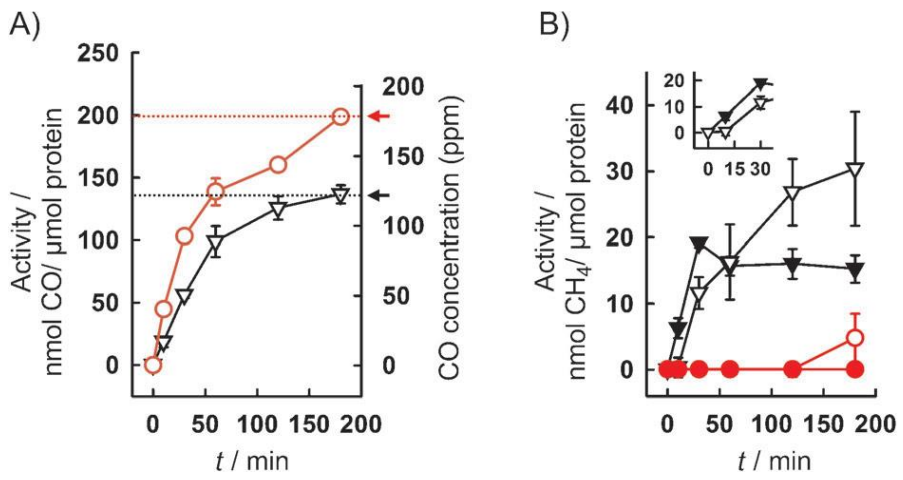

Figure 3.2. ATP-independent reduction of CO_2 to C1 products by VFe protein. A) Time-dependent formation of CO from CO_2 in H_2O (▽) or D_2O (○). B) Comparison of the time-dependent formation of CH_4 from CO_2-reduction in H_2O (▽) or D_2O (○) with that from CO-reduction in H_2O (▾) or D_2O (•). CO was supplied at 136 ppm and 178 ppm, the amounts of CO formed in H_2O (▽) and D_2O (○), respectively, from CO_2 reduction at 180 min (arrows in A). Inset: first 30 min of CH_4 formation in H_2O from CO (▾) or CO_2 (▽). Data are mean ± SD (n=3) after background correction.

in the concentration achieved by the VFe protein during CO_2 reduction after 180 min (Figure 3.2, arrows), no CD_4 was detected as a product in D_2O (Figure 3.2, •), whereas CH_4 formation reached 18 nmol/µmol protein within 30 min in H_2O (Figure 3.2, ▽). This increase in activity was similar to the increase (12 nmol/µmol protein) between 10 and 30 min when CO_2 was supplied, following a delay of 10 min in which no CH_4 was detected (Figure 3.2, ▾). Beyond 30 min, however, CH_4 formation reached a plateau when CO was the substrate (Figure 2 B, ▾), whereas it continued to increase with CO_2 (Figure 3.2, ▽). The similarity between the initial phases of CO- and CO_2-based CH_4 formation (Figure 3.2 B, inset) suggests that a portion of CH_4 is formed by CO_2-derived CO, particularly given the 10 min delay in the CO_2-based reaction (correlating with the time required to accumulate a sufficient amount of CO from CO_2 reduction). The disparity between the two reactions beyond 30 min, however, implies that a certain portion of CH_4 is generated directly by CO_2 reduction; this could account for the different shapes of the time courses of CH_4 formation, as well as the total amounts of CH_4 produced in the CO- and CO_2-based reactions.

3.3.2 Hydrocarbon Chain Products from CO_2 Reduction

Other than reducing CO_2 to the C1 hydrocarbon product CH_4, the VFe protein can use CO_2 as a substrate for ATP-independent C-C coupling into hydrocarbon products up to C4 (Figure 3.3). Unlike in the formation of CH_4, there was a dramatic increase in C2–C4 hydrocarbon formation upon substitution for H_2O by D_2O: formation of C_2D_4, C_2D_6, C_3D_6, C_3D_8, C_4D_8, and C_4D_{10} reached 18, 12, 14, 5, 4.5 and 2.0

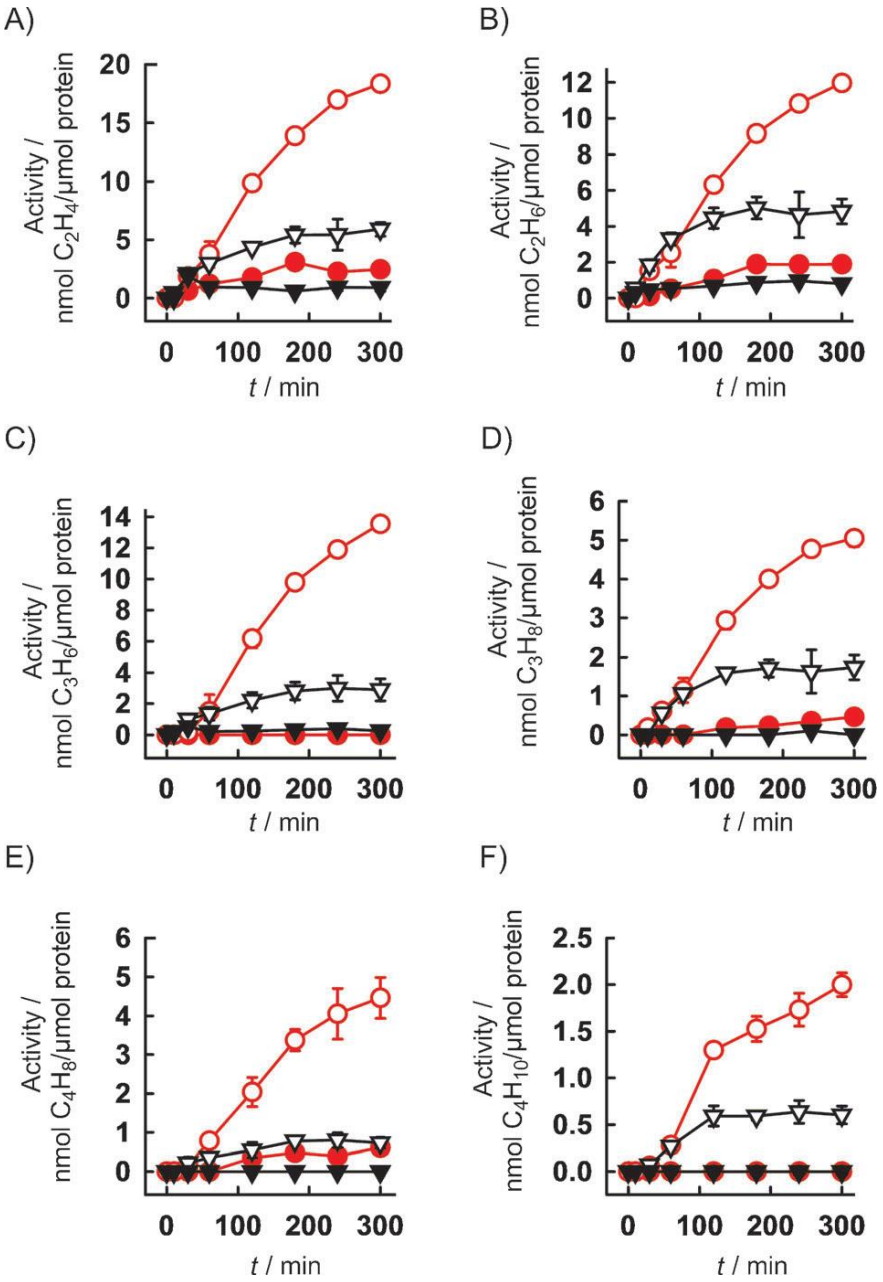

Figure 3.3. ATP-independent reduction and coupling of CO_2 into C2–C4 products by VFe protein. Comparison of time-dependent formation of A) C_2H_4, B) C_2H_6, C) C_3H_6, D) C_3H_8, E) C_4H_8, and F) C_4H_{10} from CO_2-reduction in H_2O (▽) or D_2O (○) with those from CO reduction in H_2O (▼) or D_2O (•). CO was supplied at 136 ppm (▼) and 178 ppm (•), the amounts of CO formed in H_2O and D_2O, respectively, from CO_2-reduction by VFe protein at 180 min (arrows in Figure 2 A). Data are mean ±SD (n=3) after background correction.

nmol/μmol protein, respectively, after 300 min (Figure 3.3 A-F, ○), whereas in the presence of H_2O, formation reached a plateau between 120 and 180 min at 6, 5, 3, 1.7, 0.8, and 0.6 nmol/μmol protein, respectively (Figure 3.3 A-F, ▽). When CO was supplied in a concentration reflecting that achieved from CO_2 reduction by VFe protein at 180 min (Figure 3.2 A, arrows), little or no C2–C4 product was detected in the presence of either D_2O (Figure 3.3 A–F, •) or H_2O (Figure 3.3 A–F, ▾), thus suggesting that these products were formed directly from CO_2 reduction instead of indirectly from CO_2-derived CO.

3.3.3 Tracing the Carbon Source of the Hydrocarbon Products

GC-MS analysis further confirmed the source of carbon in the C1–C4 hydrocarbon products as CO_2: mass shifts of +1, +2, +3, and +4 of C1, C2, C3, and C4 products, respectively, upon substitution of $^{13}CO_2$ for $^{12}CO_2$ in H_2O-based reactions (Figure 3.4 A, B). In addition, this demonstrated that the source of hydrogen in these products was H_2O: mass shifts of +4, +6, and +8 for products containing 4, 6, and 8 hydrogen atoms, respectively, upon substitution of D_2O for H_2O in $^{12}CO_2$-based reactions (Figure 3.4 A, C), and additional mass shifts of +2, +3, and +4 (C2, C3, and C4 products, respectively) upon further substitution of $^{13}CO_2$ for $^{12}CO_2$ (Figure 3.4 C, D) occurred. In the case of C_4H_{10} and C_4D_{10}, the base peaks were monitored to circumvent the problem of the detection limit: m/z 43.087, 46.064, 50.098, and 58.108 represent the predominant fragment ions formed for $^{12}C_4H_{10}$, $^{13}C_4H_{10}$, $^{12}C_4D_{10}$, and $^{13}C_4D_{10}$, respectively (Figure 3.4).

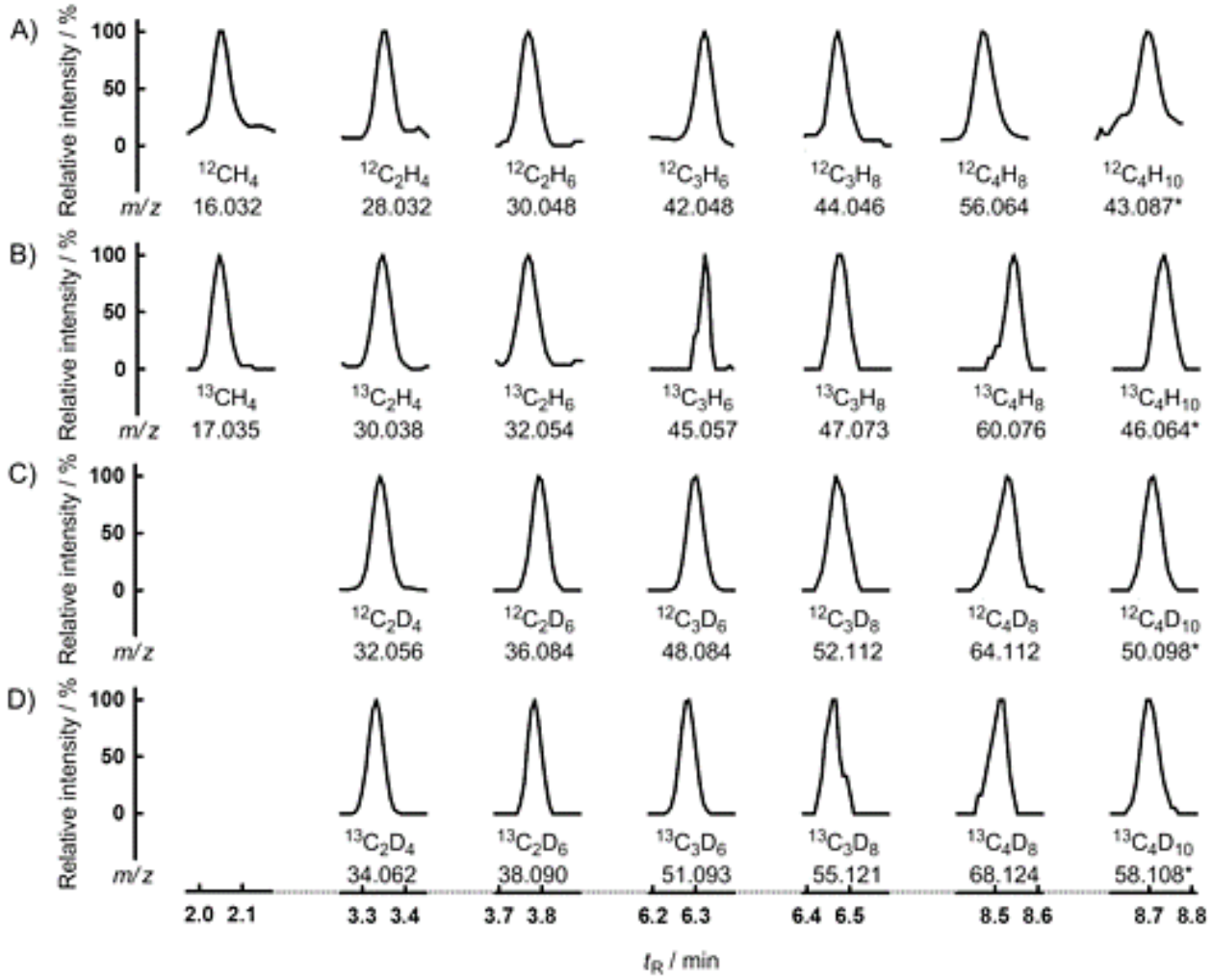

Figure 3.4. GC-MS analysis of hydrocarbons generated by VFe protein in the ATP-independent reaction of CO_2 reduction. The products were generated in H_2O with A) $^{12}CO_2$ or B) $^{13}CO_2$ as the substrate, or in D_2O with C) $^{12}CO_2$ or D)$^{13}CO_2$. The m/z ratios at which the products were traced are indicated. For C_4H_{10} and C_4D_{10}, the base peaks (*), or the tallest peaks representing the most common fragment of these species, were monitored to overcome the problem of detection limit.

3.4 Summary and Conclusion

The total activity of C-C coupling (i.e., formation of ≥C2 products) by VFe protein in the ATP-independent, Eu^{II} DTPA-driven reaction (Figure 3.1, System II) was higher than that by the FeVco in the ATP-independent, SmI_2-driven reaction (Figure 3.1, System III) (Figure 3.5 A,

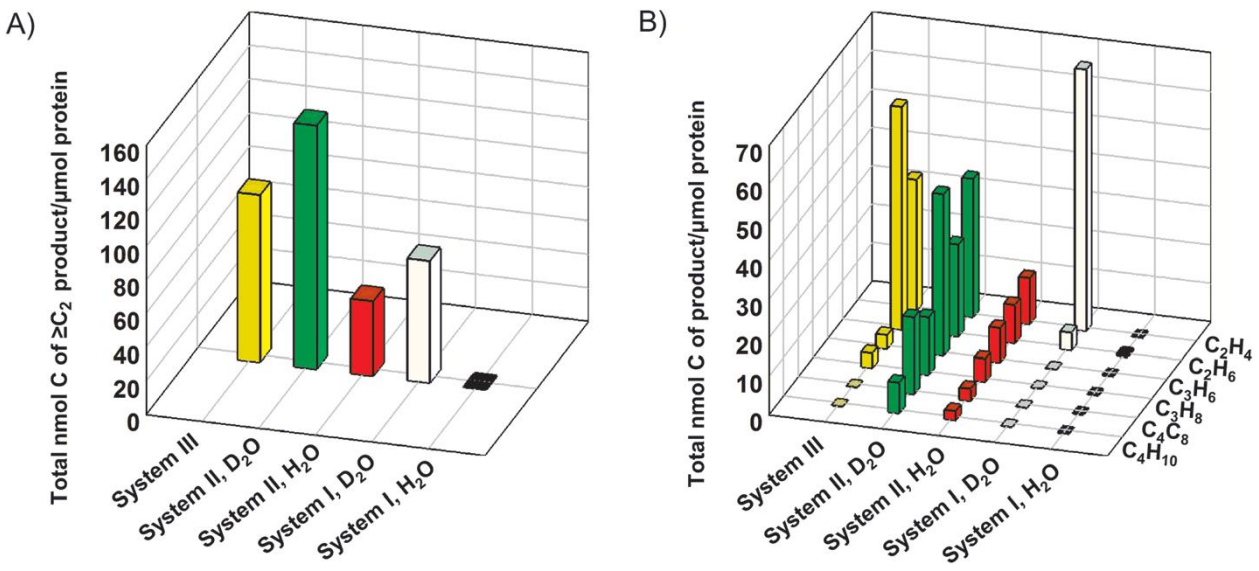

Figure 3.5. C-C coupling from CO_2 reduction by the three V nitrogenase-based systems. A) Total, and B) individual activities of C–C coupling by Systems I, II, and III. Activities were calculated based on the sums of carbons in hydrocarbon products ≥C2. The data for Systems I and III are from refs. [5] and [6], respectively.

green versus yellow) or by V nitrogenase in the ATP-dependent reaction (Figure 3.1, System I) in D_2O (Figure 3.5 A, white) or H_2O (Figure 3.5 A, black). Moreover, compared to Systems I and III, System II showed a greater tendency to reduce CO_2 to longer carbon chains and a broader product profile, both in D_2O (Figure 3.5 B, green) and in H_2O (Figure 3.5 B, red). Furthermore, system II is the only system which can reduce CO_2 not only under heavy water (D_2O) but also under H_2O to hydrocarbon chains. Given the absence of Fe protein in System II, the active V cluster site is likely more "exposed" in this system than that in System I (Figure 3.1); this might explain the improved ability of system II to extend the carbon chain and generate larger hydrocarbon products. Another explanation for this observation could be the speed of the electron delivery. Since Eu^{II} DTPA renders the association and dissociation between VFe and Fe protein for electron transfer obsolete, the electrons are presumably faster available to the cofactor, the V cluster. Moreover, the protein scaffold that houses the

V cluster in system II, likely provides stability to the cluster and modulates its redox potential; this might account for the higher activity by a weaker reductant (Eu^{II} DTPA) in System II, relative to the lower activity by a stronger reductant (SmI_2) in System III (Figure 3.5 A, green versus yellow). Apart from the composition-dependent differences, there is a strong deuterium effect on the activity of protein-enabled CO_2 reduction in an aqueous buffer, as both Systems I and II displayed dramatically increased CO_2-reducing activity upon substitution of H_2O by D_2O (Figure 3.5), similar to the D_2O effect observed for the reduction of CO by Mo and V nitrogenase (15, 18). The D_2O-based System II is also the most efficient system in the formation of hydrocarbon chains, it routes 44 % of the electrons towards chain formation whereas only 20.8 % and 2.7 % of the electrons in System I and III, respectively, are used for the production of hydrocarbons ≥ C2. Not only that the highest number of electrons is directed towards hydrocarbon chains in System II, but also the longest chains C4 (i.e. butene and butane) were identified for the same system. Although systematic studies are required to elucidate the mechanism of CO_2 reduction by V nitrogenase, these observations afford initial insights into the characteristics of this unique reaction and provide a potential template for the future design of nitrogenase-based catalysts to recycle the greenhouse gas CO_2 into useful hydrocarbon products.

3.5 Acknowledgments

I would like to thank Dr. Yilin Hu (University of California, Irvine) for the construction of the *A. vinelandii* strain YM68A. I also thank John Wiley and Sons for the permission to include portions of Chapter 3 in my dissertation, which were originally published in *ChemBioChem* (19). This work is supported by the National Institute of Health Grant GM 67626.

3.6 References

1. Wiig JA, Rebelein JG, & Hu Y (2014) Nitrogenase Complex. in *eLS* (John Wiley & Sons Ltd, Chichester).
2. Burgess BK & Lowe DJ (1996) Mechanism of Molybdenum Nitrogenase. *Chem Rev* 96(7):2983-3012.
3. Rivera-Ortiz JM & Burris RH (1975) Interactions among substrates and inhibitors of nitrogenase. *J Bacteriol* 123(2):537-45.
4. Yates MG (1992) *Biological Nitrogen Fixation* (Chapman and Hall, New York).
5. Rebelein JG, Hu Y, & Ribbe MW (2014) Differential reduction of CO(2) by molybdenum and vanadium nitrogenases. *Angew Chem Int Ed Engl* 53(43):11543-6.
6. Lee CC, Hu YL, & Ribbe MW (2015) Catalytic Reduction of CN-, CO, and CO2 by Nitrogenase Cofactors in Lanthanide-Driven Reactions. *Angewandte Chemie-International Edition* 54(4):1219-22.
7. Lee CC, Hu Y, & Ribbe MW (2015) Catalytic reduction of CN-, CO, and CO2 by nitrogenase cofactors in lanthanide-driven reactions. *Angew Chem Int Ed Engl* 54(4):1219-22.
8. Danyal K, Inglet BS, Vincent KA, Barney BM, Hoffman BM, Armstrong FA, Dean DR, & Seefeldt LC (2010) Uncoupling nitrogenase: catalytic reduction of hydrazine to ammonia by a MoFe protein in the absence of Fe protein-ATP. *J Am Chem Soc* 132(38):13197-9.
9. Vincent KA, Tilley GJ, Quammie NC, Streeter I, Burgess BK, Cheesman MR, & Armstrong FA (2003) Instantaneous, stoichiometric generation of powerfully

reducing states of protein active sites using Eu(II) and polyaminocarboxylate ligands. *Chem Commun (Camb)* (20):2590-1.

10. Ribbe MW, Hu Y, Guo M, Schmid B, & Burgess BK (2002) The FeMoco-deficient MoFe protein produced by a nifH deletion strain of Azotobacter vinelandii shows unusual P-cluster features. *J Biol Chem* 277(26):23469-76.
11. Hu Y, Fay AW, Dos Santos PC, Naderi F, & Ribbe MW (2004) Characterization of Azotobacter vinelandii nifZ deletion strains. Indication of stepwise MoFe protein assembly. *J Biol Chem* 279(52):54963-71.
12. Burgess BK, Jacobs DB, & Stiefel EI (1980) Large-scale purification of high activity Azotobacter vinelandII nitrogenase. *Biochim Biophys Acta* 614(1):196-209.
13. Hu Y, Fay AW, & Ribbe MW (2005) Identification of a nitrogenase FeMo cofactor precursor on NifEN complex. *Proc Natl Acad Sci U S A* 102(9):3236-41.
14. Glasoe PK & Long FA (1960) Use of glass electrodes to measure acidities in deuterium oxide. *J Phys Chem* (64):188-9.
15. Hu Y, Lee CC, & Ribbe MW (2011) Extending the carbon chain: hydrocarbon formation catalyzed by vanadium/molybdenum nitrogenases. *Science* 333(6043):753-5.
16. Lee CC, Hu Y, & Ribbe MW (2010) Vanadium nitrogenase reduces CO. *Science* 329(5992):642.
17. Lee CC, Hu Y, & Ribbe MW (2009) Unique features of the nitrogenase VFe protein from Azotobacter vinelandii. *Proc Natl Acad Sci U S A* 106(23):9209-14.
18. Hu Y, Lee CC, & Ribbe MW (2012) Vanadium nitrogenase: a two-hit wonder? *Dalton Trans* 41(4):1118-27.

19. Rebelein JG, Hu Y, & Ribbe MW (2015) Widening the Product Profile of Carbon Dioxide Reduction by Vanadium Nitrogenase. *ChemBioChem* 16(14):1993-6.

Chapter 4: The Interconversion between Carbon Monoxide and Carbon Dioxide by Nitrogenase Iron Proteins

4.1 Introduction

The iron (Fe) proteins of the homologous molybdenum (Mo) and vanadium (V) nitrogenases, designated NifH and VnfH, respectively, are the reductase component of nitrogenase (see Chapter 1). NifH and VnfH from the soil bacterium *Azotobacter vinelandii* are highly homologous, sharing a sequence identity of 91% with each other. Both are homodimers carrying a subunit-bridging [Fe_4S_4]-cluster and a nucleotide-binding site that is harbored within each subunit. During substrate turnover, the Fe protein (NifH or VnfH) forms a functional complex with its catalytic partner (NifDK or VnfDGK), permitting ATP-dependent transfer of electrons from the former to the latter and the subsequent reduction of substrates at the cofactor site (M or V cluster) of the latter upon accumulation of a sufficient amount of electrons (see Chapter 1.2.1) (1-5). Such a two-component catalytic system enables two reactions that are important for energy- and environment-related areas: (*i*) the reduction of nitrogen (N_2) to ammonia (NH_3) (1, 3, 4); and (*ii*) the reduction of carbon monoxide (CO) or carbon dioxide (CO_2) to hydrocarbons under ambient conditions (6, 7).

While running control experiments for the ATP-dependent reduction of CO_2 by Mo and V nitrogenase (Chapter 2), we noticed surprising results. Fe protein (NifH and VnfH) under dithionite was able to reduce CO_2 in low amounts to CO. Prompting the questions of whether the actions of Fe proteins can be uncoupled from their respective catalytic partners, and if so what interesting chemistry can be performed by these unique reductases on their own.

4.2 Materials and Methods

4.2.1 Reagents

Unless specified otherwise, all chemicals were purchased from Fisher Thermo Scientific (Waltham, MA) and Sigma-Aldrich (St. Louis, MO). ^{12}CO (99.9% purity) and $^{12}CO_2$ (99.998% purity) were purchased from Praxair (Danbury, CT). ^{13}CO (99% purity) and $^{13}CO_2$ (99% purity) were purchased from Cambridge Isotope Laboratories (Tewksbury, MA).

4.2.2 Protein Purification

Azotobacter vinelandii strains expressing non-tagged *vnfH*- and *nifH*-encoded Fe proteins of Mo and V nitrogenases (designated VnfH and NifH) respectively, were grown as described elsewhere (8, 9). Published methods were used for the purification of VnfH and NifH from their respective wildtype strains and variant strains containing deletions of genes encoding their catalytic partners (VnfDGK and NifDK) (8, 9).

4.2.3 *In vitro* CO_2 Reduction Assays

The *in vitro* CO_2 reduction assays were carried out under 100% CO_2 in 9.4 mL assay vials. Each assay contained, in a total volume of 1.5 mL, 500 mM Tris-HCl (pH 10.0), 20 mg VnfH or NifH, 15 mM sodium dithionite, and either no nucleotide or 21.6 mM MgATP. Of the nucleotide-free assays, some contained the same components except for the substitution of 15 mM europium(II) diethylenetriaminepentaacetate (Eu^{II} DTPA) for dithionite; whereas others contained the same components except for the absence of dithionite and the substitution of 20 mg oxidized VnfH or NifH for reduced VnfH or NifH. The oxidized VnfH or NifH was prepared by incubation of the protein with excess indigo disulfonate (IDS), followed by a single passage of the incubation mixture through an anion exchange column as described earlier (10). Assays containing crude extracts or partially purified proteins were

scaled up and contained a total of 70 mg protein in a total volume of 2.5 mL. All assays were assembled as described above without protein, flushed/exchanged repeatedly with 100% CO_2, and equilibrated for 30 min until pH stabilized at approximately 8.1. Subsequently, the reaction was initiated by addition of NifH or VnfH and incubated with continuous shaking at 30 °C. Headspace samples were taken at 0, 30, 60, 120, 180, 240, 300 and 360 min, and examined for the amounts of CO generated at these time points (see Chapter 4.2.6).

4.2.4 *In vitro* CO Oxidation Assays

The *in vitro* CO oxidation assays were carried out under 99.9% CO in 9.4 mL assay vials. Each assay contained, in a total volume of 1 mL, 250 mM Tris-HCl (pH 8.0), 10 mg VnfH or NifH, and 20 mM IDS. Assays containing crude extracts or partially purified proteins were scaled up and contained a total of 70 mg protein in a total volume of 2.5 mL. All assays were assembled as described above without protein and IDS, flushed/exchanged repeatedly with 100% Ar, flushed/filled with 100% CO, and equilibrated for 30 min. Subsequently, NifH or VnfH was added, and the reaction was initiated by addition of IDS and incubated with continuous shaking at 30 °C. Headspace samples were taken at 0, 30, 60, 120, 180, 240, 300 and 360 min following the release of dissolved CO_2 by addition of 100 µL concentrated hydrochloric acid (HCl) to the liquid phase, and examined for the total amounts of CO_2 generated at these time points (see Chapter 4.2.6).

4.2.5 *in vivo* CO_2 Reduction Assays

A. vinelandii strains expressing VnfH and NifH, respectively, in genetic backgrounds lacking the encoding genes for their catalytic partners were inoculated into 250 mL Erlenmeyer flasks containing 100 mL Burke's minimal medium supplemented with 2 mM ammonium acetate and either 30 µM Na_3VO_4 (in the case of the VnfH-expressing strain) or 11 µM

Na_2MoO_4 (in the case of the NifH-expressing strain). The cultures were grown with shaking at 200 rpm at 30 °C, and their growth rates were monitored by following cell densities at 436 nm using a Genesys 20 spectrophotometer (Spectronic, Westbury, NY). When OD_{436} of the cultures reached approximately 1.1, the Erlenmeyer flasks were capped airtight, and CO was added at 0, 20%, 30%, 40%, 50% and 100%, respectively, to the headspaces of these flasks. The cultures were incubated at 30 °C with shaking at 200 rpm for 14 h before their gas phases were examined for the amounts of CO (see Chapter 4.2.6). The amount of Fe protein in the culture was determined based on the activity of the crude extract (containing NifH or VnfH only) upon supplementation of the purified catalytic partner of the Fe protein (NifDK or VnfDGK) in an *in vitro* activity assay, and how it compared with standards containing known amounts of purified nitrogenase component proteins (8).

4.2.6 Quantification of CO and CO_2

The amount of CO or CO_2 generated in the *in vitro* and *in vivo* assays was determined through headspace analysis using a Thermo Scientific Trace 1300 GC-FID Instrument, of which the detector was interfaced with a methanizer (Thermo Electron North America LLC, Madison, WI). CO or CO_2 in the headspace sample was separated on a TG-BOND Msieve 5A column (30 m x 0.32 mm ID x 30 μm film) (Thermo Electron North America LLC, Madison, WI), which was held at 45 °C for 1 min before it was heated to 245 °C at a rate of 25 °C/min. Subsequently, CO or CO_2 was hydrogenated at 350 °C by the methanizer, and the resulting CH_4 was measured by GC-FID. The amount of CO or CO_2 was determined based on a linear standard curve ($R_2 \geq 99.5$) that was derived from the measurement of varying amounts of ^{12}CO (99.9% purity) or $^{12}CO_2$ (99.998% purity) using the same instrument. The detection limit for CO or CO_2 was 2 ppm.

4.2.7 Formate Assays

Production of formate in CO_2 reduction assays was examined by GC-MS analysis of its derivatized ester using the reagent, pentafluorobenzyl bromide (PFBBr) (11). Samples were prepared as described in Chapter 4.2.5, followed by removal of the protein using Amicon Ultra centrifugal filter units (Ultra-15, MWCO 30 kDa). An aliquot of 0.2 mL of the protein-free solution was then mixed with 0.4 mL of a 100 mM PFBBr solution (in acetone), vortexed for 1 min, and incubated at 60 °C for 40 min. Subsequently, 1 mL hexane was added and the mixture was vortexed for 5 min at room temperature, followed by centrifugation at 13,000 rpm for 5 min. 1 μL of the organic layer was analyzed by GC-MS using a Thermo Scientific Trace 1300 GC system coupled to a Thermo ISQ QD (Thermo Electron North America LLC, Madison, WI), which was equipped with an Agilent DB-5 capillary column (30m, 0.32 mm inner diameter). The carrier gas was helium (1 mL/min), with the injector temperature set at 200 °C, and the transfer line set at 250 °C. The GC temperature program was set as follows: start at 55 °C, hold for 4 min, increase to 215 °C at 20 °C/min, and then hold for 4 min. The pentafluorobenzyl-formic ester was analyzed at m/z = 226 ion in SIM mode. Quantitation was achieved using formate standards with concentrations ranging from 0 to 5 mM, and the detection limit for the formate was 0.015 mM.

4.2.8 Western Blot Analysis

The expression of VnfH and NifH in *A. vinelandii* strains was examined by Western blot analysis. *A. vinelandii* strains expressing VnfH and NifH, respectively, were cultivated with or without ammonia acetate until OD_{436} of the cell densities reached approximately 1.1 (see Chapter 4.2.5). Subsequently, 4 μL crude extracts of the VnfH- and NifH-expressing strains grown in the presence and absence of ammonia, respectively, along with ~0.4 μg of purified

NifH and VnfH, were subjected to 4-15% SDS-PAGE (Mini-Protean® TGX™, Bio-Rad, Hercules, CA). The protein bands on the gel were then transferred onto a nitrocellulose membrane (Bio-Rad Hercules, CA) by electroblotting, and non-specific binding was blocked by soaking the membrane in a Tris-buffered saline solution containing 0.1% Tween (TBST) and 5% non-fat dry milk at room temperature for 2 h. The nitrocellulose membrane was then incubated with antibodies raised against purified NifH (12) in 2.5% non-fat dry milk in TBST at 4 °C overnight, washed three times in a TBST solution for 30 min, and incubated at room temperature for 1 h with horseradish peroxidase-conjugated secondary antibody that was diluted by a factor of 1:8000 in a TTBS solution containing 2.5% milk. The membrane was then rinsed three times in TTBS, incubated with enhanced chemiluminescent substrate (EMD Millipore, Billerica, MA), and exposed to film for 3 seconds before the film was scanned and analyzed by densitometry using ImageJ (13).

4.2.9 Midpoint Potential Determination

The midpoint potentials for the $[Fe_4S_4]^{1+/2+}$ transitions of NifH and VnfH were determined by redox titration in an anaerobic glove box at ambient temperature (14). Each reaction contained, in a total volume of 0.75 mL, 500 mM Tris-HCl (pH 10.0), 15 mM sodium dithionite, 11.25 mg VnfH or NifH, and either no nucleotide or 21.6 mM MgATP. All reaction mixtures were flushed/exchanged repeatedly with 100% CO_2, and equilibrated for 30 min until the pH of the mixture stabilized at approximately 8.1. Subsequently, one redox mediator dye, such as methyl viologen, benzyl viologen, safranin O or phenosafranin, was added to the reaction mixture at a final concentration of 10 μM. Each reaction mixture was slowly titrated with a 1 mM solution of the oxidant, potassium ferricyanide. The reduction

potential of the mixture was monitored by a combinational platinum working electrode with a saturated Ag/AgCl reference (Microelectrode Inc., Bedford, NH) and, at every 10-15 mV, the mixture was anaerobically transferred to a sealed cuvette and analyzed at 420 nm using an Evolution 260 Bio spectrophotometer (Thermo Fisher Scientific, Waltham, MA) for the intensity of a characteristic feature of the $[Fe_4S_4]^{2+}$ at this wavelength (15).

4.2.10 GC-MS Analysis

For GC-MS analysis, samples of the *in vitro* reactions of CO_2 reduction by nucleotide-free VnfH and NifH, and *in vivo* assays, were prepared in the presence of $^{12}CO_2$ or $^{13}CO_2$ (see Chapter 4.2.3 and 4.2.5). The reaction product, ^{12}CO or ^{13}CO, was then analyzed by GC-MS using a Thermo Scientific Trace 1300 GC system coupled to a Thermo ISQ QD (Thermo Electron North America LLC, Madison, WI) by comparing its mass and retention time with those of the ^{12}CO or ^{13}CO standard (≥ 99.9% purity). For each sample or standard, a total of 250 µL gas was injected into a split/splitless injector operated at 120 °C in splitless mode. Gas separation was achieved on a TG-BOND Msieve 5A column (30 m x 0.32 mm ID x 30 µm film; Thermo Electron North America LLC, Madison, WI), which was held at 45 °C for 1 min, heated to 250 °C at a rate of 25 °C/min, and held at 250 °C for 4 min. The carrier gas, helium (He), was passed through the column at a rate of 2.5 mL/min. The mass spectrometer was operated in electron impact (EI) ionization mode.

4.2.11 EPR Analysis

EPR samples were prepared in a glove box (Vacuum Atmospheres, address) with an O_2 level of less than 2 ppm. To trace the conversion of CO_2 to CO, each sample contained, in a total volume of 0.5 mL, 0.6 M Tris-HCl (for "CO_2 sample", pH 10.0; for "Ar controls", pH 8.0), 10 mg NifH or VnfH, and either no nucleotide or 7 mM MgATP. All samples were first assembled

without protein, flushed/exchanged repeatedly with 100% CO_2 ("CO_2 samples") or Ar ("Ar controls") and equilibrated for 30 min until the pH of the "CO_2 samples" stabilized at approximately 8.1. Subsequently, the dithionite- or Eu^{II} DTPA-treated NifH or VnfH was passed through a small gel filtration column (G25, General Electric, Fairfield, CT) to remove excess dithionite or Eu^{II} DTPA before 10 mg of thus-treated NifH or VnfH was added to a gas- and pH-equilibrated, protein-free solution. The mixture was then stirred for 30 min and flash frozen in liquid nitrogen. To trace the conversion of CO to CO_2, each sample contained, in a total volume of 1 mL, 0.025 mM Tris-HCl (pH 8.0), 20 mg NifH or VnfH, and 2 mM IDS. All samples were first assembled without protein and IDS, flushed/exchanged repeatedly with 100% Ar, and then flushed/filled with 100% CO ("CO samples"). The NifH or VnfH sample was first passed through a small gel filtration column (G25) to remove dithionite prior to the addition of IDS. Subsequently, 20 mg of IDS-oxidized NifH or VnfH was added to a gas- and pH-equilibrated solution and the resulting mixture was shaken at 30 °C continuously before a 200 μL sample was taken from the mixture at 5, 45, 120 and 240 min and flash frozen in liquid nitrogen. EPR spectra of these samples were recorded at 10 K by an ESP 300 E_z spectrometer (Bruker, Billerica, MA) interfaced with an ESR-9002 liquid-helium continuous-flow cryostat (Oxford Instruments, Abingdon, Oxfordshire, England) using a microwave power of 20 mW, a gain of 5.02×10^4, a modulation frequency of 100 kHz and a modulation amplitude of 9 G. Four scans of perpendicular-mode EPR were recorded using a microwave frequency of 9.46 GHz.

4.3 Results and Discussion

4.3.1 *In vitro* Interconversion between CO and CO_2 by Iron Proteins

The Fe proteins were examined for their abilities to reduce CO_2 *in vitro* in the absence of their respective catalytic partners. When dithionite was supplied as a reductant, both VnfH and NifH were capable of reducing CO_2 to CO in nucleotide-free or ATP-bound states (Figure 4.1a). The nucleotide-free VnfH and NifH generated comparable amounts of CO from CO_2 reduction over 360 min, and the formation of CO by both Fe proteins remained linear within the first 180 min (Figure 4.1a, *inset*). Gas chromatography–mass spectrometry (GC–MS) analysis further confirmed the origin of carbon in the product (CO) as that from the substrate (CO_2), showing an expected mass shift of CO by +1 upon substitution of $^{13}CO_2$ for $^{12}CO_2$ in reactions enabled by VnfH (Figure 4.1b, *top*) and NifH (Figure 4.1b, *bottom*). In the presence of an oxidant, indigo disulfonate (IDS), both VnfH and NifH became inactive in CO_2 reduction (Figure 4.1), suggesting that the activities of these Fe proteins originated from their associated $[Fe_4S_4]$-clusters that existed in the reduced, +1 state ($[Fe_4S_4]^{1+}$) in the presence of dithionite (1).

Further support for this argument came from an observed correlation between the redox potential of the Fe protein-bound $[Fe_4S_4]$-cluster and the yield of the Fe protein-enabled conversion of CO_2 to CO. Consistent with a decrease in the reduction potentials of both Fe protein-associated $[Fe_4S_4]$-clusters by ~100 mV in the presence of ATP and dithionite (Table 4.1), the yields of CO-formation by ATP-bound VnfH

Table 4.1. Reduction Potential of NifH and VnfH $[Fe_4S_4]^{+1}$-Clusters in the presence of CO_2.

Protein	No Nucleotide	+MgATP
NifH	-301	-405
VnfH	-346	-430

Potentials $E^{o'}$, mV/SHE

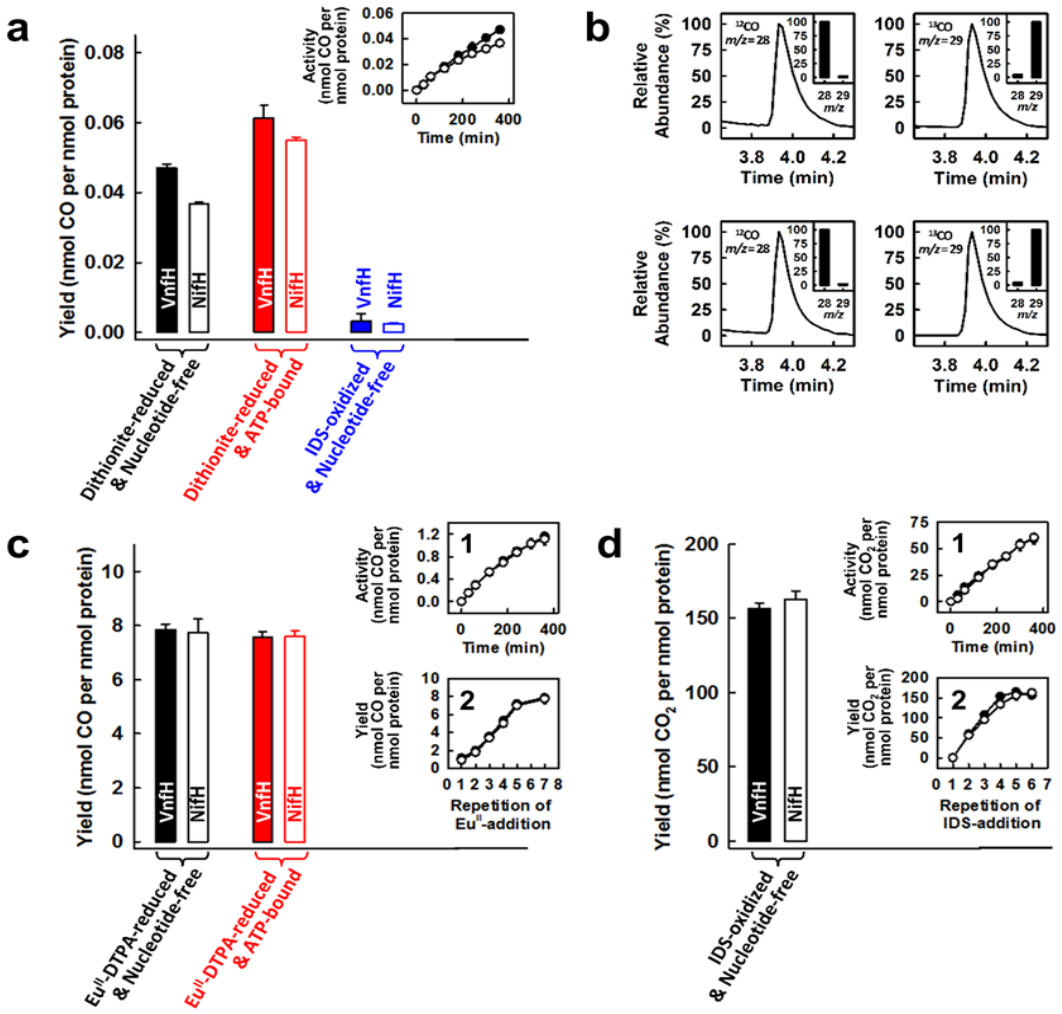

Figure 4.1. *In vitro* reduction of CO_2 to CO by Fe proteins. (a) Yield of CO from CO_2 reduction over 360 min by VnfH or NifH in dithionite-reduced/nucleotide-free, dithionite reduced/ATP-bound, and IDS-oxidized/nucleotide-free states. Inset shows time-dependent formation of CO by dithionite-reduced VnfH (*solid*) or NifH (*open*). (b) GC-MS analysis of CO generated by VnfH (*upper*) or NifH (*lower*) upon reduction of $^{12}CO_2$ (*left*) or $^{13}CO_2$ (*right*). The isotope distributions of CO (^{12}CO, m/z=28; ^{13}CO, m/z=29) generated in these reactions are shown in the insets. (c) Yield of CO from CO_2-reduction after 7 repeated additions of Eu^{II} DTPA by VnfH or NifH in nucleotide-free and ATP-bound states. Inset 1 shows time-dependent formation of CO by Eu^{II} DTPA-reduced VnfH (*solid*) or NifH (*open*) without repeated additions of Eu^{II} DTPA. Inset 2 shows the increase of CO-formation by VnfH (solid) or NifH (open) upon repeated additions of Eu^{II} DTPA. (d) Yield of CO_2 from CO oxidation after 5 repeated additions of IDS by VnfH or NifH in nucleotide-free states. Inset 1 shows time-dependent formation of CO_2 by IDS-oxidized VnfH (solid) or NifH (open) without repeated additions of IDS. Inset 2 shows increase of CO_2-formation by VnfH (solid) or NifH (open) upon repeated additions of IDS. Activities in Insets 2 were determined 360 min after each addition of Eu^{II} DTPA (c) or IDS (d). Activities (a, c, d) were determined based on 3 independent experiments (n = 6) and presented as mean ± s. d. GC-MS experiments (b) were conducted in duplicate, and representative results are shown.

and NifH were 30% and 50%, respectively, higher than nucleotide-free VnfH and NifH (Figure 4.1). Likewise, VnfH was 28% and 12%, respectively, more active than NifH in nucleotide-free and ATP-bound states (Figure 4.1a), which aligns well with the observation that the reduction potentials of VnfH were 45 and 25 mV, respectively, lower than those of NifH in nucleotide-free and ATP-bound states (Table 4.1). Upon substitution of a stronger reductant, europium (II) diethylenetriaminepentaacetate [Eu^{II} DTPA; E°' = -1.14 V at pH 8, SHE (16)], for dithionite [E°' = - 0.436 V at pH 7, SHE (17)], both VnfH and NifH reduced CO_2

a

VnfH	Total volume	Protein concentration	Total protein	Specific activity	Yield	Purification
Purification step	*ml*	*mg/ml*	*g*	*nmol CO/mg/h*	*%*	*-fold*
Crude extract	800	38	30.4	1.6	100	1
Anion exchange chromatography	60	53	3.2	3.4	23	2.19
Gel filtration chromatography	12	48	0.6	4.3	5	2.69

b

NifH	Total volume	Protein concentration	Total protein	Specific activity	Yield	Purification
Purification step	*ml*	*mg/ml*	*g*	*nmol CO/mg/h*	*%*	*-fold*
Crude extract	750	37	27.8	1.8	100	1
Anion exchange chromatography	65	49	3.2	3.3	21	1.83
Gel filtration chromatography	9	39	0.4	4.2	3	2.33

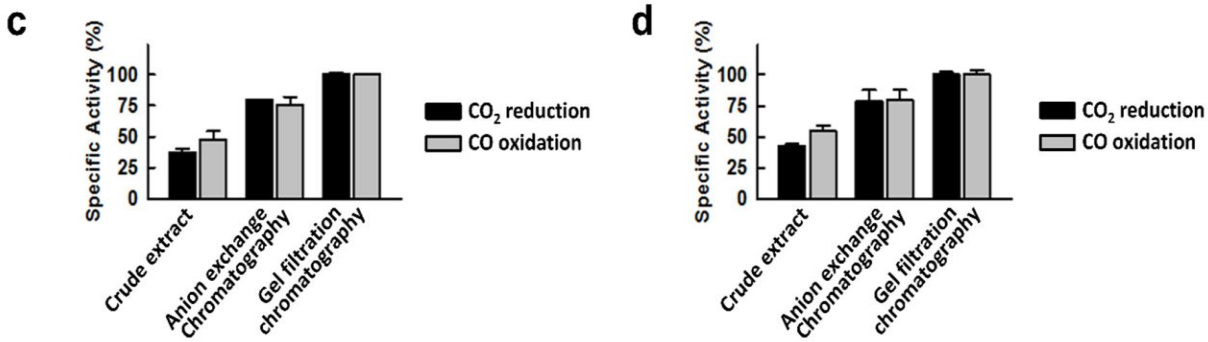

Figure 4.2. Increase of specific activities of Fe proteins during purification. (a,b) Purification tables showing the activities of VnfH (a) and NifH (b) in CO_2 reduction in the presence of Eu^{II} DTPA at different purification stages. (c, d) Increase of the specific activities of VnfH (c) and NifH (d) in CO_2-reduction in the presence of Eu^{II} DTPA (black bars) and in CO oxidation in the presence of IDS (gray bars). Activities are expressed as per mg of total proteins at different purification steps. The maximum activities of purified proteins after the last step of purification (gel filtration chromatography) were: VnfH, 4.3±0.1 nmol CO/mg/h (CO_2 reduction) and 182±10 nmol CO_2/mg/h (CO oxidation); NifH, 4.2±0.2 nmol CO/mg/h (CO_2 reduction) and 195+7 nmol CO_2/mg/h (CO oxidation). These activities are set as 100%, and the activities at earlier steps of the purification procedure (crude extract, anion exchange chromatography) are expressed accordingly (c, d). Each Fe protein was purified 6 times, 3 times from the wildtype strains and 3 times from the variant strains containing deletions of genes encoding the catalytic partners of the Fe proteins. Activities were determined based on 6 independent experiments (n = 12) and presented as mean ± s. d.

to CO at ~30-fold higher rates, reaching a catalytic turnover number (TON) of CO_2 (1.16 nmol CO/nmol protein or a TON of 1.16) over 360 min (Figure 4.1c, *inset 1*; also see Figure 4.2 and Figure 4.3). Repeated addition of Eu^{II} DTPA resulted in an initial near-linear increase of CO formation by both VnfH and NifH (Figure 4.1, *inset 2*), reaching a TON of ~8 after 7 repetitions in both VnfH- and NifH-catalyzed reactions (Figure 4.1c, *bars*).

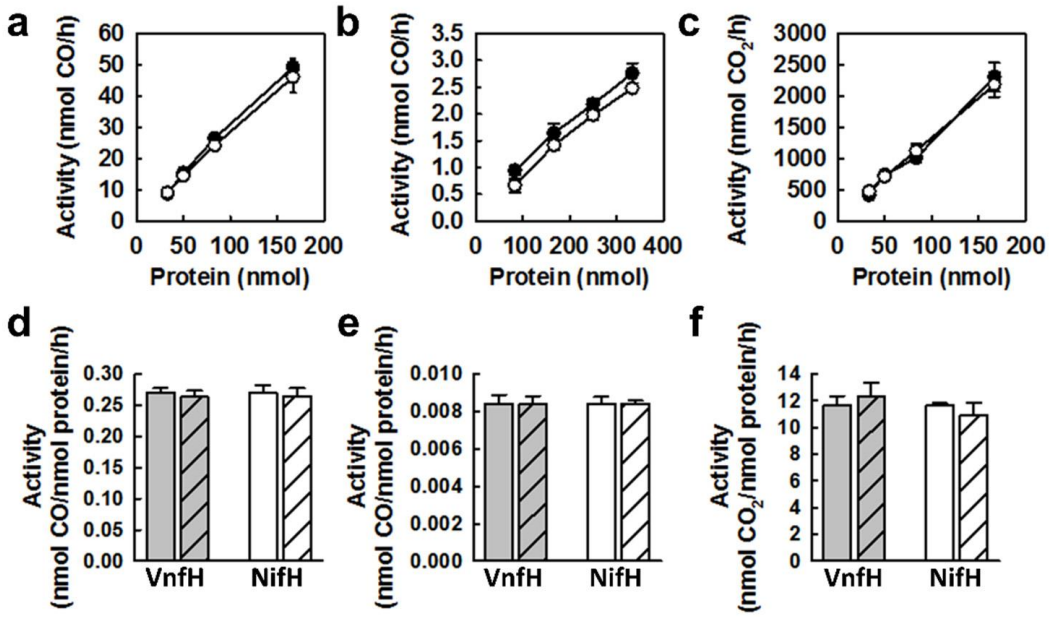

Figure 4.3. Linear correlation between the activity and amount of the purified Fe protein and reproducibility of activity from different protein preparations. (a-c) Activities of VnfH (solid circles) and NifH (open circles) in CO_2-eduction in the presence of Eu^{II} DTPA (a) and dithionite (b), and in CO oxidation in the presence of IDS (c). Activities of proteins were determined based on 2 independent experiments (n = 4) and presented as mean ± s. d. (d-f) Average activities of VnfH (gray bars) and NifH (white bars) in CO_2 reduction in the presence of Eu^{II} DTPA (d) and dithionite (e), and in CO oxidation in the presence of IDS (f). Each Fe protein was purified 6 times, 3 times from the wildtype strains (solid bars) and 3 times from variant strains containing deletions of genes encoding the catalytic partners of the Fe proteins (striped bars). Activities were determined based on 3 independent experiments (n = 6) and presented as mean ± s. d.

4.3.2 EPR Analysis of CO_2- and CO-bound Iron Proteins

EPR analysis provided further insights into the interaction between the Fe protein-bound $[Fe_4S_4]$-cluster and the substrate CO_2. In the absence of CO_2, both VnfH and NifH displayed perpendicular mode, $S = 1/2$ signals that originated from their respective $[Fe_4S_4]^{1+}$-clusters, with the signals assuming a rhombic lineshape without nucleotide and an axial lineshape upon binding of ATP (Figure 4.4a, b, *red*). Following incubation with CO_2, the signal intensities of VnfH and NifH decreased, which resulted from oxidation of the VnfH- and NifH-associated $[Fe_4S_4]^{1+}$-clusters to an EPR silent, $[Fe_4S_4]^{2+}$-state concomitant with the transfer of electrons from the reduced clusters to CO_2 (Figure 4.4a, b, *black*). However, the signals of NifH and VnfH only showed a moderate decrease of intensity in the absence of nucleotide (Figure 4.4a, b, *left*) but disappeared completely upon binding of ATP (Figure 4.4a, b, *right*), demonstrating a more efficient transfer of electrons to CO_2 in the nucleotide-bound proteins. The Eu^{II} DTPA-reduced VnfH and NifH, on the other hand, displayed a parallel mode, $g = 16.4$ signal that was characteristic of $[Fe_4S_4]$-clusters in the all-ferrous ($[Fe_4S_4]^0$) state (Figure 4.4c, d, *red*) (18). This signal disappeared completely upon incubation with CO_2 (Figure 4.4c, d, *black*), suggesting oxidation of the VnfH- and NifH-associated $[Fe_4S_4]^0$ clusters to an EPR silent, $[Fe_4S_4]^{2+}$-state following the transfer of electrons to CO_2. Moreover, in the presence of CO_2, Eu^{II} DTPA-reduced VnfH and NifH displayed a small, perpendicular-mode signal at $g = 1.99$ (Figure 4.4e, f). Such a signal was also observed when dithionite-reduced VnfH and NifH were incubated with CO_2 (Figure 4.4a, b, *arrows*), although the signals were much smaller in the spectra of ATP-bound proteins and further masked by the $S = 1/2$ signals in the spectra of nucleotide-free proteins. The appearance of this unique signal in the presence

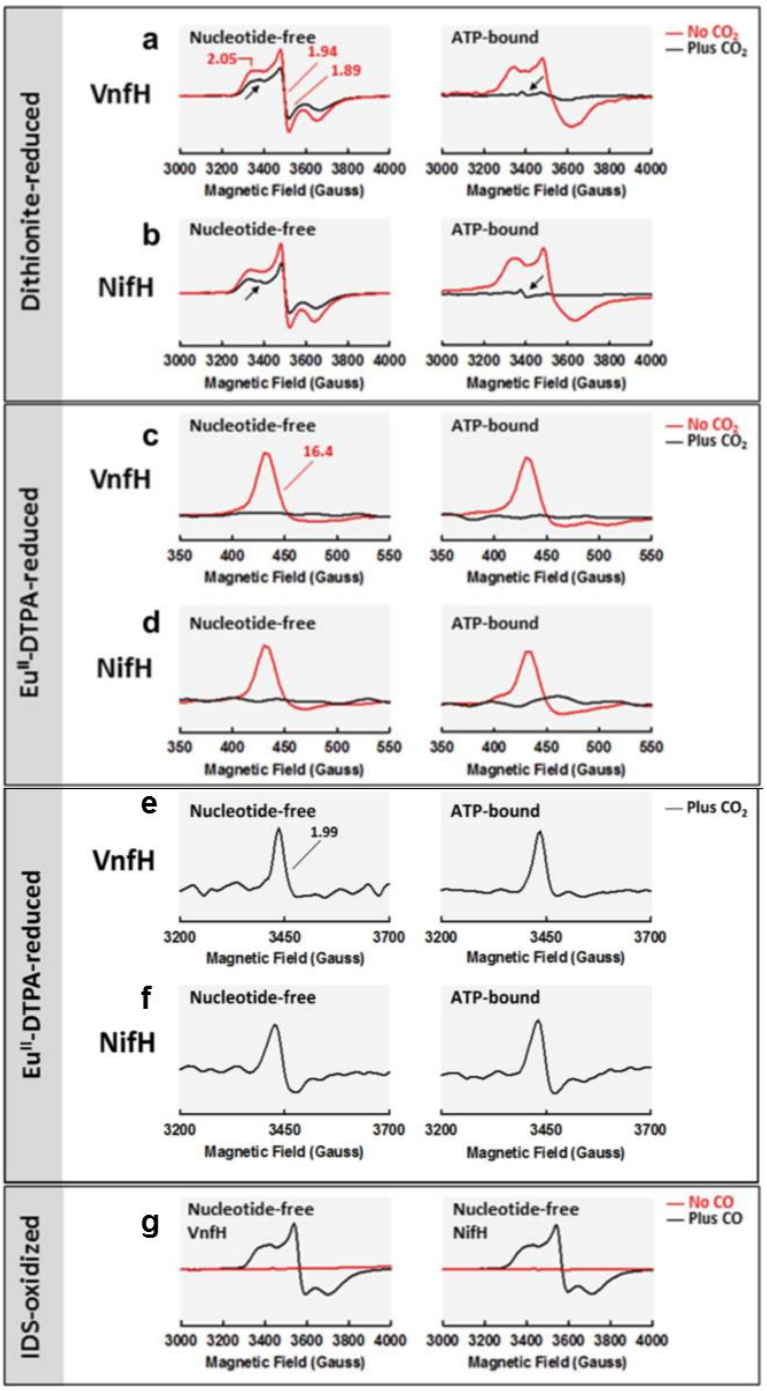

Figure 4.4. Interactions of CO_2 and CO with the $[Fe_4S_4]$-clusters of the Fe proteins. (a-f) perpendicular (a, b)- and parallel (c, f)-mode EPR spectra of nucleotide-free (*left*) and ATP-bound (*right*) VnfH and NifH in dithionite- and Eu^{II} DTPA-reduced states in the absence (*red*) or presence (*black*) of CO_2. (g) Perpendicular mode EPR spectra of nucleotide-free VnfH (*left*) and NifH (*right*) in IDS-oxidized states in the absence (*red*) or presence (*black*) of CO. The perpendicular EPR feature that appeared upon interaction of CO_2 with the VnfH- or NifH associated $[Fe_4S_4]$-cluster is indicated by an arrow (a, b). The same feature is also observed in the perpendicular mode EPR spectra of Eu^{II} DTPA-reduced VnfH and NifH upon incubation with substrate CO_2 (e, f). Spectra were recorded at 10 K. The *g* values are indicated.

of CO_2 suggests an impact of interaction with, or binding of, CO_2 or CO_2-derived intermediates on the electronic properties of the $[Fe_4S_4]$-clusters within these Fe proteins.

4.3.3 Comparison of Fe Proteins with Carbon Monoxide Dehydrogenase

The ability of Fe protein to catalyze the interconversion between CO and CO_2 establishes this protein as an enzymatic mimic of CO dehydrogenase (CODH) (19, 20), the only other enzyme known to catalyze the same reversible reactions. In the presence of dithionite, NifH and VnfH are able to reduce CO_2 and form ~0.04 nmol CO/nmol protein without nucleotide (Figure 4.1a). Under Eu^{II} DTPA this product formation increases 30-fold to ~1.2 nmol CO/nmol protein over a period of 360 min (Figure 4.1c *inset 1*). Readding Eu^{II} DPTA 7-times further prolongs the turnover and results in a TON of 8 (Figure 4.1c). After incubating dithionite and Eu^{II} DTPA reduced NifH and VnfH with CO_2 the $[Fe_4S_4]^{+1}$- (Figure 4.4a, b) and the $[Fe_4S_4]^0$-state (Figure 4.4c, d), respectively, disappear and the $[Fe_4S_4]$-cluster takes on the EPR-silent $[Fe_4S_4]^{+2}$-state (Figure 4.4a-d, *black lines*). Presumably, this change in the EPR signal derives from the electron transfer from the $[Fe_4S_4]$-cluster to the substrate CO_2.

Moreover, in the presence of IDS, the nucleotide-free VnfH and NifH were capable of oxidizing CO to CO_2 (Figure 4.1d). Both proteins generated ~60 nmol CO_2/nmol protein (or a TON of ~60) from CO oxidation over 360 min (Figure 4.1d, *inset 1*; also see Figure 4.2 and Figure 4.3), and repeated addition of IDS led to an initial near-linear increase of CO_2-formation by both proteins (Figure 4.1d, *inset 2*), reaching a TON of ~160 after 6 repetitions (Figure 4.1d, *bars*). Following incubation with CO, the IDS-oxidized VnfH and NifH transitioned from an EPR-silent, $[Fe_4S_4]^{2+}$-state (Figure 4.4g, *red*) to one that displayed the $[Fe_4S_4]^{1+}$-characteristic, $S = 1/2$ signal (Figure 4.4g, *black*), which resulted from reduction of the $[Fe_4S_4]^{2+}$-cluster concomitant with transfer of electrons from CO to the oxidized cluster.

The considerably higher rates of CO oxidation than CO_2 reduction by both Fe proteins likely contributes to the low efficiencies of these proteins in CO_2-conversion.

Compared to the Fe protein, CODHs catalyze the interconversion between CO_2 and CO at considerably higher rates (21-23). The CODH from *Rhodospirillum rubrum* (21), for example, catalyzes CO_2 reduction at turnover rates between 0.19 and 45 s^{-1} and CO oxidation at a turnover rate as high as 40,000 s^{-1}. Interestingly, while the Fe protein resembles CODH in having a higher rate of CO oxidation than CO_2 reduction, the equilibrium seems to be shifted towards CO_2 reduction, given a substantially lower (by ~1-2 orders of magnitude) ratio between the rates of CO oxidation and CO_2 reduction by Fe proteins as compared to the ratios reported so far for the CODHs.

4.3.4 *In vivo* Reduction of CO_2 to CO

Excitingly, conversion of CO_2 to CO could be achieved *in vivo* by *A. vinelandii* strains expressing VnfH and NifH, respectively, as the sole components of Mo and V nitrogenases under N_2-fixing conditions. When the growth medium was supplemented with ammonia, the expression of VnfH (Figure 4.5, *lane 3*) or NifH (Figure 4.5, *lane 6*) was repressed and, consequently, CO could hardly be detected as a product of CO_2 reduction by either strain (Figure 4.6a, c, *gray bars*). Upon depletion of ammonia in the growth medium, however, the expression of VnfH (Figure 4.5, *lane 2*) or NifH

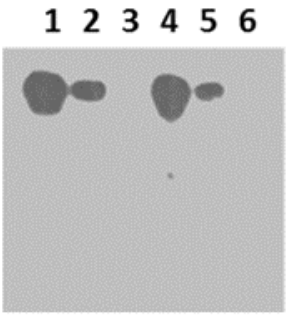

Figure 4.5. Western blot analysis of Fe protein expression. Lane 1, purified VnfH; lane 2, crude extract of VnfH-expressing *A. vinelandii* strain grown in the absence of ammonia; lane 3, crude extract of VnfH-expressing *A. vinelandii* strain grown in the presence of ammonia; lane 4, purified NifH; lane 5, crude extract of NifH-expressing *A. vinelandii* strain grown in the absence of ammonia; lane 6, crude extract of NifH-expressing *A. vinelandii* strain grown in the presence of ammonia. The western blot analysis was conducted in triplicate, and the representative result is shown.

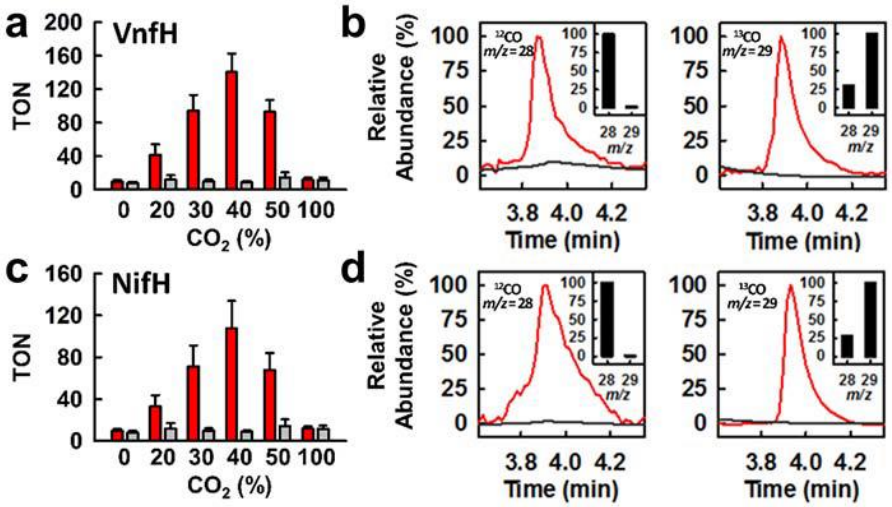

Figure 4.6. *In vivo* reduction of CO_2 to CO by Fe proteins. Formation of CO from CO_2 reduction by *A. vinelandii* strains expressing VnfH (**a**) and NifH (**c**) in the absence (*red*) or presence (*gray*) of ammonia when CO_2 was supplied as a substrate at different concentrations. GC-MS analysis of CO generated by *A. vinelandii* strains expressing VnfH (**b**) or NifH (**d**) in the absence of ammonia (*red traces*) upon reduction of $^{12}CO_2$ (*left*) or $^{13}CO_2$ (*right*). No CO was detected by GC-MS analysis when these strains were grown in the presence of ammonia (*gray traces*). The isotope distributions of CO (^{12}CO, m/z=28; ^{13}CO, m/z=29) generated in these reactions are shown in the insets. Activities (a, c) were determined based on 4 independent experiments (n = 8) and presented as mean ± s. d. GC-MS experiments (b, d) were conducted in duplicate, and representative results are shown.

(Figure 4.5, *lane 5*) was up-regulated concomitant with a significant increase of the activities of both strains to reduce CO_2 to CO (Figure 4.6a, c, *red bars*). Both VnfH- and NifH-expressing strains displayed maximum CO_2 reducing activities at 40% CO_2, showing TONs of 140 (Figure 4.6a) and 110 (Figure 4.6c), respectively, over 14 h. GC–MS analysis further confirmed that the carbon in CO was derived from CO_2 in the *in vivo* reactions catalyzed by VnfH (Figure 4.6b) and NifH (Figure 4.6d). More importantly, VnfH and NifH demonstrated considerably higher CO_2 reducing activities *in vivo* (up to an average TON of 10 per h; *see* Figure 4.6a) than *in vitro* (up to an average TON of 0.2 per h; *see* Figure 4.1c, *inset 2*), which could originate from a reducing intracellular environment of *A. vinelandii* rendered by its well-known O_2-protection mechanisms and abundance of ferredoxins (24) and/or the presence of a

physiological electron donor(s) (25, 26) that permit(s) the VnfH- and NifH- associated clusters to shuttle between 0 and +2 states to supply electrons for the *in vivo* CO_2 reduction. The latter scenario is particularly interesting, as it bears relevance to the long-standing debate of whether the $[Fe_4S_4]^{0/2+}$-couple is used by the Fe protein under physiological conditions (27, 28) and, if so, which spin state (S = 0 or S = 4) is adopted by the all-ferrous $[Fe_4S_4]^0$-cluster (18, 25-28).

4.4 Summary and Conclusion

The fact that CO_2 can be activated and reduced by Fe proteins under ambient conditions is important because it represents a potential template for the future development of strategies for the removal and sequestration of CO_2 concomitant with the conversion of this greenhouse gas into valuable chemical products. The capability of Fe protein, a homometallic FeS enzyme, to effect ambient CO_2 reduction via a distinct mechanism than the heterometallic CODH enzymes opens up new avenues for studies that aim at understanding and improving the process of CO_2 conversion. Moreover, the observation of the *in vivo* reduction of CO_2 to CO by Fe proteins in the non-carboxydotrophic organism *A. vinelandii* suggests a possible biotechnological advantage of this system in CO production, as the CODHs predominantly function in the production of energy (via CO oxidation) and biomass (via CO_2 reduction coupled with carbon fixation) in carboxydotrophic organisms rather than releasing CO as an unwanted product of CO_2 reduction. The utility of the Fe protein-catalyzed reactions, therefore, can be appreciated both from a theoretical standpoint and in a practical vein. Alone, the Fe protein can either be used as a simple, FeS-based mechanistic model for investigations of CO_2 activation, or it can be exploited for its ability to conduct ambient

reduction of CO_2 to syngas CO *in vivo*. As the reductase component of V nitrogenase, the Fe protein (VnfH) was recently shown to work in concert with its catalytic partner (VnfDGK) to enable the *in vivo* conversion of CO to hydrocarbons (see Chapter 5). This exciting discovery suggests a realistic possibility to engineer an *A. vinelandii*-based whole-cell system, which couples the *in vivo* conversion of CO_2 to CO (by VnfH) and the *in vivo* conversion of CO to hydrocarbons (by VnfH/VnfDGK) into a two-step process for recycling CO_2 into useful chemical/fuel products.

4.5 Acknowledgments

I would like to thank Dr. Chi Chung Lee (University of California, Irvine) for determining the reduction potential of the NifH and VnfH $[Fe_4S_4]^{+1}$-clusters and carrying out the formate assays, and Dr. Martin Stiebritz (University of California, Irvine) for the DFT calculations. I also thank the Nature Publishing Group for publishing portions of this Chapter in *Nature Chemical Biology* (29). This work is supported by UCI startup funds and a Hellman Fellowship to Dr. Yilin Hu.

4.6 References

1. Burgess BK & Lowe DJ (1996) Mechanism of Molybdenum Nitrogenase. *Chem Rev* 96(7):2983-3012.
2. Hu Y & Ribbe MW (2015) Nitrogenase and homologs. *J Biol Inorg Chem* 20(2):435-45.
3. Hoffman BM, Lukoyanov D, Yang ZY, Dean DR, & Seefeldt LC (2014) Mechanism of nitrogen fixation by nitrogenase: the next stage. *Chem Rev* 114(8):4041-62.

4. Rees DC, Akif Tezcan F, Haynes CA, Walton MY, Andrade S, Einsle O, & Howard JB (2005) Structural basis of biological nitrogen fixation. *Philos Trans A Math Phys Eng Sci* 363(1829):971-84; discussion 1035-40.

5. Eady RR (1996) Structure-Function Relationships of Alternative Nitrogenases. *Chem Rev* 96(7):3013-30.

6. Hu Y, Lee CC, & Ribbe MW (2011) Extending the carbon chain: hydrocarbon formation catalyzed by vanadium/molybdenum nitrogenases. *Science* 333(6043):753-5.

7. Lee CC, Hu Y, & Ribbe MW (2010) Vanadium nitrogenase reduces CO. *Science* 329(5992):642.

8. Lee CC, Hu Y, & Ribbe MW (2009) Unique features of the nitrogenase VFe protein from Azotobacter vinelandii. *Proc Natl Acad Sci U S A* 106(23):9209-14.

9. Hu Y, Fay AW, & Ribbe MW (2005) Identification of a nitrogenase FeMo cofactor precursor on NifEN complex. *Proc Natl Acad Sci U S A* 102(9):3236-41.

10. Bursey EH & Burgess BK (1998) The role of methionine 156 in cross-subunit nucleotide interactions in the iron protein of nitrogenase. *J Biol Chem* 273(45):29678-85.

11. Kage S, Kudo K, Ikeda H, & Ikeda N (2004) Simultaneous determination of formate and acetate in whole blood and urine from humans using gas chromatography-mass spectrometry. *J Chromatogr B Analyt Technol Biomed Life Sci* 805(1):113-7.

12. Ribbe MW, Bursey EH, & Burgess BK (2000) Identification of an Fe protein residue (Glu(146)) of Azotobacter vinelandii nitrogenase that is specifically involved in FeMo cofactor insertion. *J Biol Chem* 275(23):17631-8.

13. Schneider CA, Rasband WS, & Eliceiri KW (2012) NIH Image to ImageJ: 25 years of image analysis. *Nat Methods* 9(7):671-5.

14. Rupnik K, Lee CC, Hu Y, Ribbe MW, & Hales BJ (2011) [4Fe4S]2+ clusters exhibit ground-state paramagnetism. *J Am Chem Soc* 133(18):6871-3.

15. Eady RR, Richardson TH, Miller RW, Hawkins M, & Lowe DJ (1988) The vanadium nitrogenase of Azotobacter chroococcum. Purification and properties of the Fe protein. *Biochem J* 256(1):189-96.

16. Vincent KA, Tilley GJ, Quammie NC, Streeter I, Burgess BK, Cheesman MR, & Armstrong FA (2003) Instantaneous, stoichiometric generation of powerfully reducing states of protein active sites using Eu(II) and polyaminocarboxylate ligands. *Chem Commun (Camb)* (20):2590-1.

17. Mayhew SG (1978) The redox potential of dithionite and SO-2 from equilibrium reactions with flavodoxins, methyl viologen and hydrogen plus hydrogenase. *Eur J Biochem* 85(2):535-47.

18. Angove HC, Yoo SJ, Munck E, & Burgess BK (1998) An all-ferrous state of the Fe protein of nitrogenase. Interaction with nucleotides and electron transfer to the MoFe protein. *J Biol Chem* 273(41):26330-7.

19. Kung Y & Drennan CL (2011) A role for nickel-iron cofactors in biological carbon monoxide and carbon dioxide utilization. *Curr Opin Chem Biol* 15(2):276-83.

20. Jeoung JH, Fesseler J, Goetzl S, & Dobbek H (2014) Carbon monoxide. Toxic gas and fuel for anaerobes and aerobes: carbon monoxide dehydrogenases. *Met Ions Life Sci* 14:37-69.

21. Ensign SA (1995) Reactivity of carbon monoxide dehydrogenase from Rhodospirillum rubrum with carbon dioxide, carbonyl sulfide, and carbon disulfide. *Biochemistry* 34(16):5372-8.

22. Lindahl PA, Munck E, & Ragsdale SW (1990) CO dehydrogenase from Clostridium thermoaceticum. EPR and electrochemical studies in CO2 and argon atmospheres. *J Biol Chem* 265(7):3873-9.

23. Kumar M, Lu WP, & Ragsdale SW (1994) Binding of carbon disulfide to the site of acetyl-CoA synthesis by the nickel-iron-sulfur protein, carbon monoxide dehydrogenase, from Clostridium thermoaceticum. *Biochemistry* 33(32):9769-77.

24. Orme-Johnson WH & Sands RH (1973), ed Lovenberg W (Academic Press, New York and London), pp 195-238.

25. Lowery TJ, Wilson PE, Zhang B, Bunker J, Harrison RG, Nyborg AC, Thiriot D, & Watt GD (2006) Flavodoxin hydroquinone reduces Azotobacter vinelandii Fe protein to the all-ferrous redox state with a S = 0 spin state. *Proc Natl Acad Sci U S A* 103(46):17131-6.

26. Jacobs D & Watt GD (2013) Nucleotide-assisted [Fe4S4] redox state interconversions of the Azotobacter vinelandii Fe protein and their relevance to nitrogenase catalysis. *Biochemistry* 52(28):4791-9.

27. Howard JB & Rees DC (2006) How many metals does it take to fix N2? A mechanistic overview of biological nitrogen fixation. *Proc Natl Acad Sci U S A* 103(46):17088-93.

28. Erickson JA, Nyborg AC, Johnson JL, Truscott SM, Gunn A, Nordmeyer FR, & Watt GD (1999) Enhanced efficiency of ATP hydrolysis during nitrogenase catalysis utilizing

reductants that form the all-ferrous redox state of the Fe protein. *Biochemistry* 38(43):14279-85.

29. Rebelein JG, Stiebritz M, Lee CC, & Hu Y (2016) Activation and Reduction of Carbon Dioxide by Nitrogenase Iron Proteins. *Nat Chem Biol* (In Press).

Chapter 5: *in vivo* Hydrocarbon formation by Vanadium Nitrogenase

5.1 Introduction

Recently, nitrogenase was shown to reduce carbon monoxide (CO) to hydrocarbons *in vitro*, an important reaction of potential significance for the future development of strategies to recycle the toxic CO gas - a waste product of steel, PVC and ferroalloys industries - into useful chemical and fuel products, such as ethylene (C_2H_4) and propane (C_3H_8) (1, 2). The "conventional" molybdenum (Mo) and "alternative" vanadium (V) nitrogenases (3) are two homologous members of this enzyme family. Both enzymes comprise a reductase component (*nifH*- or *vnfH*-encoded Fe protein) and a catalytic component (*nifDK*-encoded MoFe protein or *vnfDGK*-encoded VFe protein) (see Chapter 1). Catalysis by both nitrogenases involves the formation of a functional complex between their respective component proteins, which facilitates adenosine triphosphate (ATP)-dependent transfer of electrons from the reductase component to the cofactor site of the catalytic component, where substrate reduction takes place. Interestingly, the V nitrogenase of *Azotobacter vinelandii* is considerably more active than its Mo-counterpart in CO reduction, catalyzing this reaction at a rate of 16 nmol reduced carbon/nmol protein/min as compared to a rate of 0.02 nmol reduced carbon/nmol protein/min by the Mo nitrogenase (1, 4). This observation in conjunction with the recent finding that *A. vinelandii* strains expressing VnfH and NifH, respectively, as the sole components of Mo and V nitrogenases can convert CO_2 to CO *in vivo* under N_2-fixing conditions (see Chapter 4.3.4), has led to questions of whether the cells expressing the entire V nitrogenase, consisting of Fe and VFe protein, can also reduce CO to hydrocarbons *in vivo* and, if so, whether these cells incorporate the CO-derived carbon into the cell mass or if they simply release the products of the CO reduction as byproducts.

5.2 Materials and Methods

5.2.1 Reagents

Unless otherwise specified, all chemicals were purchased from Fisher (Pittsburgh, PA) or Sigma-Aldrich (St. Louis, MO). Natural-abundance ^{12}CO (99.9% purity) was purchased from Praxair (Danbury, CT), whereas ^{13}CO (≥ 98% isotopic purity) was purchased from Cambridge Isotope Labs (Tewksbury, MA).

5.2.2 Analysis of *in vivo* CO Reduction by Nitrogenase-expressing Strains of *A. vinelandii*

A. vinelandii strains expressing the Mo and V nitrogenases, respectively (1, 5), were grown in two 500 mL Erlenmeyer flasks, each containing 250 mL Burke's minimal medium supplemented with 2 mM ammonium acetate (NH_4OAc) and either 11 μM Na_2MoO_4 (in the case of the strain expressing Mo nitrogenase) or 30 μM Na_3VO_4 (in the case of the strain expressing V nitrogenase). The cultures were grown at 30 °C with shaking at 200 rpm, and the growth rates were monitored by measuring cell densities at 436 nm using a Genesys 20 spectrophotometer (Spectronic, Westbury, NY). After 20 h and 23 h, when OD_{436} of the cultures started to plateau at ~2.4 (the strain expressing Mo nitrogenase) and ~1.4 (the strain expressing V nitrogenase), respectively, the Erlenmeyer flasks were capped by airtight stoppers, and CO was added at a concentration of 10% to the head spaces of these flasks. Subsequently, the cultures were allowed to grow at 30 °C with shaking at 200 rpm, and 250 μL of headspace sample was taken from each culture at 0, 1, 2, 3, 4, 5, 6, 7 and 8 h after CO addition and examined for hydrocarbon formation. As controls, *A. vinelandii* cultures expressing the Mo and V nitrogenases, respectively, were prepared by the same procedure as described above except that CO was not added when ammonia was exhausted in the

growth media. Hydrocarbon products were quantified by GC-FID using a previously described procedure (1, 2). Specifically, each 250 μL headspace sample was injected onto an activated alumina column (Grace, Columbia, MD), which was held at 55 °C for 1 min, heated to 155 °C at 12.5 °C /min, and held at 155 °C during the course of measurement. The quantities of all products were determined by using a Scott gas mixture containing 15 ppm of each hydrocarbon compound (Houston, TX). The detection limits were 10.27, 6.22, 9.73 and 2.79 nmol/L, respectively, for CH_4, C_2H_4, C_2H_6 and C_3H_8.

5.2.3 Determination of Optimal CO Concentration for *in vivo* Hydrocarbon Formation

A. vinelandii strains expressing Mo and V nitrogenases, respectively, were grown as described in Chapter 5.2.2, in three set of 500 mL Erlenmeyer flasks (six flasks/set), each containing 250 mL Burke's minimal medium supplemented with 2 mM NH_4OAc and (i) and (ii) 30 μM Na_3VO_4 (in the case of the strain expressing V nitrogenase); and (iii) 11 μM Na_2MoO_4 (in the case of the strain expressing Mo nitrogenase). When OD_{436} of the cultures reached ~2.4 (the strain expressing Mo nitrogenase) and ~1.4 (the strain expressing V nitrogenase), respectively, the six cultures of set ii were supplemented with 2 mM NH_4OAc. Subsequently, all flasks were capped airtight, followed by addition of CO at 0, 7.5%, 15%, 22.5%, 30% and 37.5%, respectively, to the gas phases of the six flasks in each set of cultures. The cultures were then allowed to grow at 30 °C with shaking at 200 rpm for 8 h, and 250 μL of headspace sample was taken from each culture and examined by GC-FID for hydrocarbon formation (see above). The concentration of the VFe protein was determined based on the average yield of five independent purifications (5).

5.2.4 Improvement of *in vivo* Hydrocarbon Formation by Intermittent Air Exposure

A 250 mL culture of the *A. vinelandii* strain expressing the V nitrogenase was grown in a 500 mL Erlenmeyer flask as described in Chapter 5.2.2 until the cell density started to plateau. At this point, the flask was capped airtight, and CO was added at a concentration of 15% to the gas phase of this culture. The culture was then allowed to grow at 30 °C with shaking at 200 rpm for 4 h before 250 μL of the headspace sample was taken and examined by GC-FID for hydrocarbon formation (see Chapter 5.2.2). Following this procedure, the airtight stopper of the flask was replaced by a sterile foam plug, and the culture was incubated at 30 °C with shaking at 200 rpm for 20 min. Subsequently, the flask was capped airtight again, followed by addition of 15% CO to the gas phase, incubation of culture with CO for 4 h, determination of hydrocarbon formation by GC-FID, and aeration of the culture for 20 min as described in Chapter 5.2.4. This procedure was repeated for a total of 20 times until the linear increase of hydrocarbon formation started to plateau.

5.2.5 GC-MS Analysis of Hydrocarbons Generated by *in vivo* CO Reduction

A. vinelandii strain expressing the V nitrogenase was grown as described in Chapter 5.2.2 until the cell density started to plateau, when the flask was capped airtight, followed by addition of ^{13}CO at a concentration of 15% to the gas phase of this culture. The culture was grown for another 8 h before 250 μL headspace sample was taken and analyzed by GC-MS using a Thermo Scientific Trace 1300 GC system coupled to a Thermo ISQ QD (Thermo Electron North America LLC, Madison, WI) and a previously described procedure (1, 2). Specifically, a 250 μL gas sample was injected into a split/splitless injector operated at 120 °C in in split mode, with a split ratio of 5. A 1-mm ID liner was used to optimize the sensitivity of gas separation, which was achieved on an HP-PLOT-Q capillary column

(0.320 mm ID x 30 m length, Agilent Technologies, Santa Clara, CA) that was held at 40 °C for 2 min, heated to 180 °C at a rate of 10 °C /min, and held at 180 °C for 1 min. The carrier gas, helium, was passed through the column at a rate of 1.1 mL/min. The mass spectrometer was operated in electron impact (EI) ionization mode, and the identities of C_2H_4, C_2H_6 and C_3H_8 were confirmed by comparing their masses and retention times with those of the Scott standard alkane and alkene gas mixture.

5.2.6 NanoSIMS Analysis of *A. vinelandii* Cultures Incubated with ^{12}CO and ^{13}CO

For experiments presented in Figure 5.3, *A. vinelandii* strain expressing the V nitrogenase was grown in two 250 mL Erlenmeyer flasks, each containing 100 mL Burke's minimal medium (which contained sucrose as the carbon source) (6) supplemented with 2 mM ammonium acetate and 30 μM Na_3VO_4. The cultures were incubated at 30 °C with shaking at 200 rpm until the cell densities started to plateau. Subsequently, the Erlenmeyer flasks were capped airtight, followed by addition of 15% ^{12}CO and ^{13}CO, respectively, to the gas phases of the two cultures. The cultures were allowed to undergo 13 repetitions of 4 h-CO incubation with 20 min-aeration, with the formation of hydrocarbons monitored throughout the process. For experiments presented in Figure 5.4, three 100 mL cultures were prepared as described in Chapter 5.2.2 by growing cells till the cell densities started to plateau, followed by exchange of the gas phases into gas mixtures containing (i) 65% $^{15}N_2$, 15% $^{14}N_2$ and 20% O_2; (ii) 65% $^{15}N_2$, 15% ^{13}CO and 20% O_2; and (iii) 65% $^{14}N_2$, 15% ^{12}CO and 20% O_2, respectively. The CO-free culture was then grown for 4 h; whereas the ^{12}CO- and ^{13}CO-containing cultures were allowed to undergo 13 repetitions of 4 h-CO incubation with 20 min-aeration periods. For nanoSIMS analysis, an aliquot of 250 μL of each culture (diluted to the same OD_{436}) was pipetted on a silicon wafer (University Wafer, Boston, MA) with a

diameter of 2.5 cm. The samples were subsequently fixed with a phosphate-buffered saline (PBS) solution containing 4% formaldehyde for 1 h at room temperature, washed sequentially with PBS, 1:1 PBS/ethanol and ethanol, and dried on the wafer (7). The secondary ion ($12C^-$ and $13C^-$) and secondary electron images were acquired with a CAMECA NanoSIMS 50L ion microprobe (Caltech, Pasadena, CA). A +8 keV primary Cs+ beam of ~1 pA was used to raster the samples in 12x12, 10x10, or 2x2 microns areas. Secondary ion ($12C^-$ and $13C^-$) images of -8 keV were collected simultaneously with electron multiplier (EM) detectors. The interference from $12CH^-$ to $13C^-$ was separated with a mass resolving power (MRP) of ~5000. Ion images of 256x256 pixels were collected in 3 different regions of interest (ROI)/sample, 2 or 3 frames/ROI, and 15 min/frame, and processed with L'image software (http://limagesoftware.net/). The standard used for calculations of $\delta^{13}C$ and $\delta^{15}N$ values were a $^{13}C/^{12}C$ isotope ratio of 0.011237 (8) and a $^{15}N/^{14}N$ isotope ratio of 0.003677 (8-10), respectively.

5.2.7 LC-MS analysis of Acetyl-CoA Formation by CO-incubated *A. vinelandii* Cultures

A. vinelandii strain expressing the V nitrogenase was grown in three 250 mL batches in 500 mL Erlenmeyer flasks as described Chapter 5.2.2 until OD_{436} of these cultures reached approximately 1.4. Subsequently, these cultures were harvested individually by centrifugation at 15,000 g, 4 °C for 10 min, followed by resuspension of each pellet in 250 mL Burke's minimal medium that contained no ammonia and a limited amount of sucrose (2 g/L; equivalent to 1/10 of that normally used in the Burke's minimal medium). The flasks were then capped airtight, followed by addition of no CO, 15% ^{12}CO and 15% ^{13}CO, respectively, to the headspaces of these re-suspended cultures, continued incubation of these cultures at 30 °C with shaking at 200 rpm for 18 h, harvesting of cells by centrifugation at 15,000 g, 4 °C

for 10 min, and storage of pellets at -80 °C. An amount of 0.5 *g* of each pellet was lysed by addition of 1.5 mL of 10% perchloric acid, followed by vigorous vortexing of the mixture. The cell lysate was then allowed to sit for 10 min before the pH of the solution was adjusted to 7.4 by 1 M Tris-HCl (pH 7.5). Each lysate was then filtered using Amicon Ultra 30,000 MWCO centrifugal filters (EMD Millipore, Billerica, MA) and analyzed for acetyl-CoA by LC-MS analysis. Specifically, acetyl-CoA was separated by a Thermo Scientific Dionex Ultimate 3000 UHPLC system on an Acclaim 120 C18 column (4.6x100 mm, 5 μm particle size), which is directly coupled with an MSQ Plus single quadruple mass spectrometer (Thermo Electron North America LLC, Madison, WI). The column was first equilibrated with 100% buffer A (95%:5% H_2O/acetonitrile, 5 mM ammonia formate, pH 7.5) for 15 min. Each run was initiated upon injection of a 100 μL sample onto the column, followed by application of an isocratic flow of 100% buffer A for 5 min, a linear gradient of 0–100% buffer B over 5 min, and an isocratic flow of 100% buffer B for 10 min. To re-equilibrate the column after each run, a linear gradient of 100–0% buffer B was applied for 5 min, followed by an isocratic flow of 100% buffer A for 5 min over the column. The flow rate was kept at 0.5 mL/min, while the column was maintained at 30 °C throughout the runs. A purchased standard of acetyl-CoA (Sigma-Aldrich, St Louis, MO) was used to establish the retention time of this molecule on this column. Mass determination of different acetyl-CoA species was performed via electrospray ionization in positive ion mode (ESI+) with the following mass spectrometer parameters: capillary voltage, 3,000 V; sample cone voltage, 30 V; desolvation temperature, 120 °C; and source temperature, 120 °C. The masses 810 (acetyl-CoA), 811 (one ^{13}C-incorporated acetyl-CoA) and 812 (two ^{13}C-incorporated acetyl-CoA) were traced using SIM mode.

5.3 Results and Discussion

5.3.1 In vivo Hydrocarbon Formation from CO Reduction by *A. vinelandii*

To examine the ability of nitrogenase to perform *in vivo* CO reduction, *A. vinelandii* strains carrying the encoding genes for the Mo and V nitrogenases, respectively, were first grown in 250 mL growth media supplemented with ammonia, an externally supplied nitrogen source which suppressed the expression of nitrogenase while allowing accumulation of cell mass (Figure 5.1a). The growth of the two cultures started to plateau after 20 h and 23 h, respectively, indicating a depletion of ammonia in the growth media that served as a signal to turn on the expression of Mo and V nitrogenases in the respective cultures. At this point, the culture flasks were capped by airtight stoppers, and CO was added at 10% to the gas phases of these nitrogenase-expressing cultures (Figure 5.1a, arrows). The cultures were then allowed to grow in the absence of ammonia while being monitored for the *in vivo* hydrocarbon formation through an hourly analysis of the headspace of each culture by gas chromatography (GC). Excitingly, the culture expressing the V nitrogenase was capable of *in vivo* production of 1390 nmol C_2H_4, 86 nmol C_2H_6 and 8 nmol C_3H_6, respectively, over a time period of 8 h (Figure 5.1Fb, blue). Gas chromatography-mass spectrometry (GC-MS) analysis further demonstrated mass shifts of +2, +2 and +3, respectively, of products C_2H_4, C_2H_6 and C_3H_6 upon substitution of ^{13}CO for ^{12}CO, confirming CO as the carbon source of these hydrocarbon products (Figure 5.1c, d). The culture expressing the Mo nitrogenase, on the other hand, was unable to generate detectable amounts of hydrocarbon products under the same *in vivo* conditions (Figure 5.1b, black), consistent with the previous observation that the Mo nitrogenase was only 0.1% as active as the V nitrogenase in the in vitro reaction of CO reduction (1). Such an impaired ability of Mo nitrogenase to reduce CO to hydrocarbons

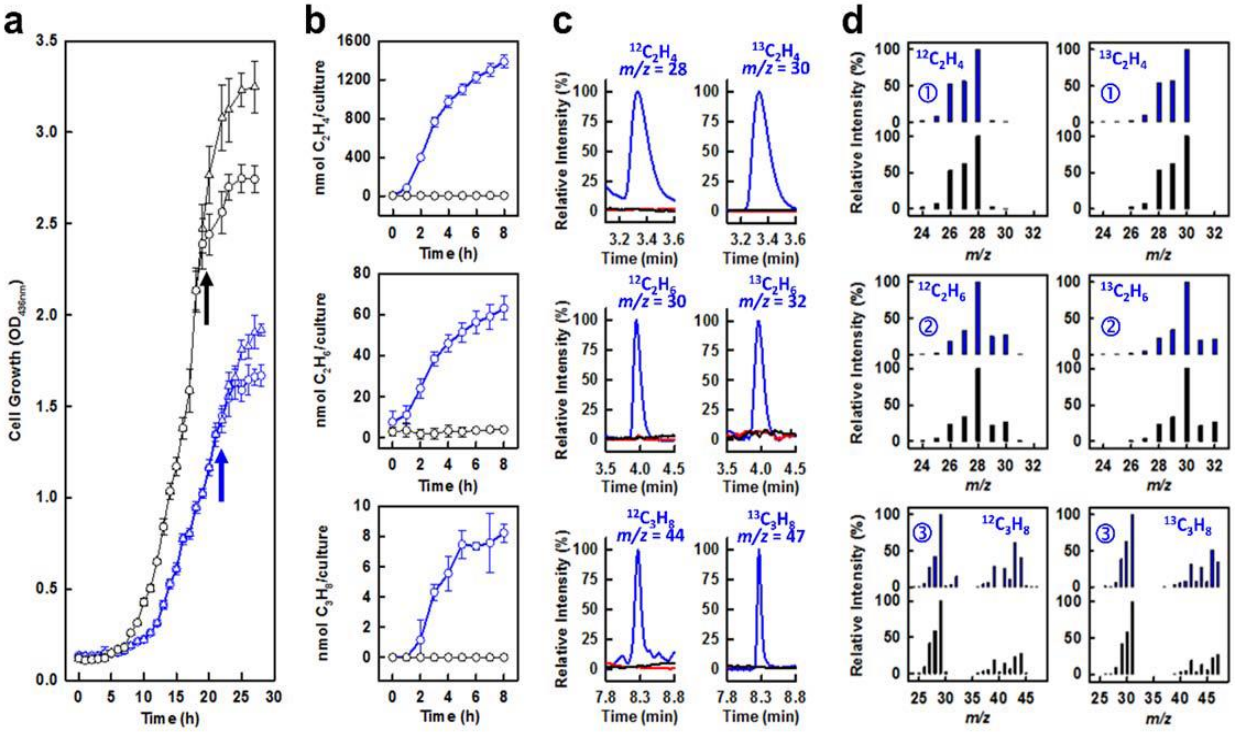

Figure 5.1. ***In vivo*** **hydrocarbon formation from CO reduction by** ***A. vinelandii*****.** a) Growth curves of *A. vinelandii* strains expressing Mo (black) and V (blue) nitrogenases in the presence (○) and absence (△) of 10% CO. The arrows indicate the time points of CO addition to the two cultures, when ammonia was depleted and nitrogenase expression was turned on. (b) Time-dependent formation of C_2H_4, C_2H_6 and C_3H_8 by 250 mL cultures of *A. vinelandii* strains expressing Mo (black) and V (blue) nitrogenases. The 250 mL culture expressing the V nitrogenase yielded 1387 nmol C_2H_4, 63 nmol C_2H_6 and 8 nmol C_3H_8, respectively, when 1.7 mmol CO was supplied in a 250 mL gas phase. (c) GC-MS analysis of C_2H_4 (upper), C_2H_6 (middle) and C_3H_8 (lower) formed by *A. vinelandii* strain expressing V nitrogenase in the presence of ^{12}CO (left) and ^{13}CO (right). The products were traced in the SIM mode of GC-MS at masses indicated in the figure. The peak intensities of products generated by the culture expressing the V nitrogenase (blue) were set at 100%. Note the absence of product formation when CO was supplied to controls that either expressed the Mo nitrogenase in the absence of ammonia (black) or did not express the V nitrogenase in the presence of ammonia (red). (d) GC-MS fragmentation patterns of C_2H_4 (①, blue), C_2H_6 (②, blue) and C_3H_8 (③, blue) formed by the *A. vinelandii* strain expressing the V nitrogenase in the presence of ^{12}CO (left) and ^{13}CO (right). The corresponding fragmentation patterns of standards are presented based on information obtained from the NIST mass spectrometry database (black) (http://webbook.nist.gov). The intensities of base peaks were set at 100% in all panels. Data of cell growth and activity analysis (a, b) were obtained from 3 independent experiments (n = 6) and presented as mean ± s. d. GC-MS experiments (c, d) were conducted 3 times, and representative results are shown.

in vivo was further demonstrated by subjecting the culture expressing the Mo nitrogenase to different amounts of CO (between 0 and 37.5% at a step increase of 7.5%), where no

hydrocarbons were detected at any CO concentration (Figure 5.2a). In contrast, the activities of *in vivo* hydrocarbon formation when CO was supplied at all tested concentrations, reaching a maximum of 1556 nmol products/250 mL culture at 15% CO (Figure 5.2a). Quantification of V nitrogenase expressed in the culture further revealed formation of a

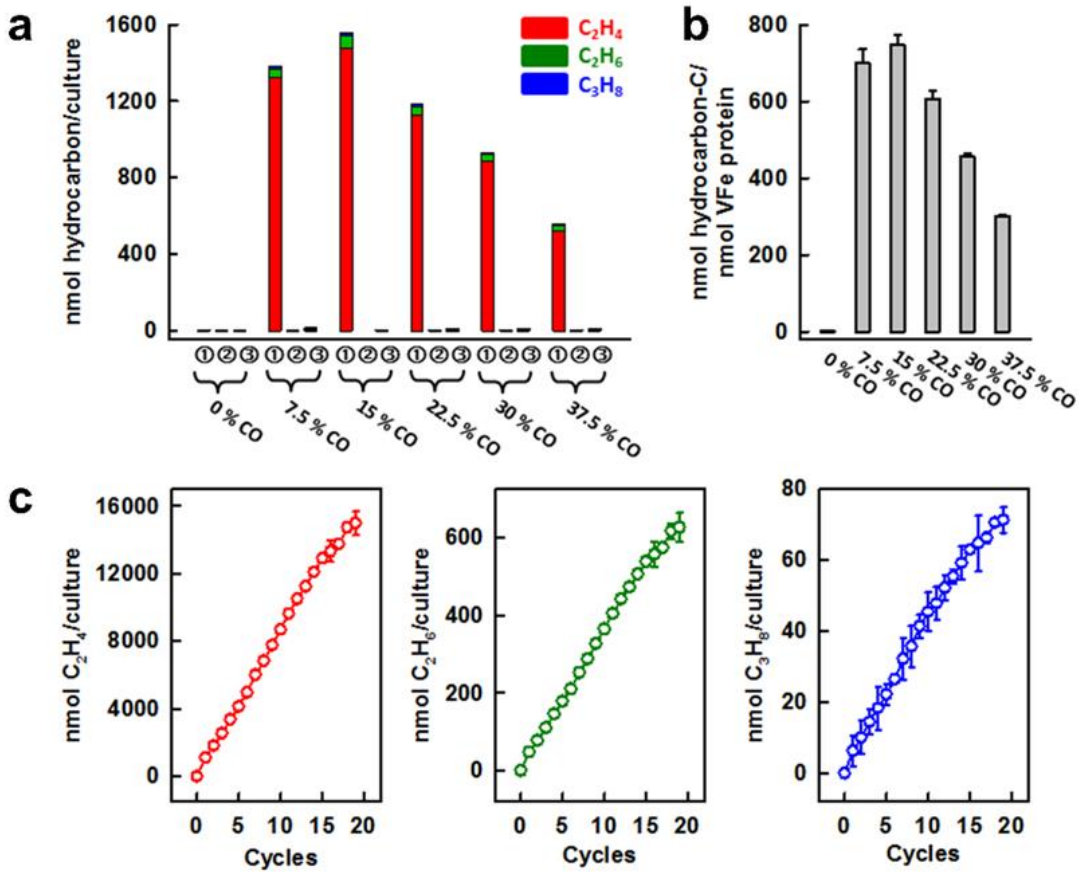

Figure 5.2 Optimization of *in vivo* hydrocarbon production from CO reduction. (a) Hydrocarbon formation by 250 mL cultures of *A. vinelandii* strains carrying encoding genes for V (①,②) and Mo (③) nitrogenases upon incubation with various CO concentrations for 8 h. CO was added upon depletion of ammonia without (①,③) or with (②) supplementation of additional ammonia to the growth media. (b) Specific yield of *in vivo* hydrocarbon formation by V nitrogenase upon incubation with various CO concentrations for 8 h. (c) Linear increases of C_2H_4 (left), C_2H_6 (middle) and C_3H_8 (right) formation by a 250 mL culture of the V nitrogenase-expressing *A. vinelandii* strain every 4 h upon repeated addition of CO with intermittent 20 min aeration. A 250 mL culture expressing the V nitrogenase yielded 14981 nmol C_2H_4, 626 nmol C_2H_6 and 71 nmol C_3H_8, respectively, after 20 cycles of repeated addition of 2.6 mmol CO in a 250 mL gas phase with intermittent aeration, which was equivalent to 1.2% carbon conversion. Data of activity analysis were obtained from 3 independent experiments (n = 6) and presented as mean ± s. d.

maximum of 750 nmol reduced carbon/nmol VFe protein, or a turnover number of as high as 750, at 15% CO over 8 h (Figure 5.2b). Importantly, CO could not be reduced to hydrocarbons when the expression of V nitrogenase was suppressed by the addition of excess ammonia in the growth media (Figure 5.2a). Moreover, the culture expressing the V nitrogenase closely resembled the purified V nitrogenase in the distribution of products (1), producing C_2H_4 as the overwhelmingly predominant product (95%; Figure 5.2a, red) of CO reduction over C_2H_6 (3.9%; Figure 5.2a, green) and C_3H_8 (1.1%; Figure 5.2a, blue) (1, 2). Together, these observations established a direct link between the V nitrogenase in the culture and the *in vivo* activity of hydrocarbon formation.

The observation of good turnover numbers of the *in vivo* CO reduction compelled us to further explore the possibility to improve the yield of hydrocarbon production in this reaction. Noticeably, the *in vivo* production of hydrocarbons by V nitrogenase started to plateau after the cell culture was incubated with CO for 4 h (see Figure 5.1b). Additionally, there was a decline of *in vivo* hydrocarbon formation when CO was supplied at a concentration beyond ~15% (see Figure 5.2a). These results could be explained by inhibition of the respiratory chain and/or other key metabolic pathways of *A. vinelandii* by CO, as well as accumulation of toxic waste products and/or inhibitors of V nitrogenase upon CO reduction, leading to an inability of cells and/or the V nitrogenase to function normally with prolonged exposure to high concentrations of CO. To alleviate the inhibitory effect of CO, the culture expressing V nitrogenase was placed under air after incubation with 15% CO for 4 h, permitting the cells to "relax" for 20 min before 15% CO was re-introduced into the gas phase of the culture. Remarkably, such a treatment led to a complete revitalization of the culture in its ability to produce hydrocarbons, as the culture displayed a linear increase of

product formation after nearly 20 repetitions of this procedure (Figure 5.2*c*). The amounts of C_2H_4, C_2H_6 and C_3H_8 accumulated after 20 repetitions were 15680, 625 and 71 nmol/250 mL culture, respectively (Figure 5.2*c*), demonstrating the possibility of biotechnological adaptation of this protocol for *in vivo* hydrocarbon production in the future. Moreover, a dramatic increase of CO consumption was achieved by this procedure, providing a necessary tool for the determination of whether CO was used as a carbon source and incorporated into cell mass or if it was processed into hydrocarbons in a novel, secondary metabolic pathway.

5.3.2 The Physiological Role of the *in vivo* CO Reduction by V nitrogenase

Seeing the high efficiency of the hydrocarbon formation of *A. vinelandi* expressing V nitrogenase we were wondering whether CO reduction has a physiological role. To determine whether the carbon of CO is incorporated into the cell mass of *A. vinelandii* cultures expressing V nitrogenase were prepared in the presence of 15% ^{12}CO or ^{13}CO with intermittent "relaxation" every 4 h by a short, 20 min exposure to air. This procedure was repeated 13 times to allow isotope enrichment and, subsequently, equal amounts of the ^{12}CO- and ^{13}CO-treated cells were fixed, dried and analyzed by nanoscale secondary ion mass spectrometry (CAMECA nanoSIMS 50L instrument) (7, 11, 12). Secondary electron images of samples incubated with ^{12}CO (Figure 5.3a) and ^{13}CO (Figure 5.3c) confirmed the identities of the images as those derived from cells and not from random particles; whereas the secondary ion images demonstrated nearly identical $\delta^{13}C$ value of the ^{12}CO-incubated (Figure 5.3b) and ^{13}CO-incubated (Figure 5.3d) samples. Analysis of the $\delta^{13}C$ values of three different regions of interest (ROI) in each sample further confirmed that the abundance of

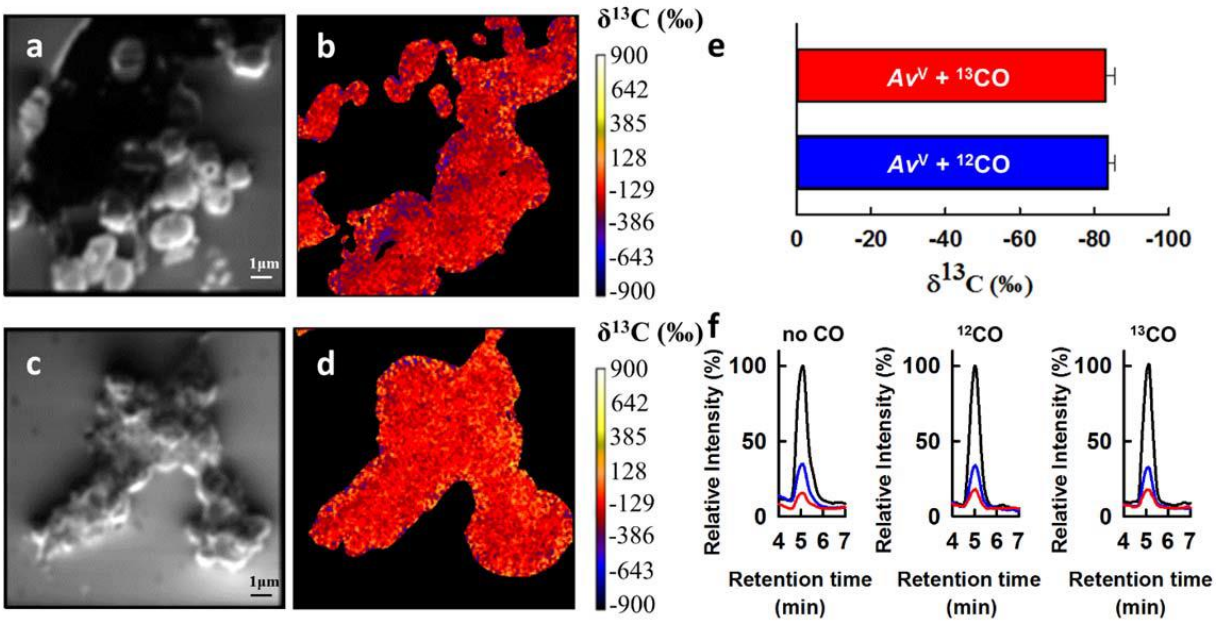

Figure 5.3. *In vivo* CO reduction as a secondary metabolic pathway. (a-d) Secondary electron images (a, c) and secondary ion ($^{13}C^-$ and $^{12}C^-$) images (b, d) derived from nanoSIMS analysis of *A. vinelandii* cells expressing V nitrogenase in the presence of ^{12}CO (a, b) or ^{13}CO (c, d). The nanoSIMS experiment was performed twice. Each time, data was collected at 3 different regions of interest (ROI) in each sample. Representative nanoSIMS data are shown in a-d. (e) Average $\delta^{13}C$ values of *A. vinelandii* cells expressing V nitrogenase in the presence of ^{12}CO (blue) or ^{13}CO (red). The average $\delta^{13}C$ value of each sample was calculated based on data collected in 3 different ROI (n = 9). (f) LC-MS analysis of acetyl-CoA formed by *A. vinelandii* cells expressing V nitrogenase in the absence (left) and presence of ^{12}CO (middle) or ^{13}CO (right). Natural-abundance (black), one (blue) and two (red) ^{13}C-substituted acetyl-CoA molecules were traced at masses 810, 811 and 812, respectively. The LC-MS experiment was performed 4 times. Representative results are shown in f.

^{13}C in the ^{13}CO-incubated sample was indistinguishable from that in the ^{12}CO-incubated sample (Figure 5.3e), suggesting that the carbon of CO was not incorporated into the cellular components. To demonstrate the ability of nanoSIMS to detect enrichment of isotopes in cells, the incorporation of $^{15}N_2$ by *A. vinelandii* was traced (Figure 5.4). Furthermore, the incorporation of $^{15}N_2$ was also traced in the presence of 15% ^{12}CO, as expected the incorporation of $^{15}N_2$ was significantly lower (Figure 5.4). Nonetheless the

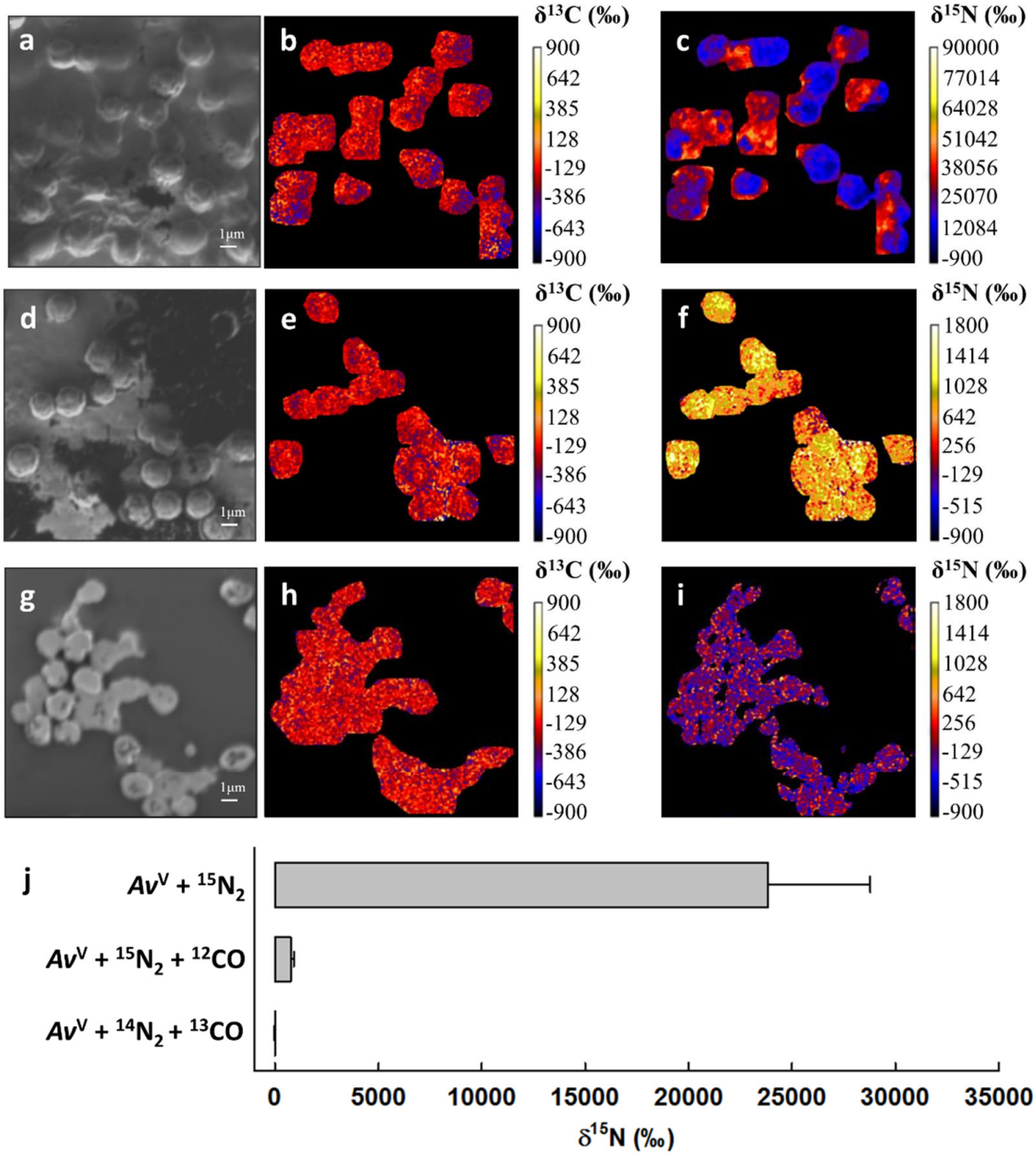

Figure 5.4. Assimilation of N via N_2 reduction by *A. vinelandii*. (a-i) Secondary electron (a, d, g) and secondary ion (b-h, c-i) images derived from nanoSIMS analysis of *A. vinelandii* cells expressing the V-nitrogenase in the presence of $^{15}N_2$ (a-c), $^{15}N_2$ plus ^{12}CO (d-e), and $^{14}N_2$ plus ^{13}CO (g-i) (see Chapter 5.2.6 for experimental details). For each sample, data was collected at 3 different regions of interest (ROI), 2 frames/ROI. Representative nanoSIMS data are shown in a-i. (j) Average $\delta^{15}N$ values of *A. vinelandii* cells expressing the V-nitrogenase in the presence of $^{15}N_2$, $^{15}N_2$ plus ^{12}CO, and $^{14}N_2$ plus ^{13}CO. The average $\delta^{15}N$ value of each sample was calculated based on data collected in 3 different ROIs (n = 6).

^{15}N-incorporation was significantly higher than the background (Figure 5.4j).

A second line of evidence, that CO was not used as a carbon source for anabolism is provided by liquid chromatography-mass spectrometry (LC-MS). LC-MS showed indistinguishable ratios between the natural-abundance (Figure 5.3f, black), one ^{13}C-incorporated (Figure 5.3f, blue), and two 13C-incorporated (Figure 5.3f, red) acetyl-CoA molecules in *A. vinelandii* cells incubated without CO (Figure 5.3f, left), with ^{12}CO (Figure 5.3f, middle), and with ^{13}CO (Figure 5.3f, right) concomitant with the expression of V nitrogenase, providing further support that CO was not used as a carbon source to generate the central metabolite, acetyl-CoA, during cell growth. Combined results from these studies conclusively defined the *in vivo* CO reduction by V nitrogenase as a novel, secondary metabolic pathway for the conversion of CO into hydrocarbons.

5.4 Summary and Conclusions

Nature has developed some effective strategies for microbes to utilize CO as an electron and/or carbon source for cell growth (13, 14). The *in vivo* conversion of CO to alkanes/alkenes by *A. vinelandii* represents a previously-unidentified strategy utilized by microbes to cope with CO. It has been postulated that the Earth atmosphere was rich in CO and methane (CH_4) in the Archean Eon (15) and that microbes living in this environment were adapted to strategies to effectively utilize these carbon-containing molecules, alone or in symbiosis. It is plausible, therefore, that the host of the ancestral, "prototype nitrogenase" was well-tuned toward reducing CO to small alkenes and alkanes, and these products were then assimilated and used as the sole carbon/energy source either by the host itself or by other microbes that could not generate these products on their own. Interestingly, while

nitrogenase-expressing organisms like *A. vinelandii* seem to have lost the ability to use small hydrocarbons for cell growth during the course of evolution, various alkane/alkene assimilating organisms are known to exist today (16-18), implying that a nitrogenase-based, symbiotic CO-utilizing strategy may still be in use. Moreover, the possible evolvement of nitrogenase from an enzyme specialized in processing carbon compounds into one specialized in processing nitrogen compounds establishes this enzyme as an evolutionary link between the carbon and nitrogen cycles on Earth.

Regardless of its evolutionary relevance, the fact that CO is reduced by *A. vinelandii* to hydrocarbons as secondary metabolites gives this *in vivo* reaction a clear biotechnological advantage in maximizing the product yield and cost efficiency. Indeed, the yield of ethylene production by this reaction (1 μmol C_2H_4 per *g* dry cell per h) is already within the range of the existing methodologies for bio-ethylene production (0.1-3000 μmol C_2H_4 per *g* dry cell per h) (19) prior to any optimization. Further, despite a low percentage of carbon conversion, the specific activity of this reaction (0.1 μmol hydrocarbons/g V nitrogenase/s) is comparable to the specific activities of the less efficient Fischer-Tropsch catalysts or those discovered at the early developmental stage of this industrial process (0.024-0.3 μmol hydrocarbons/g catalyst/s) (20, 21). Importantly, contrary to the Fischer-Tropsch process or fermentation-based methodologies for hydrocarbon production, the *A. vinelandii*-enabled reaction is an ambient, feedstock-free process that directly converts a toxic waste (CO) into useful hydrocarbon products. Perhaps even more excitingly, it was discovered recently that *A. vinelandii* strains expressing the respective Fe protein components of Mo and V nitrogenases alone were capable of *in vivo* conversion of CO_2 to CO (see Chapter 4), a process that could be coupled with the *in vivo* conversion of CO to hydrocarbons by *A. vinelandii* into

a whole cell system for hydrocarbon production from the greenhouse gas CO_2. Such a two-step system will circumvent the problem that a direct conversion of CO_2 to hydrocarbons by nitrogenase is of extremely poor efficiency (see Chapter 2 and 3) (22, 23). Additionally, both steps in this system can be optimized for improved product yield or desired product profile and, on their own or in combination, they represent attractive templates for the future development of strategies that effectively recycle carbon wastes into useful chemical and fuel products.

5.5 Acknowledgements

I would like to thank Dr. Yilin Hu (University of California, Irvine) for the construction of the *A. vinelandii* strain YM68A and Dr. Chi Chung Lee (University of California, Irvine) for carrying out the LC-MS analysis of acetyl-CoA. I also thank the Nature Publishing Group for publishing portions of this Chapter in *Nature Communications* (24). This work was supported by DOE (BES) Award DE-SC0014470, funds from UC Irvine to Dr. Markus W. Ribbe and Dr. Yilin Hu and a Hellman Fellowship to Dr. Yilin Hu.

5.6 References

1. Hu Y, Lee CC, & Ribbe MW (2011) Extending the carbon chain: hydrocarbon formation catalyzed by vanadium/molybdenum nitrogenases. *Science* 333(6043):753-5.
2. Lee CC, Hu Y, & Ribbe MW (2010) Vanadium nitrogenase reduces CO. *Science* 329(5992):642.
3. Eady RR (1996) Structure-Function Relationships of Alternative Nitrogenases. *Chem Rev* 96(7):3013-30.

4. Hu Y, Lee CC, & Ribbe MW (2012) Vanadium nitrogenase: a two-hit wonder? *Dalton Trans* 41(4):1118-27.

5. Lee CC, Hu Y, & Ribbe MW (2009) Unique features of the nitrogenase VFe protein from Azotobacter vinelandii. *Proc Natl Acad Sci U S A* 106(23):9209-14.

6. Burgess BK, Jacobs DB, & Stiefel EI (1980) Large-scale purification of high activity Azotobacter vinelandII nitrogenase. *Biochim Biophys Acta* 614(1):196-209.

7. Pernthaler A, Dekas AE, Brown CT, Goffredi SK, Embaye T, & Orphan VJ (2008) Diverse syntrophic partnerships from deep-sea methane vents revealed by direct cell capture and metagenomics. *Proc Natl Acad Sci U S A* 105(19):7052-7.

8. Craig H (1957) Isotopic Standards for Carbon and Oxygen and Correction Factors for Mass-Spectrometric Analysis of Carbon Dioxide. *Geochim Cosmochim Acta* 12(1-2):133-49.

9. Bièvre PD, Valkiers S, Peiser HS, Taylor PDP, & Hansen P (1996) Mass-spectrometric methods for determining isotopic composition and molar mass traceable to the SI, exemplified by improved values for nitrogen. *Metrologia* 33(5):447.

10. Junk G & Svec HJ (1958) The absolute abundance of the nitrogen isotopes in the atmosphere and compressed gas from various sources. *Geochim Cosmochim Acta* 14(3):234-43.

11. Gao D, Huang X, & Tao Y (2016) A critical review of NanoSIMS in analysis of microbial metabolic activities at single-cell level. *Crit Rev Biotechnol* 36(5):884-90.

12. Dekas AE, Poretsky RS, & Orphan VJ (2009) Deep-Sea Archaea Fix and Share Nitrogen in Methane-Consuming Microbial Consortia. *Science* 326(5951):422-6.

13. Svetlichny VA, Sokolova TG, Gerhardt M, Ringpfeil M, Kostrikina NA, & Zavarzin GA (1991) Carboxydothermus-Hydrogenoformans Gen-Nov, Sp-Nov, a Co-Utilizing Thermophilic Anaerobic Bacterium from Hydrothermal Environments of Kunashir-Island. *Syst Appl Microbiol* 14(3):254-60.

14. Ragsdale SW & Pierce E (2008) Acetogenesis and the Wood-Ljungdahl pathway of CO(2) fixation. *Biochim Biophys Acta* 1784(12):1873-98.

15. Glikson AY (2008) Milestones in the evolution of the atmosphere with reference to climate change. *Aust J Earth Sci* 55(2):125-39.

16. Roslev P, Iversen N, & Henriksen K (1997) Oxidation and assimilation of atmospheric methane by soil methane oxidizers. *Appl Environ Microbiol* 63(3):874-80.

17. Coleman NV & Spain JC (2003) Distribution of the coenzyme M pathway of epoxide metabolism among ethene- and vinyl chloride-degrading Mycobacterium strains. *Appl Environ Microbiol* 69(10):6041-6.

18. Jaekel U, Musat N, Adam B, Kuypers M, Grundmann O, & Musat F (2013) Anaerobic degradation of propane and butane by sulfate-reducing bacteria enriched from marine hydrocarbon cold seeps. *ISME J* 7(5):885-95.

19. Eckert C, Xu W, Xiong W, Lynch S, Ungerer J, Tao L, Gill R, Maness PC, & Yu J (2014) Ethylene-forming enzyme and bioethylene production. *Biotechnol Biofuels* 7(1):33.

20. Mims CA, McCandlish LE, & Melchior MT (1988) Fischer-Tropsch Synthesis-a C-2 Initiator for Hydrocarbon Chain Growth on Ruthenium. *Catalysis Letters* 1(5):121-5.

21. Jahangiri H, Bennett J, Mahjoubi P, Wilson K, & Gu S (2014) A review of advanced catalyst development for Fischer-Tropsch synthesis of hydrocarbons from biomass derived syn-gas. *Catalysis Science & Technology* 4(8):2210-29.

22. Rebelein JG, Hu Y, & Ribbe MW (2015) Widening the Product Profile of Carbon Dioxide Reduction by Vanadium Nitrogenase. *ChemBioChem* 16(14):1993-6.

23. Rebelein JG, Hu Y, & Ribbe MW (2014) Differential reduction of CO(2) by molybdenum and vanadium nitrogenases. *Angew Chem Int Ed Engl* 53(43):11543-6.

24. Rebelein JG, Lee CC, Hu Y, & Ribbe MW (2016) In vivo Hydrocarbon Formation by Vanadium Nitrogenase: A Novel Secondary Metabolic Pathway. *Nat Commun* (In Press).